Russian Original Vol. 42, No. 3, March, 1977

September, 1977

SATEAZ 42(3) 191-288 (1977)

pts Xerox
p224-225

SOVIET ATOMIC ENERGY

АТОМНАЯ ЭНЕРГИЯ
(ATOMNAYA ÉNERGIYA)

TRANSLATED FROM RUSSIAN

c/b CONSULTANTS BUREAU, NEW YORK

SOVIET ATOMIC ENERGY

Soviet Atomic Energy is a cover-to-cover translation of *Atomnaya Énergiya*, a publication of the Academy of Sciences of the USSR.

An agreement with the Copyright Agency of the USSR (VAAP) makes available both advance copies of the Russian journal and original glossy photographs and artwork. This serves to decrease the necessary time lag between publication of the original and publication of the translation and helps to improve the quality of the latter. The translation began with the first issue of the Russian journal.

Consultants Bureau journals appear about six months after the publication of the original Russian issue. For bibliographic accuracy, the English issue published by Consultants Bureau carries the same number and date as the original Russian from which it was translated. For example, a Russian issue published in December will appear in a Consultants Bureau English translation about the following June, but the translation issue will carry the December date. When ordering any volume or particular issue of a Consultants Bureau journal, please specify the date and, where applicable, the volume and issue numbers of the original Russian. The material you will receive will be a translation of that Russian volume or issue.

Subscription
$117.50 per volume (6 Issues)
2 volumes per year

Single Issue: $50
Single Article: $7.50

Prices somewhat higher outside the United States.

CONSULTANTS BUREAU, NEW YORK AND LONDON

227 West 17th Street
New York, New York 10011

Published monthly. Second-class postage paid at Jamaica, New York 11431.

Soviet Atomic Energy is abstracted or indexed in *Applied Mechanics Reviews, Chemical Abstracts, Engineering Index, INSPEC—Physics Abstracts and Electrical and Electronics Abstracts, Current Contents,* and *Nuclear Science Abstracts.*

SOVIET ATOMIC ENERGY

A translation of *Atomnaya Énergiya*

September, 1977

Volume 42, Number 3 March, 1977

CONTENTS

CONTENTS

(continued)

CONTENTS

(continued)

Engl./Russ.

The Russian press date (podpisano k pechati) of this issue was 2/24/1976. Publication therefore did not occur prior to this date, but must be assumed to have taken place reasonably soon thereafter.

DETERMINATION OF MINERALIZATION TIME FROM THE ISOTOPIC COMPOSITION OF LEAD SULFIDES

G. E. Ordynets

UDC 550.93

Isotopic analysis is being used successfully in the study of ore deposits. The results of isotopic studies are being widely used for the solution of problems involving the age of ores and the source of ore materials. There is interest in the use of the isotopic-lead method for evaluation of the time of mineralization and for refinement of the sequence of mineralization. For this purpose, an analysis was made of the lead in sulfides of various ages from a hydrothermal uranium deposit in a uranium sulfide formation.

The deposit is located in the peripheral region of the central massif at the junction of two large tectonic blocks. The enclosing rock is in the form of metamorphized precambrian amphibolites, gneisses, and magmatites containing seams of marbles and limestones with veins and intersecting dikes of pegmatites and aplites. The

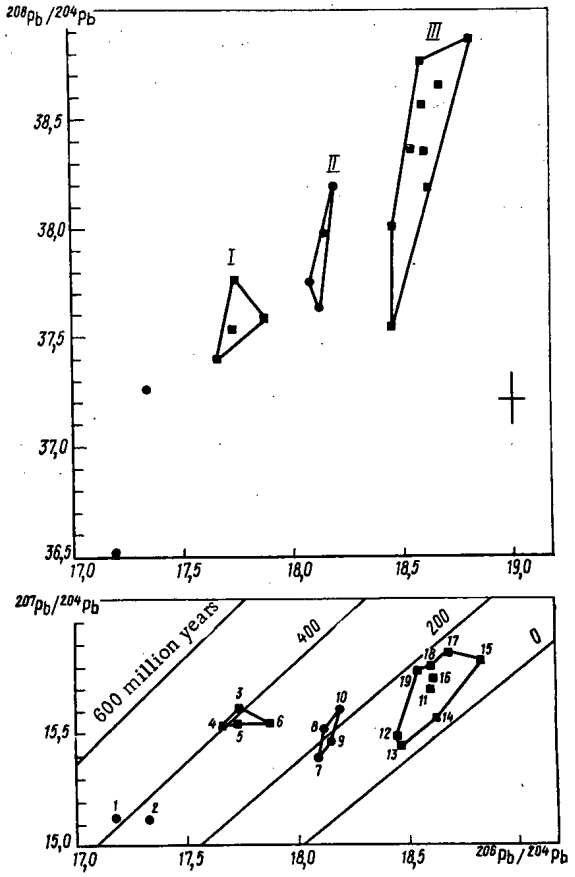

Fig. 1. Diagram of isotopic ratios of leads in sulfides: +) analytic uncertainty; ●) pyrite; ■) galena.

Translated from Atomnaya Énergiya, Vol. 42, No. 3, pp. 171-176, March, 1977. Original article submitted April 9, 1976.

TABLE 1. Isotopic Composition of Lead Sulfide

Type of sample	204Pb, %	206Pb, %	207Pb, %	208Pb, %	206Pb/204Pb	207Pb/204Pb	208Pb/204Pb	206Pb/207Pb	208Pb/207Pb	208Pb/(206Pb+207Pb)
					Group I					
Pyrite impregnated in limestone	1,419	25,09	21,67	51,82	17,68	15,27	36,52	1,158	2,391	1,11
Recalculated	1,432	24,61	21,67	52,29	17,19	15,13	36,52	1,136	2,413	1,13
Pyrite impregnated in limestone	1,414	24,52	21,38	52,69	17,34	15,12	37,26	1,147	2,464	1,14
Galena impregnated in limestone	1,387	24,60	21,64	52,37	17,74	15,60	37,76	1,137	2,420	1,13
The same	1,397	24,67	21,68	52,25	17,66	15,52	37,40	1,138	2,410	1,13
" "	1,393	24,70	21,63	52,28	17,73	15,53	37,53	1,142	2,417	1,13
Galena together with quartz and sphalerite in the zone of crushing	1,389	24,83	21,57	52,21	17,88	15,53	37,58	1,151	2,420	1,13
Av. value for galenas	1,392	24,70	21,63	52,28	17,75	15,54	37,57	1,142	2,417	1,13
					Group II					
Pyrite scattered in graphitized paragneisses	1,358	25,06	21,28	52,29	18,09	15,37	37,75	1,178	2,457	1,13
The same	1,384	25,09	21,45	52,08	18,13	15,50	37,63	1,170	2,428	1,12
Pyrite in ground graphitized material of the cracked zone* (recalculated)	1,378	25,01	21,09	52,32	18,15	15,45	37,97	1,175	2,457	1,13
The same	1,370	24,93	21,38	52,32	18,20	15,60	38,19	1,166	2,447	1,13
Average value	1,372	25,02	21,35	52,25	18,14	15,48	37,88	1,172	2,447	1,13
					Group III					
Galena in carbonate–polymetallic vein (average of two laboratories)	1,350	25,13	21,18	52,34	18,61	15,69	38,77	1,186	2,471	1,13
The same (av. of two analyses)	1,380	25,47	21,35	51,80	18,46	15,47	37,54	1,193	2,426	1,11
Galena in carbonate–polymetallic vein	1,372	25,34	21,16	52,13	18,47	15,43	38,00	1,198	2,464	1,12
The same	1,363	25,39	21,21	52,04	18,63	15,56	38,18	1,197	2,454	1,12
" " (av. of two analyses)	1,342	25,28	21,22	52,16	18,84	15,82	38,87	1,191	2,458	1,12
Galena in polymetallic vein	1,357	25,27	21,34	52,03	18,62	15,73	38,34	1,184	2,438	1,12
The same	1,348	25,19	21,36	52,10	18,69	15,85	38,65	1,179	2,439	1,12
" "	1,352	25,16	21,35	52,13	18,61	15,79	38,56	1,178	2,442	1,12
" "	1,358	25,15	21,41	52,08	18,55	15,77	38,35	1,175	2,432	1,12
Average value	1,358	25,26	21,29	52,09	18,61	15,68	38,36	1,187	2,447	1,12
					Group IV					
Galena in calcite vein	1,312	28,17	20,81	49,71	21,47	15,86	37,89	1,354	2,389	1,01
Pyrite in calcite vein	1,308	29,08	20,33	49,28	22,23	15,54	37,68	1,430	2,424	1,00

*Results recalculated by the Brown method.

main ore-monitoring structures are large discontinuous tectonic zones of submeridional direction. As a rule, they follow a course consistent with the enclosing rock and are traced over distances up to 20 km. The ore bodies are coordinated with the near-meridional longitudinal tectonic zones and with the shallower dislocations of northwesterly direction resting on them. In tectonic zones from 2 to 25 m thick, which are ordinarily in the form of intensely crushed, graphitized, and pyritized fine-grained plagioclase–biotite gneisses, there appear numerous veins of variously aged carbonates together with uraninites and selenides and impregnated-vein uranium ores.

The geostructural and mineralogic features of the deposit were discussed previously [1, 2]. A study of its mineral composition made it possible to pick out five successive stages of mineralization: graphite–pyrite, quartz–pyrite, carbonate–sulfide, carbonate–chlorite–uraninite, and calcite–pyrite.

TABLE 2. Results of Comparative Analyses of Isotopic Lead Composition in Galenas

Sample no.	^{204}Pb	^{206}Pb	^{207}Pb	^{208}Pb
3	1,385 *	24,46	21,57	52,58
	1,389†	24,73	21,71	52,17
11	1,352 *	24,99	21,03	52,63
	1,348†	25,25	21,37	52,03

*Data of V. M. Eloev and A. S. Samoletov.
†Data of Ya. Legierskii.

Only the sequence of formation of the concluding stages is established from direct geological observations. The age interrelations of the initial stages were established from general geological considerations and by analogy with deposits in the region such as the age of uraninites, which is 270 million years [3-5].

To determine the isotopic composition of lead, samples of galenas and pyrites were collected from various mineral complexes in the deposit. The lead was extracted with dithizone after acid leaching. Analysis of the isotopic composition was performed on MI-1305 and MI-1311 mass spectrometers by the single-beam method using a silicate emitter. Four groups of lead-containing sulfides were picked out in accordance with geological location and isotopic composition (Table 1, Fig. 1).

Group I includes sulfides dispersed in limestones and belonging to the quartz–pyrite stage. The occurrence of this sulfide mineralization in Precambrian strata remains unclear; it is either metamorphogenic, associated with metamorphosis of the enclosing rock, or is hydrothermal-metasomatic, resulting from the initial stages of ore formation.

The pyrites 1 and 2, separated from samples of average-grain limestones, are almost indistinguishable with respect to the isotopic composition of lead and occupy the extreme lower-left position in Fig. 1. A correction was introduced for contamination by uranium lead in the isotopic lead composition of pyrite 1 using the method proposed by Brown [6, 7] based on the ratio $^{208}Pb/(^{206}Pb + ^{207}Pb)$, which is usually 1.13 for ordinary uncontaminated lead. On the average, this value corresponds to 52.37% ^{208}Pb and a deviation of 1% is sufficient to demonstrate contamination. One can assume that lead with a content less than 52% ^{208}Pb is contaminated by uranium lead, and with a content greater than 52.75% by thorium lead. In pyrite 1, the concentration of ^{208}Pb is 51.82%, which points to an admixture of uranium lead. The correction is introduced in the following manner: dividing the value of 51.82 by 1.13, we obtain the percent sum of the uranium lead concentration ($^{206}Pb + ^{207}Pb$) in the uncontaminated lead, which (45.86%) is 0.90% less than that actually measured in the sample (46.76%); we subtract this excess of uranium lead (0.70% for ^{206}Pb and 0.20% for ^{207}Pb) from the corresponding measured values (25.09-0.70 = 24.39% and 21.67-0.20 = 21.47%); we sum the resultant values with the concentrations of ^{204}Pb and ^{208}Pb and take the sum (1.419 + 24.39 + 21.47 + 51.82 = 99.099) as 100% and then calculate the percent content of each isotope in the corrected (recalculated) isotopic composition for lead. Figure 1 shows the values of the recalculated isotopic composition of lead. A similar correction was introduced in the compositions of pyrites 9 and 10. In pyrites 1, 9, and 10, the ratio $^{208}Pb/(^{206}Pb + ^{207}Pb)$ was 1.10-1.11 before the introduction of corrections, which indicates contamination with uranium lead. Luminescence analysis of the pyrites revealed 0.0004-0.0005% of uranium in them.

The maximum ^{204}Pb content (1.41-1.53%) in pyrites 1 and 2 indicates the greatest age of the lead in these minerals. According to J. Brown, a ^{204}Pb concentration of 1.40% and above should correspond to Precambrian. All the remaining parameters, particularly the ^{206}Pb and ^{207}Pb concentrations and the $^{206}Pb/^{204}Pb$ and $^{206}Pb/^{207}Pb$ ratios, correspond to a time between Precambrian and Fanerozoic. It can be assumed that the lead in these pyrites are Late Precambrian or Early Paleozoic. Lead of such an isotopic composition has not been known in the region before now.

Galenas 3, 4, 5, and 6, which were collected in the same place as the pyrites discussed, are characterized by identical lead composition within the limits of error of the method and form a rather compact group in Fig. 1.

TABLE 3. Model-Based Age of Lead Sulfides

Sample no.	Isotopic ratio		Age, million yr	
	$^{206}Pb/^{207}Pb$	$^{208}Pb/^{207}Pb$	$^{206}Pb/^{207}Pb$	$^{208}Pb/^{207}Pb$
1	1,136	2,413	360	340
2	1,147	2,464 *	310	120 *
3	1,137	2,420	360	310
4	1,138	2,410	350	360
5	1,142	2,417	330	330
6	1,151	2,420	280	310
Average for Group I	1,142	2,417	330	330
7	1,178	2,457	140	150
8	1,170	2,428	190	280
9	1,175	2,457	160	150
10	1,166	2,447	210	190
Average for Group II	1,172	2,447	175	190
11	1,186	2,471	100	80
12	1,193	2,426	60	280
13	1,198	2,464	40	110
14	1,197	2,454	40	160
15	1,191	2,458	70	140
16	1,184	2,438	110	230
17	1,179	2,439	140	230
18	1,178	2,442	140	210
19	1,175	2,432	160	260
Average for Group III	1,187	2,447	100	190

*Not included in calculation of the average because of anomalously high value for ^{208}Pb content.

The isotopic lead composition of these samples shows that the sulfide mineralization scattered in limestone is the oldest in the deposit. Furthermore, as follows from Table 1 and Fig. 1, the pyrites differ markedly from the galenas in isotopic lead composition. It can be assumed that the formation of these sulfides was associated with the initial hydrothermal-metasomatic process, probably in early Paleozoic time. The greater age of the pyrite is apparently the result of the addition of Precambrian lead from enclosing formations.

Group II combines pyrites that form scattered impregnations in deformed and graphitized paragneisses of the main tectonic zone. Although they also belong to the earliest graphite–pyrite stage, the formation of these pyrites is associated with various mineral complexes that are spatially combined within the limits of the tectonic zone. It did not appear possible to separate the analyzed pyrites from the tectonic zone with respect to production; they were separated from crushed samples in the form of a 90-95% concentrate after washing with methylene iodide.

As indicated above, some samples in this group (9, 10) are characterized by an increased uranium content (0.0004-0.0005%) and by an isotopic composition shifted in the direction of an excess of uranium lead. Recalculated results from the method of J. Brown are given for these samples in Table 1.

The isotopic lead composition is much the same for all pyrites in Group II. They form an independent group differing markedly in isotopic composition from the sulfide of Group I. The average values for the isotopic lead composition of these pyrites ($^{206}Pb/^{204}Pb = 18.14$; $^{207}Pb/^{204}Pb = 15.48$; $^{208}Pb/^{204}Pb = 37.88$) can be used as geochemical characteristics of their conditions of formation in the basic tectonic zones.

Group III contains the galenas 11-19. They were collected from northeastern veins, which are composed of minerals of the carbonate–sulfide stage. Analytical results for galenas 16-19 were kindly furnished by Ya. Legierskii.

In order to check the possibility of using the results from two different isotope laboratories, parallel analyses were made of the isotopic lead composition in two galenas (Table 2). The results were in satisfactory agreement with the best being those for the determination of ^{204}Pb.

Despite some spread in the data resulting from varying material composition of the veins, their differing thicknesses, and the effect of enclosing rock, we note that the isotopic lead composition of the galenas in Group III varies insignificantly. These samples form an isolated group in Fig. 1. Galenas 12 and 13 differ slightly

from the others. In them, the ^{204}Pb concentration is somewhat high, and correspondingly the ratios of ^{206}Pb, ^{207}Pb, and ^{208}Pb to ^{204}Pb are a little low in comparison with the average values. The higher ^{204}Pb content can be explained by the fact that in thin polymetallic veins, where samples 12 and 13 were collected, the old lead of the enclosing rock has a greater effect.

The galenas of Group III differ markedly from the sulfides of Groups I and II with respect to isotopic lead composition and are characterized by a specific lead, the mean isotopic composition of which (18.61; 15.68; 38.36), corresponds to the Mesozoic age and can serve as a reliable isotopic characteristic of the carbonate–sulfide stage of mineralization.

If one assumes the age of uraninites to be 270 million years [4, 5], the disparity between the Mesozoic age of the carbonate–sulfide stage and its position to the sequence scheme [2] before the carbonate–chlorite–uraninite stage becomes obvious. The results are evidence of the fact that formation of carbonate–sulfide veins occurred after carbonate–chlorite–uraninite veins. Therefore, the existing scheme for the sequence of mineralization requires refinement.

The galena 20 and pyrite 21, which were collected from the most recent veins, make up Group IV. The lead in these samples differs considerably from the preceding samples by reason of a marked excess of uranium lead which is obviously anomalous. This appears most clearly in the markedly lower ^{204}Pb concentrations (around 1.31%), the anomalously high values for ^{206}Pb (28-29%), etc. (Table 1). The isotopic lead composition of these sulfides is evidence that buildup of radiogenic uranium lead (^{206}Pb), which was captured by the most recent sulfides concluding the hydrothermal process, occurred in the ore bodies of the deposit. Furthermore, anomalies in the composition of lead sulfides are noted in the neighborhood of aggregates of uraninites of the calcite–chlorite–uranium stage. Since the anomalous radiogenic lead was not observed at marked separation from ore bodies, its use as a survey criterion, as was established in many uranium deposits of other types [8-10], is obviously limited. The values of $^{208}Pb/^{204}Pb$, which are 37.89 and 37.68, do not differ from the values corresponding to ordinary lead ore, which indicates the absence of high concentrations of thorium in the ores because one would otherwise expect anomalously high values of this ratio in the lead of recent sulfides.

The results presented indicate that several types of lead are obviously distinguishable in the sulfides of the deposit under consideration. Furthermore, each type corresponds to one or another period of mineralization and is characterized by a definite isotopic composition which varies in regular manner from the oldest lead of the early stages (Group I) to the youngest lead of the carbonate–sulfide veins (Group III). These data are evidence of the pulsational nature of the hydrothermal-metasomatic process, each stage of which is characterized by definite conditions for formation.

An attempt was made to determine the age of the lead in these sulfides from existing isotopic data. However, one should keep in mind that one does not ordinarily determine the age of mineralization from the isotopic composition of lead ore since it will depend on the model assumed for the evolution of lead in the earth's crust. In addition, natural lead does not fall within the framework of the assumed model as a rule, and varying isotopic ratios in a specific sample yield markedly divergent values for the age. Thus for the average isotopic composition of lead in Hercynian deposits (about 150 samples), the age calculated by various methods varies from 260 to 490 million years [4].

A model proposed by Legierskii and based on the use of $^{206}Pb/^{207}Pb$ and $^{208}Pb/^{207}Pb$ ratios [4, 5] was accepted for the calculation of the age of lead in the various stages of mineralization. The interpretation of the resultant age values (Table 3) may not be unique. Nevertheless, it should be emphasized that the scattered sulfide mineralization in limestone (Group I) is oldest (about 330 million years according to the calculation). The age of the lead in the graphite–pyrite stage (Group II) is 175-190 million years. However, as already pointed out, the pyrites were represented by several generations and the values obtained probably do not reflect the true age of this stage. For lead in the galenas of carbonate–sulfide veins (Group III), the greatest spread is noted in the age values calculated from the two isotopic ratios and the age of the lead in this stage of ore formation is either Cretaceous (100 million years from the $^{206}Pb/^{207}Pb$ ratio) or Lower Jurassic (190 million years from the $^{208}Pb/^{207}Pb$ ratio) depending on the ratio accepted. In any case, acknowledge that the formation of carbonate–sulfide veins occured in Kimmeridgian time.

The hydrothermal process of ore formation at the deposit studied continued for a period of 150-200 million years and was accompanied by a regular variation in the isotopic lead composition. Each stage of mineralization is characterized by an isotopic lead composition typical of it alone, which is a definite geochemical criterion for mineral formation. The results of this work are evidence of the Kimmeridgian age of the carbonate–sulfide veins and indicate the need for refinement of the existing scheme for the sequence of mineralization, according to which the formation of the veins occurred in Hercynian time. Buildup of radiogenic lead,

which was captured by the sulfides of more recent stages, occurred in the ore bodies. However, anomalous lead sulfides were observed only in the immediate vicinity of the ore bodies or within them and therefore obviously cannot be used as a survey criterion. Aging of the lead in pyrites of the quartz–pyrite stage, the admixture of Precambrian lead from enclosing gneisses in the galenas of thin polymetallic veins, and the recorded regularity concerning the unity of the source of uranium, vanadium, and selenium [2], are evidence that the enclosing Precambrian formations may be the probable source of ore material.

The author is grateful to S. M. Eloev, A. S. Semoletov, and Ya. Legierskii for assistance with the work and to V. E. Boitev and B. V. Brodin for valuable discussion of the materials in the preparation of the paper.

LITERATURE CITED

1. V. E. Boitsov and K. Stukhlikova, Izv. Vyssh. Uchebn. Zaved., Geol. Razved., No. 8, 33 (1969).
2. V. E. Boitsov and Yu. M. Dymkov, in: Uranium Deposits: Zonality and Paragenesis [in Russian], Atomizdat, Moscow (1970), p. 119.
3. A. V. Zavarzin et al., in: Uranium Deposits: Zonality and Paragenesis [in Russian], Atomizdat, Moscow (1970), p. 93.
4. Ya. Legierskii, Cas. Mineral. Geol., 18, No. 1, 1 (1973).
5. Ya. Legierskii and M. Vanacek, Acta Univ. Carol. Geol., No. 2, 153 (1967).
6. J. Brown, in: Lead Isotopes in Ore Deposits [Russian translation], Atomizdat, Moscow (1969), p. 194.
7. J. Brown et al., in: Lead Isotopes in Ore Deposits [Russian translation], Atomizdat, Moscow (1969), p. 197.
8. R. Cannon et al., in: Geochemical Surveying [Russian translation], Mir, Moscow (1973), p. 228.
9. D. Ya. Surazhskii and A. I. Tugarinov, At. Energ., 9, No. 1, 21 (1960).
10. A. I. Tugarinov et al., At. Energ., 25, No. 6, 483 (1968).

INVESTIGATION OF URANIUM AND URANIUM-CONTAINING MINERALS BY THEIR LUMINESCENCE SPECTRA

B. S. Gorobets, S. S. Engoyan, and G. A. Sidorenko

UDC 535.372:549.755.35

The photoluminescence of uranium minerals has been previously studied in [1, 2]. Exact spectra of ≈20 uranium minerals were determined, including the most widely distributed minerals, which luminesce at 77 and 298°K; these were the classes of phosphates, arsenates, silicates, carbonates, sulfates, molybdates, vanadates, and hydroxides of uranium. The regular changes of the frequency values of completely symmetrical (c.s) and asymmetrical (a.s) uranyl oscillations were established as a function of the anion composition of the ligands, the presence in them of H_2O and OH, and also the appearance of a relation between the type of symmetry of the crystal field in which the uranyl exists and the ability of the latter to luminesce [1, 2]. The individuality of the low-temperature luminescence spectra of uranium minerals of different crystallochemical groups was conditioned by the diagnostic procedure of the many mineral types or their relations to a defined group, which considerably facilitated the study of the oxidation zones of uranium deposits. The advantages were shown of the luminescence method over other methods of phase analysis, involving its rapidity, the possibility of working with milligram quantities, and the retention of the substances being analyzed in the original form.

The purpose of this paper is to determine and interpret the luminescence spectra of the rare uranium minerals that have not been previously studied, so that the proposed procedure can be more versatile. The problem also includes the explanation of the chemical bond effect on the luminescence of uranium, in particular on the change of the light scale of the luminescence from bluish-green to red for minerals of different classes.

Investigated Samples and Their Luminescence

Samples were successfully found and the luminescence was investigated of 20 previously unstudied uran-

Translated from Atomnaya Énergiya, Vol. 42, No. 3, pp. 177-182, March, 1977. Original article submitted May 19, 1976.

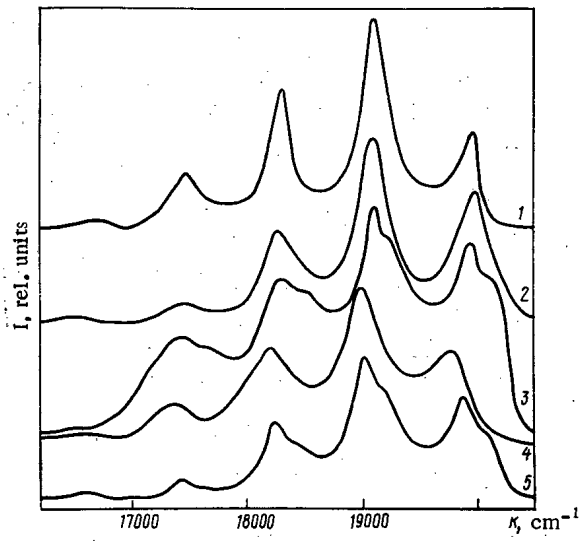

Fig. 1. Luminescence spectra of uranyl phosphates and arsenates at 298°K: 1) hydrogeneous autunite; 2) sabugalite; 3) novacekite; 4) uranospinite; 5) sodium uranospinite.

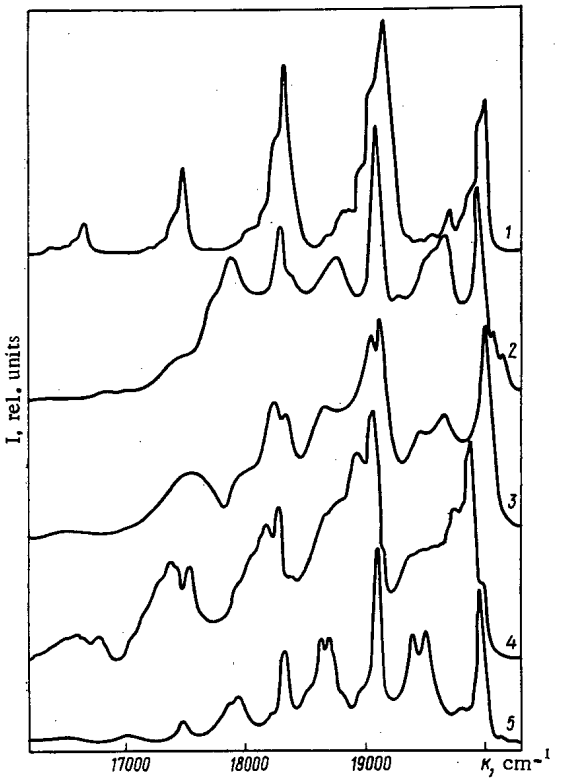

Fig. 2. Luminescence spectra of uranyl phosphates and arsenates at 77°K: 1) hydrogeneous autunite; 2) sabugalite; 3) novacekite; 4) uranospinite; 5) sodium uranospinite.

ium minerals and also four minerals containing uranium as an impurity.* All the mineral samples were examined beforehand by x-ray photography. The technique for determining the luminescence spectra is described in [1].

*The authors thank L. N. Belov, A. F. Buntikov, I. G. Zhil'tsov, V. I. Ludikova, K. V. Skvortsov, A. A. Chernikova, and co-workers of the Mineralogical Museum of the Academy of Sciences of the USSR for making the samples of rare minerals available for our study.

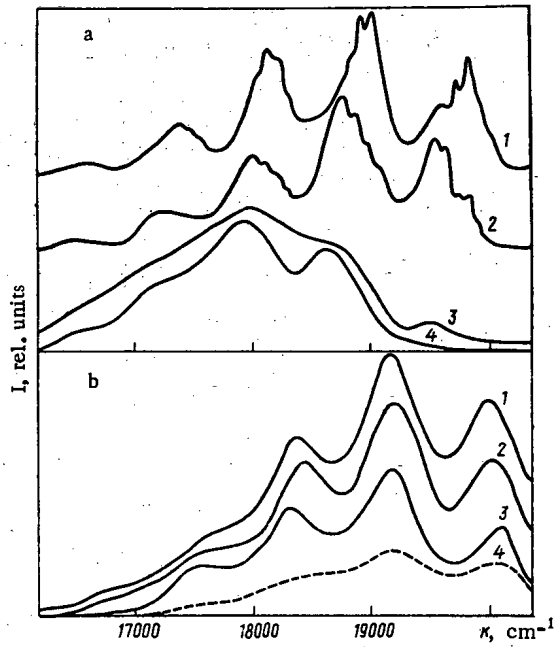

Fig. 3. Luminescence spectra at 77°K. a) Uranyl silicates: 1) Ca-ursilite; 2) (Mg, Na, Ca)-ursilite; 3) sklodowskite; 4) soddyite. b) Silica minerals: 1) chalcedony; 2) opal; 3) allophane; ----) luminescence at 298°K; $I_{298} : I_{77} = 1 : 10$ (the spectra of all the minerals are identical).

Phosphates and arsenates related to the crystallochemical group of uranium micas: hydrogenous autunite (3),* sabulgalite (1), uranospinite (1), sodium uranospinite (1), novacekite (2), and zeunerite (1), in principle, gave the same type of luminescence spectrum as the previously studied minerals of this group, e.g., autunite etc. (Figs. 1 and 2). In addition to the main series of equidistant lines I generated by the uranyl center I, in which four molecules of "ordered" water occur, disordered uranyl centers II frequently appear; the nature of the luminescence centers I and II in minerals with the autunite structure is considered in [1]. The very slight shifts of the homologous lines of series I with the various representatives of the mica group, obviously, do not always permit them to be reliably diagnosed, but in many times they may serve as additional diagnostic indicators. Only for novacekite at 298°K is a clear difference observed from the other uranium micas: the clear nonelementarity of the k_0 "lines." Series II, associated with disordered centers and appearing only at low temperatures, likewise cannot serve as a mineral diagnostic, as its position varies both with the course of time and also from region to region within the limits of the sample being studied ($k_0^{II} \approx 19.500 \pm 200$ cm^{-1}). The weak luminescence of zeunerite at 77°K is similar to that previously observed for not quite pure torbernite (phosphoric analog of zeunerite), contaminated with an autunite impurity [1]. Just like pure torbernite, pure zeunerite should not luminesce, which is also mentioned in [2]. The weak luminescence, however, is due to the intergrowth of zeunerite with another mineral, evidently uranospinite.

Arsenuranylite (found by L. N. Belov) was investigated. There is practically no difference between its luminescence spectrum and the spectra of the phosphouranylite–renardite group of minerals, which are isostructural with arsenuranylite [1, 2].

Of the uranyl silicates (in addition to those previously studied in [1]), the following were studied: soddyite, natural (1) and synthetic (more than 20), Ca-ursilite (2), (Mg, Na, Ca)-ursilite (2), sklodowskite (1), kazolite (3), chevkinlite (2), and wichtisite (1). The last three minerals do not luminesce even at low temperatures, which had been noted already in [2]. Uranyl silicates give similar (although not identical) luminescence spectra within the bounds of their crystallochemical groups: 1) sklodowskite (Fig. 3a), boltwoodite, uranophane, β-uranotil [1] ($UO_2 : SiO_4 = 1$); 2) ursilite ($UO_2 : SiO_4 < 1$); and soddyite ($UO_2 : SiO_4 > 1$).†

*The number of samples of the specified mineral is given in the brackets.

†Previously studied samples of natural soddyite were found to be contaminated and their luminescence spectrum cannot serve as a standard [1]. Seddyite, found by V. I. Ludikov, is taken as the standard, the luminescence spectrum of which coincides with the spectrum of the synthetic mineral.

TABLE 1. Spectroscopic Luminescence Characteristics at 77°K

Minerals	Uranyl electron-vibrational frequencies, cm^{-1}					
	k_0	k_1	k_2	k_3	k_4, k_5, k_6	Δk_s; $[\Delta k_a]$
Phosphates:						
hydrogenous autunite $H_2(UO_2PO_4)_2 \cdot 8H_2O$	I. 20020	19160 19070	18340 18250	17500 17420	16670, 15860, 15070	830±5 930±5
sabugalite $HAl(UO_2PO_4)_4 \cdot 16H_2O$	I. 19940 II. (19950)	19120 (18800)	18320 (18000)	17480 ?	16660	820±5 (780)
Arsenates:						
nocacekite $Mg(UO_2AsO_4)_2 \cdot 8H_2O$	I. 19960	19140 [19050]	18320 [18250]	17420 [17330]		820±5 [900±15]
	II. 19640	18940	?	?		(700)
uranospinite $Ca(UO_2AsO_4)_2 \cdot (6-8) \cdot H_2O$	I. 19890 II. 19450	19080 18780	18260 ?	17460 ?		815±10 (700)
sodium uranospinite $Na_2(UO_2AsO_4)_2(6-8) \cdot H_2O$	I. 19960	19120 [19030]	18320 [18230]	17480 [17490]	16670 ?	820±5 [905±5]
	II. (19520)	(18710)	(17930)	(17120)	(16360)	(780±20)
Carbonates:						
andersonite $Na_2Ca[(UO_2)(CO_3)_3] \cdot 6H_2O$	20790	19970	19140	18330	17490 [17420], 16690 [16600], 15870	825±5
rutherfordite UO_2CO_3	(19840)	19910 (18900)	19050 (18000)	18260 (17200)	[15790] (16350)	[900±5] (800)
Silicates						
soddyite $(UO_2)_2(SiO_4) \cdot nH_2O$	18730	18020	17300	16600	15890	710±10
ursilites $Ca[(UO_2)_2(Si_2O_5)_3] \cdot 5H_2O$	19900	19100 [19020]	18310 [18200]	17520 ?	(16700) ?	770±20 [890]
$(Mg, Ca, Na)[(UO_2)_2(Si_2O_5)_3] \cdot 5H_2O$	19570	18810	18050	17300	(16580)	760±20
sklodowskite $Mg[UO_2(SiO_3)OH]_2 \cdot 5H_2O$	18780	18000	17260	(16600)		720±30
Hydroxides and uranates						
fourmarierite $Pb[(UO_2)_4O_2(OH)_6] \cdot 4H_2O$	18800	18050	17300	(16530)		750±20
becquerelite $Ca[(UO_2)_6O_4(OH)_6] \cdot 8H_2O$	18700	17950	17300	(16500)		730±20
schoepite I $UO_2(OH)_2 \cdot H_2O$	18650	17920	17300	(16500)		750±30
schoepite II $H_2(UO_2)O_2 \cdot H_2O$ (?)	17550	16830	16100	(15400)		700—720
Uranium-containing minerals						
chalcedony SiO_2 opal $SiO_2 \cdot nH_2O$ allophane in $mAl_2O_3 \cdot nSiO_2 \cdot pH_2O$	20000—20180	19200—19340	18380—18550	(17750)	(16900)	825±5
calcites:						
single sample: phase I + phase II (weakly)	19570 19880	18810 19150	18050 18330	17300 17580		760±20 780±10
three samples: phase II	18890	19160 [19050]	18380 [18230]	17630]17530]	16820 [16710]	780±10 [900]

Notes: 1. Accuracy of determination of the narrow lines ~ 20-10 cm^{-1}. 2. In the curved brackets — frequencies of the diffuse or "floating" bands, for which their center of gravity is shown approximately. 3. In the square bracket — frequencies of the asymmetrical vibrations. 4. For brevity, the prefix "meta" is emitted in the names of the uranium micas.

The uranyl carbonates were represented by andersonite (1) and anhydrous **rutherfordine** (1). According to the luminescence spectrum at 298°K, andersonite is no different from uranothallite, bayleyite, and schroeckingerite [1]. However, these minerals are clearly different in the specific fine structure in the luminescence spectra at 77°K (Fig. 4 and Fig. 3a and b of [1]). Rutherfordine does not luminesce at 298°K and even at a low temperature the narrow lines of the fine structure are not observed in its spectrum, which confirms the greater symmetry of the crystal field, in which the luminescence centers (uranyl) are located, in comparison with other carbonates.

Hydroxides and uranates were represented by becquerelite (2), fourmarierite (4), schoepite (5), curite (1) and elarkeite (1). The last two minerals do not luminesce even at 77°K, and the reasons for this still are not explained precisely: becquerelite, fourmarierite, and two samples of yellowish-colored schoepite (schoepite I) gave identical luminescence at 77°K (Fig. 5), which confirms the previously established fact of indistinguishability of the minerals within the bounds of the class of hydroxides as a result of the absence of a marked

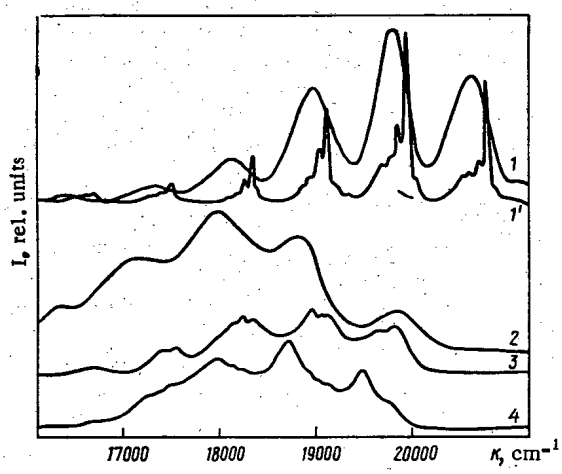

Fig. 4. Luminescence spectra of uranyl carbonates and uranium-containing calcites at 77°K; 1, 1') andersonite at 77 and 298°K; 2) rutherfordine; 3, 4) calcites from different parts of the deposit.

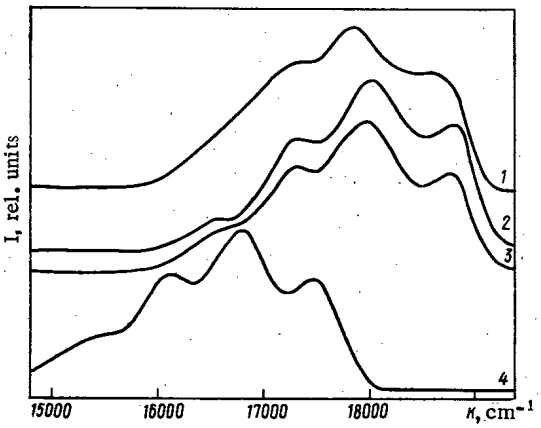

Fig. 5. Luminescence spectra of uranyl hydroxides and uranates at 77°K: 1) becquerelite; 2) fourmarierite; 3) schoepite I; 4) schoepite II.

connection between the uranyl center of luminescence with the supplementary cations Ca^{2+} and Pb^{2+} [1]. Three samples of schoepite, which had an orange color, at 77°K gave a bright red-orange luminescence with a pronounced shift to the low-frequency region of the spectrum (see Fig. 5). This unusual color luminescence of the uranyl minerals had not been observed previously. Its causes will be considered below.

Uranium-containing minerals also were studied: calcite (4), chalcedony (about 50), opal (about 40) and allophane (5). An investigation of the luminescence spectra permitted the form of entry of uranium into the mineral base to be established, which until recently was not precisely known. Uranyl does not occur isomorphically in calcites, but it is stored in the form of a finely dispersed impurity of the natural uranium minerals. At least two such phases are exhibited, most likely belonging to Ca-ursilite and (Mg, Na, Ca)-ursilite [see Fig. 4 (3, 4) and Fig. 3 (1, 2)]. We note that according to [2], the low-temperature luminescence of the uranyl in calcites is characteristic only for calcites with a low-temperature mineral formation.

For the oxides of the cryptocrystalline and amorphous group of minerals of silica, and also for aluminosilicate (allophane), it was previously shown that aquacomplexes $(UO_2nH_2O)^{2+}$ adsorbed on the surface are the predominant form of entry into them of uranium, where n = 4-6 [3, 4]. In this present paper, this conclusion is confirmed by the investigation of about 100 samples of natural and synthetic silica that have adsorbed uranium from solution with a different anion composition. It was also established that the form of entry of the uranium is identical for all the mineral types and varieties of this group: chalcedony, agate, cacholong, chrysoprase, silica, opal, hyalite, and allophane of different color, taken from many deposits.

TABLE 2. Dependence of Spectral Characteristics on the Chemical Bond in the Uranyl Minerals

Class of minerals	k_0, cm^{-1}	Δk_s, cm^{-1}	10^{-10} K, force constant, N/cm	Multiplicity of bond, n	Luminescence color
Nitrates [10]	20400—20800	840—880	7,6—7,8	2,35—2,40	Blue-green
Carbonates	19900—20700	820—840	7,0—7,6	2,20—2,35	Azure-green
Adsorbed uranyl aquacomplexes in SiO_2	19800—20100	820—830	7,0—7,3	2,20—2,25	Green
Phosphates and arsenates of the mica group	19400—20000	810—830	6,8—7,4	2,15—2,25	Yellowish-green
Phosphates and arsenates of the phosphouranylite group	18750—18850	730	5,5	1,85	Yellow
Silicates	18700—19700	710—770	5,2—6,2	1,80—2,0	»
Hydroxides	18400—18800	700—750	5,1—5,8	1,75—1,90	Yellow-orange
Uranates (schoepite II)	17500	≈ 680	4,8	1,65	Red-orange

Effect of the Chemical Bond in Uranyl Minerals on the Luminescence Spectra

It is well known that with increase of basicity of molecules in the uranyl solvation or coordination sphere, a shift occurs in the luminescence bands to the side of low frequencies [5]. This is due to an increase of the chemical bond of the uranium atom with the ligands and a corresponding weakening (stretching) of the uranyl bond $U-O_I$. As a result of this, contraction of the energy pattern of the uranyl electron-vibrational levels occurs. The contraction of the uranyl vibrational sublevels in the excited state has been known for a long time, in which the $U-O_I$ bond is longer than in the ground state; hence, the frequency of the completely symmetrical vibrations of excited uranyl is less than for nonexcited uranyl; $\Delta k_s^* < \Delta k_s$ (see [6]). During stretching of the uranyl, the electron levels of its ground and excited states, k_0 and k_0^*, must converge in proportion with the weakening of the uranyl bond in minerals of different classes. In this case, the frequency of the purely electron transition $k_0^* \rightarrow k_0$ is decreased, in consequence of which the color of the luminescence is shifted from the greenish-blue to the red region of the spectrum. At the same time, the frequency of the uranyl completely symmetrical vibrations is decreased from 800 to ~700 cm^{-1} as a result of contraction of the ground state energy sublevels $k_0 - n\Delta k_s$ (Tables 1 and 2).

Knowing the length R of the $U-O_I$ bond and its force constant K, it is possible by Gordy's formula to estimate the multiplicity of the chemical bond n in uranyl:

$$K = 1.67n\,[(x_U x_O)/R^2]^{3/4} + 0.3, \quad (1)$$

where $x_U = 1.9$ and $x_0 = 3.5$ are the electronegativities of the U^{6+} and O^{2-} ions. K can be calculated from the luminescence spectra by the formula

$$K = 0.285 \cdot 10^{-6} m_O \{(\Delta k_s)^2 + [m_U/(m_O + m_U)](\Delta k_a)^2\}, \quad (2)$$

where Δk_s and Δk_a are the frequencies of the completely symmetrical and the asymmetrical vibrations†; m_0 and m_U are the atomic masses of oxygen and uranium [6].

If the length of the bond is unknown from structural data, it can be estimated by Badger's formula [8]:

$$R = 1.08K^{-1/3} + 1.17, \quad (3)$$

or by the formula proposed by Vdovenko et al. [9]‡

$$R = 3.82 - \ln(K + 0.73). \quad (4)$$

†Δk_a is determined either directly from the luminescence spectrum (see Table 1), or by the formula $\Delta k_a = k_s\sqrt{1 + 2m_0/m_V}$ in cases when the asymmetrical vibrations do not appear in the spectrum in a clear form [6].

‡The results obtained by Eqs. (3) and (4) are very close. The differences between them are important only for chemically pure uranyl compounds, which give narrow stable lines. For minerals, the spread overlapping the accuracy of the calculation is unavoidable and amounts to ±5%.

Calculations by Eqs. (1)-(3), using luminescence data, show how the multiplicity of the bond in uranyl is reduced with increase of basicity of the ligand from 2.4 in nitrates (synthetic) to 1.8 in hydroxides (see Table 2).

Now we shall attempt to interpret the differences in the luminescence spectra of different samples of schoepite. Taking account of the shift of k_0 by almost 1000 cm^{-1} during transition from schoepite I to schoepite II, and the reduction of the band multiplicity from 1.80 to 1.65, respectively, it can be supposed that two structurally different forms of this mineral exist, despite the similarity of their radiographs. It is possible that schoepite II is a transition form from hydroxides to uranates: $(UO_2)(OH)_2 \cdot nH_2O \rightleftharpoons H_2(UO_2)O_2 \cdot nH_2O$. Actually, the large electronegativity of the O^{2-} ligand in comparison with OH, the participation in the chemical bond of H^+ and H_2O and, consequently, the possibility of the formation of hydrogen bonds between the uranyl and ligand oxygens leads to a larger stretching of the uranyl bond in schoepite II and to a reduction of its force constant in comparison with these same parameters in the hydroxides. It may be supposed that H^+ exists either in the form of oxonium H_3O^+ in the cation sphere or as a proton between the uranyl and ligand oxygens, forming hydrogen bonds.

The principal result of our work is the determination of the standard luminescence spectra of the majority of uranyl minerals in a number of uranium-containing minerals. This has permitted us to suggest a new high-speed method for their diagnosis, and also to explain the crystallochemical characteristics of uranyl minerals and to establish the form of entry of the uranium in "nonuranium" minerals. Taking account of the chemical bond, an explanation has been obtained for the luminescence color shift from bluish-green to the orange-red part of the spectrum, as a result of change of the anion composition of the uranyl minerals from carbonates to hydroxides and uranates.

LITERATURE CITED

1. B. S. Gorobets and G. A. Sidorenko, At. Energ., 36, No. 1, 6 (1974).
2. A. N. Tarashchan et al., in: The Construction and Properties of Minerals [in Russian], No. 8, Naukova Dumka, Kiev (1974), p. 107.
3. B. S. Gorobets and A. M. Portnov, Zap. Vses. Mineral. Ova, No. 3, 357 (1973).
4. B. S. Gorobets et al., in: Radioactive Elements in Geological Processes [in Russian], Institute of Geochemistry and Analytical Chemistry (GEOKhI), Akad. Nauk SSSR, Moscow (1975), p. 168.
5. G. I. Kobyshev and D. N. Suglobov, Dokl. Akad. Nauk SSSR, 120, No. 4, 330 (1958).
6. E. Rabinovich and R. Belford, Spectroscopy and Photochemistry of the Uranyl Compounds [in Russian], Atomizdat, Moscow (1968).
7. W. Gordy, J. Chem. Phys., 14, 305 (1946).
8. R. Badger, J. Chem. Phys., 3, 710 (1935).
9. V. M. Vdovenko et al., Dokl. Akad. Nauk SSSR, 167, No. 6, 1299 (1966).
10. A. N. Sevchenko and E. I. Stepanov, Zh. Eksp. Tekh. Fiz., 21, No. 2, 221 (1951).

FACILITY FOR INTRAREACTOR INVESTIGATIONS OF AN AGGREGATE OF PHYSICOMECHANICAL PROPERTIES OF MATERIALS BY A PULSED ULTRASONIC SPECTROSCOPIC METHOD

B. F. Anufriev, A. A. Balandin,
V. M. Baranov, and Yu. V. Miloserdin

UDC 620.17+534-8

The study of the changes of properties of reactor materials directly affected by intense radiation fluxes in the active zone of a nuclear reactor is an important characteristic and is of scientific interest. Ultrasonic spectroscopy methods are the most promising for measurements under irradiation, which can be used for intrareactor tests [1-3].

A method is proposed in [4, 5] for simultaneously measuring the elasticity constant (Young's modulus E and Poisson's coefficient μ), the internal friction Q^{-1} and the dynamic hardness (H_D according to Shore and the dynamic yield point P according to Tabor) on a single sample of the material being studied. It is based on the recording and subsequent analysis of the ultrasonic vibrations of the sample excited in it by a mechanical shock. The structural simplicity of the measurement unit and the feasibility of using samples of small dimensions and of simple shape allow tests to be carried out on materials under complicated conditions, which are characteristic in the operation of nuclear reactors (high temperature and intense radiation flux). In particular, the properties of materials at high temperature have been investigated by this method [6, 7]. A facility will be described later which is designed for the investigation of the changes of properties of structural and fissionable materials under the action of radiation, at a temperature created as a result of the self-heating of samples in the reactor core.

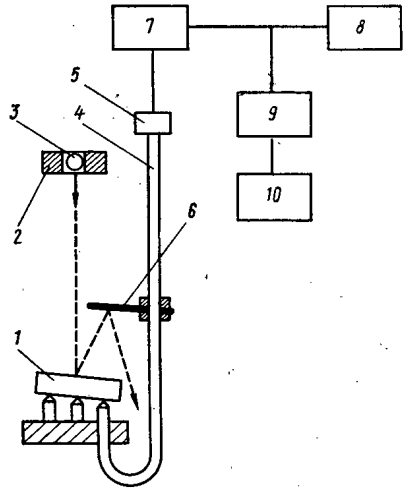

Fig. 1. Structural layout of the measurements: 1) sample being studied; 2) electromagnet; 3) small ball; 4) sound-guide; 5) piezoreceiver; 6) reflector; 7) amplifier; 8) high-frequency magnetic recorder; 9) pulse shaper; 10) electronic recorder.

Translated from Atomnaya Énergiya, Vol. 42, No. 3, pp. 183-186, March, 1977. Original article submitted August 7, 1975; revision submitted July 13, 1976.

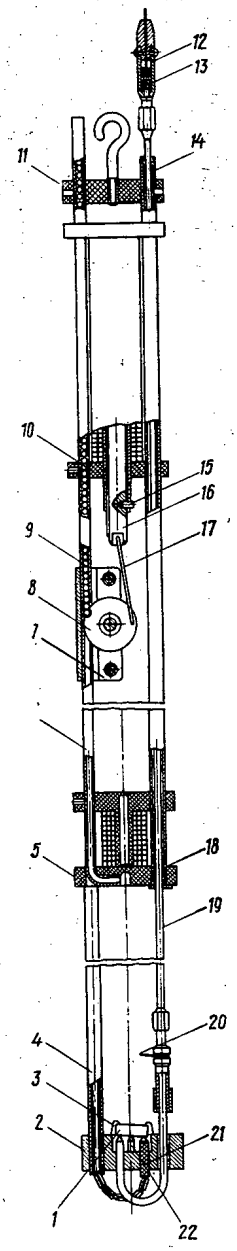

Fig. 2. Overall view of the measurement capsule of the facility: 1) sample being investigated: 2, 11) flanges; 3) clamps; 4) carrier tube; 5, 10) electromagnets; 6) tube-magazine; 7) branching; 8) plunger; 9) ball; 12) piezoholder; 13) piezotransducer; 14, 18) insulating bushes; 15) retainer; 16) shaft; 17) rigid drawbar; 19) sound-guide; 20) reflector; 21) thermocouple insert; 22) adjusting screw.

The principle of the measurement is illustrated by means of Fig. 1. The sample being studied, in the form of a disk with diameter 14-16 mm and thickness 5-8 mm is placed on three needle bearings, so that its flat surface makes a small angle (5-8°) with the horizontal plane. An electromagnet, which holds a small ball above the upper surface of the sample, is positioned over the sample. One of the bearings serves as a sound-guide for transmitting the ultrasonic vibrations of the sample to a piezoreceiver, outside of the active zone of the reactor. A reflector is secured to the sound-guide, in the form of a plate which is parallel to the plane of the sample. The ball, when dropped, impacts on the sample, causing it to vibrate at natural frequencies and thus, on rebounding at an angle to it, strikes the reflector and falls past the sample.

TABLE 1. Results of Measurements of Young's Modulus, Poisson's Coefficient, Internal Friction, Heights of Drop of the Ball (Shore hardness) and the Dynamic Yield Point of the Samples Investigated

Material	Young's modulus, 10^7 N/m^2	Poisson's coeff.	Internal friction	Drop height, cm	Dynamic yield point, 10^7 N/m^2
Duralumin D16T	7760±80 7750 7200	0,340±0,006 0,34 0,334	$(1,6\pm0,1)\cdot10^{-3}$ $1,65\cdot10^{-3}$ —	12,6±0,3 12,3 —	96±3 94 70—130
Steel Kh18N9T	20700±200 20400 20000	0,280±0,005 0,275 0,28	$(1,15\pm0,08)\cdot10^{-3}$ $0,98\cdot10^{-3}$ $\sim10^{-3}$	11,6±0,3 11,2 —	138±5 133 130—180
Copper MZ	11600±100 11500	0,335±0,006 0,35	$(1,5\pm0,1)\cdot10^{-3}$ $\sim10^{-3}$	6,0±0,2 —	42,0±1,5 40—50

Note. For all materials the values given are in the first line obtained by the method developed, in the second line the control data, and in the third line (but for copper in the second line) the handbook data.

The signals from the piezoreceiver, after amplification, are recorded by the magnetic recorder and fed to the pulse shaper, which converts the high-frequency signals into square-wave pulses, and then these are fed to a device for measuring the time between the pulses.

By analyzing the vibrations recorded, the natural frequency of the sample and the decrement of the vibrations can be determined, from which the corresponding elasticity characteristics (Young's modulus and Poisson's coefficient) and the internal friction of the material can be calculated. The natural frequency of the sample is determined by the increase of amplitude of the recorded signal, repeatedly reproduced on the screen of an oscillograph with a filter-analyzer tuned to the corresponding frequencies. The values of two natural frequencies of the sample are used to calculate the Young's modulus and Poisson's coefficient [8]. When the filter-analyzer is tuned to one of the natural frequencies of the sample, the damping decrement is determined and the internal friction is calculated.

By measuring the time interval between pulses, corresponding to the impacts of the ball on the sample and the reflector, the dynamic hardness of the material (Shore hardness) [9] and the dynamic yield point (Tabor) [10] can be calculated:

$$P=\left[0.0505\,\frac{h_2^{\frac{1}{2}}}{\left(h_1-\frac{3}{8}h_2\right)^3}\,\frac{mg}{d^3}\left(\frac{1-\mu_1^2}{E_1}+\frac{1-\mu_2^2}{E_2}\right)^{-4}\right]^{1/5},$$

where $h_2=(h_n\cos\alpha-d+gt^2/2)^2/2gt^2$ is the calculated possible height of recoil of the ball; h_n is the distance along the normal from the upper surface of the sample to the lower surface of the reflector; α is the angle between the horizontal plane and the plane of the sample; t is the time interval between impacts of the ball on the sample and the reflector; h_1 in the height of drop of the ball; m is the mass of the ball; d is the diameter of the ball; g is the acceleration of gravity; μ_1, μ_2, E_1, and E_2 are the Poisson coefficients and Young's moduli of the materials of the ball and of the sample, respectively.

The design of the intrareactor facility for the measurements by the method described has been developed for use in the vertical experimental channel of the IRT-2000 reactor, which has a diameter of 52 mm and a guaranteed neutron flux density of $\sim2\cdot10^{13}$ neutrons/(cm$^2\cdot$sec). The facility consists of the measurement system, suspended on a cable in the experimental channel of the reactor, and a system for pumping-out and filling the channel with helium. The electrical leads and the high-frequency cables are brought out through the groove of the shield plug and then through the flange of the channel to the upper platform of the reactor.

The design of the measurement system is shown in Fig. 2. The carrier unit of the structure consists of three tubes with a length of 1.5 m of Duralumin secured by upper and lower flanges. On them are assembled the unit for mounting the sample, combined with the sensor of the recording system and the unit for supplying and dropping the balls. The sample being investigated is positioned on a flange by three bearings and is tightened with clamps. One bearing is the sound-guide and another is an adjusting screw, by means of which the required inclination of the sample can be set; the third one serves as the junction of a Chromel–Alumel thermocouple, the insulating sleeve of which is rigidly fixed into the flange. The reflector is fixed on the molybdenum sound-guide with a diameter of 3 mm. The rod sound-guide, with a length of 1.5 m, is insulated from the

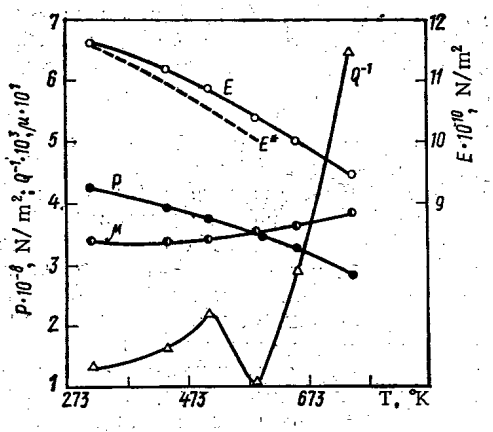

Fig. 3. Temperature dependence of Young's modulus, Poisson's coefficient, internal friction, and dynamic yield point of copper, grade MZ (E* are the handbook data).

walls of the carrier tube by fluoroplast bushes. The piezotransducer, TsTS-19 ceramic with a diameter of 8 mm and height 15 mm, is located in a holder outside the active zone of the reactor.

The unit for supplying and releasing the balls of magnetic material is located in the upper part of the measurement system. The magazine, in which 100 balls are placed, is a curved tube with an internal diameter of 3.5 mm, fixed into the flanges of the upper and lower electromagnets.

When there is no current in the winding of the electromagnet, the lower ball in the magazine is in the groove of the disk plunger with a diameter of 24 mm and thickness 3 mm, fixed on the axis in the branching. When a voltage is applied, the shaft with a step rotates the plunger through the drawbar and releases the ball which, under the action of its own weight, rolls down through the tube into a recess where it is held by the switched-on electromagnet. The ball is dropped when the power supply of the lower electromagnet is cut off.

The pumping-out and filling of the system with helium consists of a mechanical and a diffusion pump, a helium flask, vacuum valves and conduits with a length of 10 m and an internal diameter of 20 mm. After several successive pump-outs and purgings, it provides a residual air pressure of $\sim 10^{-4}$-10^{-5} mm Hg.

The principal technical data of the facility are defined by the following parameters. Operating range of temperature up to 900°K. The indentors are tempered balls of ShKh-15 steel with a diameter of 3 mm. The drop height is 300 mm. The measurement error of the natural frequencies of the sample, with a confidence coefficient of 0.95, is 0.05-0.07%, which has been established by repeated measurements of samples of different materials and by comparison of the results obtained with the data from parallel measurements by a resonance-pulse method [11]. The error in determining the relative changes of Young's modulus and Poisson's coefficient is 0.1-0.15%. The error in calculating the absolute values of E from the natural frequencies of the sample (taking account of the error in measuring the sample dimensions, determining the density, etc.) does not exceed 1%, for Poisson's coefficient it is 2%, and for the internal friction it is 7-8% [6, 7]. The error in measuring the time intervals between impacts of the ball at the sample and at the reflector is not higher than 1.5% (with a confidence coefficient of 0.95), and consequently the error in determining the Shore hardness is ~3% and for the dynamic yield point it is ~3.5%. The temperature of the sample during self-heating was determined with an error of 5-7°K. The facility can be used also for the prereactor investigation of materials over a wide range of temperatures, for which a special cryostat and a high-temperature furnace have been developed [3]. Table 1 shows the results of measurements on samples of Duralumin D16T, stainless steel Kh18N9T, and copper MZ at room temperature under laboratory conditions. For comparison, the results also are given of control measurements of these properties (the constants of elasticity and internal friction were measured by the resonance-pulse method [11], the dynamic hardness by a photoelectric method [9]), and the handbook values [12].

Figure 3 shows the temperature dependence of Young's modulus, Poisson's coefficient, internal friction, and the dynamic yield point of samples of copper MZ. The small peak of the internal friction at 510°K is due to viscous slippage along the grain boundaries [13]. The data obtained coincide well with [12], 13]. Measurements on samples of fissionable materials under laboratory conditions at 100-800°K and under irradiation in the active zone of the IRT-2000 reactor over the temperature range 350-800°K confirm the prospects of the procedure described.

LITERATURE CITED

1. Yu. V. Miloserdin, V. M. Baranov, and K. I. Molodtsov, At. Energ., 32, No. 4, 330 (1972).
2. V. M. Baranov, A. V. Rimashevskii, and V. N. Kakurin, Methods and Means of Investigating Materials and Structures Operating under the Effect of Radiation [in Russian], No. 1, Atomizdat, Moscow (1973), p. 62.
3. Yu. V. Miloserdin et al., At. Energ., 35, No. 2, 101 (1973).
4. V. M. Baranov, Yu. V. Miloserdin, and V. M. Shchavelin, Byull. Izobret., No. 34 (1970).
5. B. F. Anufriev, V. M. Baranov, and Yu. V. Miloserdin, Nauchn. Tr. Vyssh. Uchebn. Zaved. Lit. SSR, Ul'trazvuk, No. 3, 31 (1971).
6. Yu. V. Miloserdin, B. F. Anufriev, and V. M. Baranov, Zavod. Lab., 37, No. 7, 977 (1971).
7. B. F. Anufriev and V. M. Baranov, Problems of Procedure and Technique of Ultrasonic Spectroscopy [in Russian], Kiev Polytechnic Institute, Kaunas (1973), p. 101.
8. V. M. Baranov, Zavod. Lab., 38, No. 9, 1120 (1972).
9. A. A. Kul'bakh, V. M. Shavelin, and N. A. Evstyukhin, Metalloceramic and Refractory Materials [in Russian], Moscow Engineering Physics Institute, Moscow (1967), p. 29.
10. D. Tabor, Hardness of Metals, Clarendon Press, Oxford, England (1951), p. 112.
11. V. M. Baranov and Yu. V. Miloserdin, Methods of Investigating Refractory Materials [in Russian], Atomizdat, Moscow (1970), p. 61.
12. I. V. Kudryatseva (editor), Materials in Machine Construction. Handbook [in Russian], Vols. 1 and 3, Mashinostroenie, Moscow (1967).
13. M. A. Krishtal, Yu. V. Piguzov, and S. A. Golovin, Internal Friction in Metals and Alloys [in Russian], Metallurgiya, Moscow (1964).

STATISTICAL ANALYSIS OF THE JOINT EFFECT OF NICKEL, COPPER, AND PHOSPHORUS ON THE IRRADIATION EMBRITTLEMENT OF PEARLITIC STEELS

A. A. Astaf'ev, S. I. Markov, and G. S. Kark

UDC 621.039.531:669.15

A considerable amount of experimental data has been published on the radiation stability of steel used in fabricating elements for atomic power plants. However, the laws obtained are not, as a rule, of a general nature and describe only special cases of the effect one parameter or another has on the radiation stability of a material.

Attempts have recently been made to take account of the combined effect of several parameters on radiation stability. It has been discovered [1] that at an elevated irradiation temperature the presence of nickel and copper in ferritic–pearlitic steel 48TS leads to irradiation embrittlement. At a quite low impurity concentration no undesirable influence by nickel and copper was detected. It is pointed out [2] that impurities such as phosphorus have a much more pronounced effect on irradiation embrittlement at an elevated than at a low (50-80°C) irradiation temperature; at an elevated temperature nickel reduces the radiation stability of steel, evidently by amplifying the embrittling effect of phosphorus.

Information about the deleterious influence of copper and phosphorus on the radiation stability of steel is contained in a number of other papers as well, but unfortunately, there are no quantitative estimates of the joint effect of these elements and the relation between their effects and the nickel concentration.

A multifactor experiment allows such an estimate to be made. In the present paper an attempt is made to simulate such an experiment by statistical analysis of a large number of published data about the effect of the chemical composition of pearlitic steels on their radiation stability.

Translated from Atomnaya Énergiya, Vol. 42, No. 3, pp. 187-190, March, 1977. Original article submitted March 19, 1976.

The initial information was collected from ≈200 sources, primarily American, British, and Canadian publications devoted to problems of reactor materials as well as from the materials of international conferences and symposia.* The overall volume of the material collected comprised more than 1000 experiments, in each of which 10-15 factors and 5-15 output parameters were recorded.

To accomplish the task set, viz., to evaluate the combined effect of copper, phosphorus, and nickel on the irradiation embrittlement of steel, we selected those experiments (230 in all) that gave the chemical composition of the steel (including the copper and phosphorus concentration), the irradiation conditions (fluence and temperature), and the characteristic of irradiation embrittlement, i.e., an increased temperature of the brittle–ductile transition of steel (ΔT_K) as a result of irradiation. The heat-treatment parameters of the steel were not introduced into the analysis as factors, but the sampling corresponded to roughly one level of these parameters. Such factors as the reactor type, the neutron spectrum, and the size of the blanks for the samples were not taken into account; this, of course, resulted in a random spread of the experimental data with respect to the mathematical model constructed.

Tabulated below are the maximum, minimum, and mean contents (in %) of alloying elements and impurities in the chemical composition of the steels analyzed:

C	0.26; 0.02; 0.18	P	0.045; 0.004; 0.013
Si	0.41; 0.11; 0.24	S	0.05; 0.004; 0.019
Mn	1.63; 0.40; 1.18	Cu	0.35; 0.005; 0.19
Cr	1.83; 0.02; 0.85	V	0.09; 0.005; 0.04
Ni	3.28; 0.01; 0.78	Al	0.06; 0.02; 0.035
Mo	0.6; 0.003; 0.30		

The fast-neutron fluence with E > 1 MeV is $5 \cdot 10^{18}$–10^{20} neutrons/cm^2 and an irradiation temperature of 250-350°C. For a lower irradiation temperature such analysis should evidently be carried out separately since, according to the data of [2] and a number of other papers, embrittlement in this case is governed by other laws.

The mathematical apparatus of statistics was used to determine the character of the influence of one factor or another on ΔT_K, to construct empirical equations (regression equations) describing the dependence of ΔT_K on the factors, as well as to verify the significance of the coefficients in the equations and the adequacy of the statistical models. The statistical parameters were calculated on an M-220 computer.†

Possible mathematical models were constructed in the form of the regression relation

$$\Delta T_K = a_0 + \sum_{i=1}^{n} a_i x_i + \sum_{i=1}^{n} a_{ii} x_i^2 + \sum_{i,\, j=1}^{n} a_{ij} x_i x_j, \qquad (1)$$

where x_i are the influence factors; a_i and a_{ij} are regression coefficients; i, j = 1, 2, ..., n; i ≠ j; and n is the number of factors.

The criterion chosen for comparison of the various models was that of the residual variance of the experimental values of ΔT_K with respect to the regression equation. It turned out that the optimal mode, i.e., the one having the minimum residual variance with terms of no greater than second order, was a statistical model of the form

$$\Delta T_K = 110 - 1224\,[C]^2 - 76\,[Ni] + 129\,[Cu] + 4543\,]Ni]\,[P] + 164\,[Ni]\,[Cu] - 10320\,[Cu]\,[P] + 15.8F - 0.17T_{irr}, \qquad (2)$$

where the chemical symbol in brackets denotes the concentration of the element; F is the fluence,‡ 10^{19} neutrons/cm^2; and T_{irr} is the irradiation temperature, °C.

The regression equation obtained is significant since it reduces the residual variance by a factor of 4.26, which exceeds the tabulated value of the Fisher test (Φ = 1.60) for the given number of experiments and determined coefficients at a significance level of 0.99.

Verification of the significance of the regression coefficients has shown that the coefficients in front of the [Mn], [Si], [Cr], [Mo], and [S] terms are either insignificant or at the significance limit; therefore, they

*This information was collected and systematized by V. A. Yukhanov, A. N. Tarasova, V. A. Nechaev, and G. F. Prokoshina.

†N. N. Panichkin took part in the calculations.

‡In the quite narrow range investigated, $0.5 \cdot 10^{19}$–10^{20} neutrons/cm^2, the effect of the fluence on ΔT_K is described by a linear relation with satisfactory accuracy. In constructing a model for a broader range of fluence values, it is desirable to use more complex relations such as $\Delta T_K \approx F^{1/n}$ or $\Delta T_K \approx \log F + C$, which have been given in the literature.

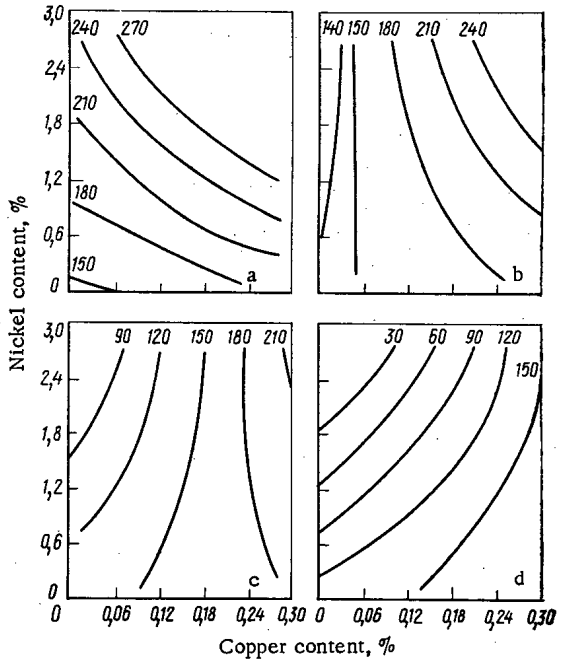

Fig. 1. Two-dimensional section of model diagram of irradiation embrittlement of reactor pressure-vessel steel (the numbers next to the curves denote the values of ΔT_K, °C).

have not been incorporated into Eq. (2). The conclusion that these elements exert a weak influence is, in the main, in agreement with the data of one of the most detailed investigations on the effect that alloying elements have on the radiation stability of iron–carbon alloys [3]. The authors of that paper show that in the case of irradiation at 300-350°C a change in the manganese, chromium, and molybdenum content does not affect the sensitivity of the material to radiation embrittlement. It was also shown [4] that at this irradiation temperature manganese at not does have any effect. Concerning the influence of molybdenum, V. I. Badanin and I. A Razov [3] note that an addition of ~0.2% molybdenum enhances the radiation stability of iron–carbon alloys but this stability remains unchanged as the molybdenum concentration rises further to 1%. In Eq. (2) the coefficient in front of [Mo] proved to be insignificant, probably because the overwhelming majority of reactor pressure-vessel steels analyzed contained molybdenum in quantities exceeding the threshold quantity.

In analyzing a statistical model, particular attention should be paid to the terms characterizing the effects of interactions, i. e., [Ni] [P], [Ni] [Cu], and [Cu] [P]. Initially, the various possible interactions between pairs in the model were verified: [Ni] [S], [Cr] [C], [Ni] [Cr], [Ni] [P], etc. However, only the products [Ni] [P], [Ni] [Cu], and [Cu] [P] significantly reduce the residual variance, i.e., affect ΔT_K. This means that the influence of nickel on the radiation stability of steel depends on the quantity of phosphorus and copper in steel, and even the character of this influence (increasing or decreasing ΔT_K) may differ at different concentrations of phosphorus and copper.

It is interesting that taking account of the effect of the interactions of nickel with phosphorus and copper not only reduces the residual variance but also significantly changes the coefficient in front of [Ni] which is +47.0 without allowance for the interactions and which, when these interactions are taken into account, changes sign and takes the value −76.0. This gives rise to a very important conclusion about the fact that in a number of experiments there has been a tendency for ΔT_K to increase with the nickel concentration, this being due not to the influence of nickel itself but to its interaction with copper and phosphorus and occurring only at some critical concentrations such that the positive sum of the contributions of the interactions of nickel with phosphorus and copper is greater than the negative contribution of [Ni] to ΔT_K.

Unfortunately, this result cannot yet be compared with published data since practically no information is available about the systematic study of the influence of nickel on the irradiation embrittlement of reactor-vessel steels with a high concentration of phosphorus and copper. Data are available about the influence of nickel on the behavior of steel with a low concentration of phosphorus, but with the copper concentration that is usual in the commercial metal. Thus, increasing the nickel concentration in steel 15Kh2MFA with a phosphorus concentration of less than 0.01% does not intensify irradiation embrittlement [1] and is, therefore, desirable as well

as allowable since it increases the margin of ductility of the steel and its hardenability. The review [5] notes that in order to explain the role of nickel in irradiation embrittlement it is necessary to investigate the influence at a low copper concentration.

Equation (2), obtained by statistical analysis, allows the influence of nickel to be predicted with the simultaneous reduction of the phosphorus and copper concentrations in steel (for example, 30% of the analyzed melts contained less than 0.01% phosphorus and 0.1% copper). It is seen that as [P] and [Cu] decrease, the embrittling effect of nickel decreases, to become neutral at some critical values of [P] and [Cu]. At an impurity concentration below the critical values, an increase in [Ni] decreases ΔT_K. Therefore, analysis of the model (2) permits the assumption that by reducing the copper and phosphorus concentrations in steel below the critical values it is possible to reveal the favorable influence of nickel itself on the radiation stability and, by increasing its content, to reduce ΔT_K.*

Depending on the requirements imposed on the steel, (such as maximum allowable ΔT_K, prescribed limits of strength properties, etc.), all the critical concentrations can be determined by the techniques of nonlinear programming and optimization.

For a graphic representation of the combined effect of nickel, copper, and phosphorus on the irradiation embrittlement of steel, a two-dimensional section has been built built of the seven-dimensional surface corresponding to the model (2) (diagrams of irradiation embrittlement) for fixed carbon concentrations, fluence, and irradiation temperature. The concentrations of elements were taken according to the data of chemical analysis of a commercial melt of reactor pressure-vessel steel; the fluence and irradiation temperature were taken to be $7 \cdot 10^{19}$ neutrons/cm^2 and 290°C. On each section of the irradiation embrittlement diagram were lines of identical values of ΔT_K in coordinates [Ni] – [Cu] for phosphorus concentrations of 0.024, 0.015, 0.009, and 0.003%. The calculations were carried out on an M-220 computer. The sections so constructed graphically illustrate the basis laws governing the combined effect of nickel, copper, and phosphorus on ΔT_K (Fig. 1). It is seen that at phosphorus concentrations of 0.024% and higher (a) in the steel, nickel increases the irradiation embrittlement over the entire range of concentrations studied. At a phosphorus concentration of 0.015% (b) nickel intensifies the embrittlement of the steel only at copper concentrations exceeding 0.06-0.07%. When the phosphorus concentration is reduced further (c), the range of copper concentrations at which nickel is observed to have a favorable effect is extended and, along with this, the magnitude of the shift of the temperature of the brittle-ductile transition, ΔT_K, is decreased. And, finally, at a phosphorus concentration of 0.003% (d), increasing the nickel content right up to 3% reduces ΔT_K practically over the entire range of copper concentrations allowable for the given steel (the lower the copper concentration, the more effective the reduction). An increase in the nickel concentration to 2.0-2.5% at [P] = 0.03% and [Cu] = 0.04-0.07% reduces ΔT_K to 30-40°C. Raising the copper concentration to 0.2-0.25% even with such a low phosphorus concentration increases ΔT_K to 120-150°C.

Thus, analysis has made it possible quantitatively to evaluate the influence of nickel, copper, and phosphorus on the irradiation stability of steel, confirmed the earlier known fact that the radiation stability of steel increased when it is purified of impurities, and showed that in this case a further margin of increase in radiation stability lies in a possible increase in the nickel content (> 1.5-2.5%), depending on the copper and phosphorus concentration.

LITERATURE CITED

1. V. A. Nikolaev and V. I. Badanin, At. Energ., 37, No. 6, 491 (1974).
2. V. A. Nikolaev and V. I. Badanin, Izv. Akad. Nauk SSR, Met., No. 2, 126 (1975).
3. V. I. Badanin and I. A. Razov, Vopr. Sudost., No. 19, 92 (1975).
4. M. Brumovski, Author's Abstract of Dissertation, Moscow Engineering Physics Institute, Moscow (1971).
5. L. Steele, Neutron Irradiation Embrittlement of Reactor Pressure Vessel Steels, Tech. Rep. Ser. 163, IAEA, Vienna (1975).

ANION-EXCHANGE REFINEMENT OF PLUTONIUM AND NEPTUNIUM SEPARATED DURING EXTRACTION REPROCESSING OF VVÉR FUEL ELEMENTS

V. I. Anisimov, A. G. Kozlov,
V. P. Lanin, A. K. Polunin,
L. N. Fedotova, and V. A. Shurmel'

UDC 541.183.5:546.799.4:546.799.3

When spent fuel elements from VVÉR reactors (water-moderated water-cooled) are reprocessed by extraction with a 30% solution of tri-n-butyl phosphate in synthine at the stage of reduction re-extraction of plutonium with uranium (IV), solutions containing the bulk of the plutonium and neptunium are formed [1, 2]. The plutonium and neptunium can be separated and their decontamination from uranium and fission products can be completed by extraction [2] and sorption [3-5] methods. Of greatest interest is sorption with hexanitrate complexes of actinides (IV) [6] on highly alkaline vinyl pyridine anion-exchange resins. References [5, 7] describe the reprocessing of plutonium and neptunium concentrates from an extraction system for the regeneration of spent fuel elements from an atomic power plant with a VVÉR-440 reactor by sorption of actinides on VP-1AP anion-exchange resin with good technological characteristics.

The present paper gives the results of anion-exchange refinement of plutonium from a reduction re-extract from extraction regeneration of spent fuel elements from a VVÉR of the Novovoronezh Atomic Power Plant with a 26-month cooling period (effective operating period 200 days). Sorption was carried out with an AB-23M highly alkaline vinyl pyridine anion-exchange resin with a gel structure and a grain size of 0.4-0.6 mm.

The re-extract of plutonium and neptunium fed in for anion-exchange refinement contained 1.2 g Pu/liter, 0.09 g Np/liter, 0.5-8 g U/liter, and 0.8 M HNO_3; the fission products were characterized by an exposure dose rate (e.d.r.) of 0.45 $\mu R/(sec \cdot m^2 \cdot liter)$. As a result of the high specific e.d.r. [~ 375 $\mu R/(sec \cdot m^2 \cdot kg\ Pu)$] the solutions were reprocessed according to a two-cycle flowsheet (Fig. 1).

In the process considered, an evaluation was made of how the method used to prepare the valence forms Pu(IV) and Np(IV) affected their separation from the actinides and fission products in the stage of joint sorption of Pu(IV) and Np(IV) in the first cycle and how the method of separation of Pu and Np affected the degree of their mutual decontamination in the second cycle.

In the first cycle, joint sorption of Pu(IV) and Np(IV) was effected with 7.5 M HNO_3; to obtain the required valence forms of the extracted metal the initial solution was acidified to 7.5 M with respect to HNO_3, and subsequently had iron (II) and hydrazine nitrates added to it to a concentration of 0.2 and 0.1 M, respectively, [8]. The solution was allowed to stand for 45 min and then sent on for sorption.

TABLE 1. Characteristics of Solutions of I Anion-Exchange Cycle

Variant of flowsheet	Charge, g/liter		Content, % of initial				Comp. of desorbate				Extraction, %	
			filtrate		scrubbing water							
	Pu	Np	Pu	Np	Pu	Np	Pu, g/liter	Np mg/liter	U, mg/liter	e.d.r. $\cdot 10^3$, $\mu R/sec \cdot m^2 \cdot liter$	Pu	Np
First	14,3	1,1	0,6	1,2	0,1	0,7	3,57	286	12,0	4,4	99,3	98,6
Second	14,3	1,1	0,9	4,1	0,1	0,4	3,56	262,5	5,0	3,5	98,9	94,8

Translated from Atomnaya Énergiya, Vol. 42, No. 3, pp. 191-194, March, 1977. Original article submitted April 9, 1976.

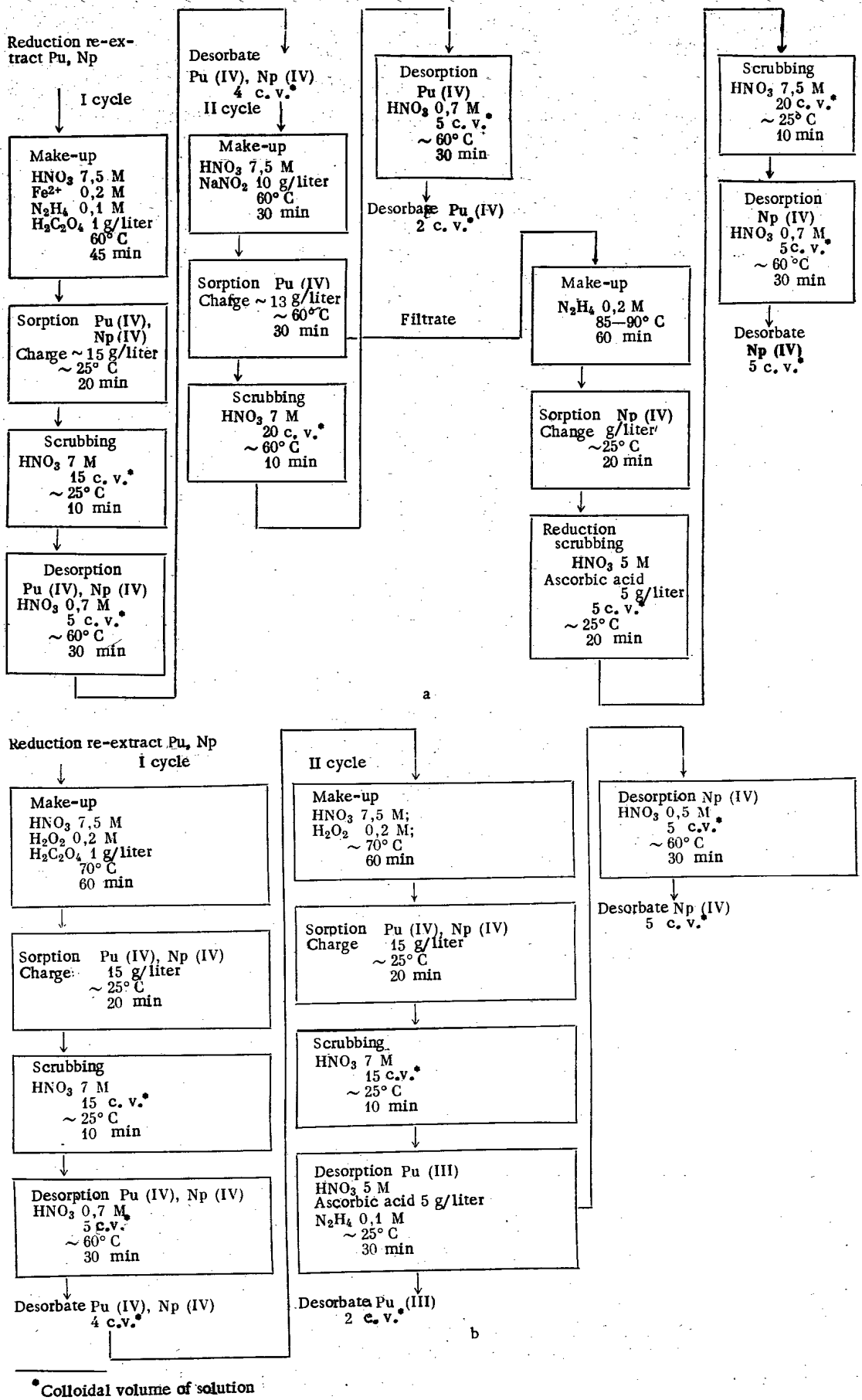

Fig. 1. Flowsheet of two-cycle anion-exchange separation of plutonium and neptunium and their decontamination from uranium and fission products: a) first variant; b) second variant.

TABLE 2. Characteristics of Solution of II Anion-Exchange Cycle

Variant of flowsheet	Charge, g/liter		Content, % of initial					Comp. of desorbate								Extraction, %	
			filtrate		scrubbing with 7 M HNO_3		reduction scrubbing	Pu				Np					
	Pu	Np	Pu	Np	Pu	Np	Np	Pu, g/liter	Np, g/kg Pu	U, g/kg Pu	e.d.r., $\mu R/m^2 \cdot sec \cdot kg$ Pu	Np, mg/liter	Pu, g/kg Np	U, g/kg Np	e.d.r., $\mu R/m^2 \cdot sec \cdot kg$ Np	Pu	Np
First Sorption	13,0	—	0,6	—	1,0	—	—	5,8	0,86	0,52	0,75	—	—	—	—	98,5	—
	—	4,0	—	5,8	—	0,1	0,03	—	—	—	—	752,3	0,93	4,0	1,52	—	94,0
Second	13,2	0,96	0,08	1,3	0,09	1,6	—	5,9	0,81	0,5	0,28	186,0	26,9	16,1	5,9	98,6	95,9

TABLE 3. Coefficients of Purification of Plutonium and Neptunium from Each Other and from Fission Products in Operations of Anion-Exchange Refinement

Cycle	Variant	Decontamination factors					
		plutonium from			neptunium from		
		U	Np	fission products	U	Pu	fission products
I	First	$1,96 \cdot 10^3$	—	$3 \cdot 10^2$	$1,27 \cdot 10^3$	—	$3 \cdot 10^2$
	Second	$4,8 \cdot 10^2$	—	$3,8 \cdot 10^2$	$4,4 \cdot 10^3$	—	$3,4 \cdot 10^2$
II	First	6,5	$1 \cdot 10^2$	1,7	10,5	$1,3 \cdot 10^4$	10
	Second	2,8	$1 \cdot 10^2$	3,5	1,2	$5 \cdot 10^2$	2,3
In two cycles	First	$1,3 \cdot 10^4$	$1 \cdot 10^2$	$5 \cdot 10^2$	$2,1 \cdot 10^4$	$1,4 \cdot 10^4$	$3 \cdot 10^3$
	Second	$1,3 \cdot 10^4$	$1 \cdot 10^2$	$1,3 \cdot 10^3$	$5,3 \cdot 10^3$	$5,5 \cdot 10^2$	$7,9 \cdot 10^2$

In the second variant, Pu(IV) – Np(IV) couples obtained in a joint re-extract of plutonium and neptunium acidified to 7.5 M HNO_3 were decontaminated with 0.2 M H_2O_2 [8].

After the sorbed metals were scrubbed from fission products with 7.5 M HNO_3, plutonium and neptunium were jointly desorbed with 0.7 M HNO_3.

The desorbate of plutonium and neptunium was made up with HNO_3 (to 7.5 M). Selective sorption was carried out in the first variant. To obtain Pu(IV) – Np(V, VI) couples, sodium nitrite was introduced into the acidified desorbate of the first cycle. After that, sorption of the plutonium (IV) was carried out and neptunium remainded in the filtrate in quantity. After scrubbing with 7 M HNO_3, the sorbed plutonium was desorbed with 0.7 M HNO_3. The filtrate, containing neptunium, was treated with hydrazine nitrate.

Sorption of the neptunium (IV) took place at ~25°C. For quantitative separation of neptunium and plutonium the neptunium was subjected to reduction scrubbing with a 5 M solution of HNO_3, containing ascorbic acid and hydrazine. Once the sorbent had been scrubbed, desorption of the neptunium was carried out.

In the second variant, Pu(IV) and Np(IV) were sorbed jointly from the first-cycle desorbate of plutonium and neptunium. After the sorbed metals were scrubbed to remove fission products, reduction desorption of the plutonium was effected with ascorbic acid. The neptium was desorbed with 0.7 M HNO_3.

The coefficients obtained for decontamination of the plutonium and neptunium from uranium, from all of the fission products, and from each other in each cycle of the considered variants of the technological flowsheets for anion-exchange refinement are presented in Tables 1-3.

When iron (II) was used to obtain Pu(IV) – Np(IV) couples in the operation of making up the solution before the first cycle, the filtrate had a lower plutonium and neptunium content than when hydroxide peroxide was used. In the first variant the values were 0.6 and 1.2%, respectively, and in the second, 0.9 and 4.1%, respectively. With iron (II) the decontamination of plutonium and neptunium from uranium and fission products decreased (see Tables 1 and 3).

The separation of plutonium and neptunium in the operation of plutonium (IV) sorption, when neptunium (V, VI) remains in the filtrate (see Fig. 1), is more quantitative (separation factor $\sim 1.3 \cdot 10^4$) than in the stage of reduction elution of plutonium after joint sorption of Pu(IV) and Np(IV). The separation factor in this case did not exceed $\sim 5 \cdot 10^2$.

The principal decontamination factors are listed in Table 3.

The exposure dose rate of the plutonium desorbate in the first variant (0.745 μR/sec $\cdot$ m^2 $\cdot$ kg Pu) was determined from the radioactivity, in %, of: ^{144}Ce + ^{144}Pr 1.1; ^{106}Ru + ^{106}Rh 3.6; ^{134}Cs + ^{137}Cs 1.9; ^{95}Zr 9.7; ^{95}Nb 86; in the second cycle (0.28 μR/sec $\cdot$ m^2 $\cdot$ kg Pu), ^{144}Ce + ^{144}Pr 1.3; ^{106}Ru + ^{106}Rh 3.6; ^{134}Cs + ^{137}Cs 2.9; ^{95}Zr 21.4; ^{95}Nb 71.4.

With the gamma spectrum of plutonium taken into account, the factor of plutonium decontamination from its various fission products in two cycles were: in the first variant, from ^{144}Ce + ^{144}Pr $2.2 \cdot 10^3$; ^{106}Ru + ^{106}Rh $7.5 \cdot 10^3$; ^{134}Cs + ^{137}Cs $2.7 \cdot 10^3$; ^{95}Zr $1.6 \cdot 10^3$; ^{95}Nb $2 \cdot 10^2$; in the second variant ^{144}Ce + ^{144}Pr $3.8 \cdot 10^3$; ^{106}Ru + ^{106}Rh $8.3 \cdot 10^3$; ^{134}Cs + ^{137}Cs $6.1 \cdot 10^3$; ^{95}Zr $1.9 \cdot 10^3$; ^{95}Nb $6 \cdot 10^2$.

LITERATURE CITED

1. V. B. Shevchenko et al., in: Proceedings of the COMECON Symposium–Studies on the Reprocessing of Spent Fuel, Vol. 1, Prague, Czechoslovak Atomic Energy Commission (1972), p. 259.
2. V. B. Shevchenko et al., Fourth Geneva Conference (1971), Paper USSR No. 435.
3. G. Burney and G. Thompson, Radiochem. Radioanal. Lett., 12, 207 (1972).
4. N. G. Chernorukov, in: Eleventh Mendeleev Conference on General and Applied Chemistry [in Russian], Vol. 1, Nauka (1975), p. 270.
5. V. I. Paramonova, Radiokhimiya, 17, No. 6, 994 (1975).
6. E. D. Kiseleva and K. V. Chmutov, Zh. Fiz. Khim., 49, No. 8, 2127.
7. V. I. Paramonova and N. B. Vysokoostrovskaya, Summaries of Papers on the Chemistry of Plutonium [in Russian], Nauka, Leningrad (1975), p. 1.
8. V. S. Koltunov, Kinetics of Actinide Reactions [in Russian], Atomizdat, Moscow (1974).

RECRYSTALLIZATION OF γ- AND β-HARDENED COMMERCIAL URANIUM

G. I. Tomson and Yu. I. Petrov

UDC 669.822.017

Comparison of the results of research on the recrystallization of hardened uranium, [1-4] and other papers, shows that the recrystallization rate depends essentially not only on the impurity content, the α-annealing temperature, and from what γ or β range the hardening took place. Accordingly, studies were undertaken on the causes of the different capacities of γ- and β-hardened uranium for recrystallization.

Research Material and Technique. The investigations were carried out on rolled specimens of commercial-purity uranium measuring 2 × 10 × 30 mm. The content of impurities in uranium (mass %), $5 \cdot 10^{-2}$ C; $8 \cdot 10^{-3}$ Fe; $5 \cdot 10^{-3}$ Si; $4 \cdot 10^{-4}$ Ni; $7 \cdot 10^{-4}$ Mn and $7 \cdot 10^{-4}$ Cu, did not exceed the solubility limit in the β range.

Previously, the specimens were subjected to homogenizing annealing at 950°C for 2 h, followed by slow cooling in a furnace ($V_{cool} \sim 5 \cdot 10$°C/min). The specimens were heat-treated in a resistance furnace in quartz ampuls with continuous evacuation ($p_{res} \sim 2 \cdot 10^{-2}$ mm Hg). The temperature was measured by a PSP 1-60 potentiometer with a Chromel–alumel thermocouple.

The initial γ and β hardening was effected from temperatures of 950 and 740°C, respectively; after soaking for 30 min, the specimens were cooled in water at 20°C. Brief heating of the specimens in the β and γ ranges in

Translated from Atomnaya Énergiya, Vol. 42, No. 3, pp. 195-198, March, 1977. Original article submitted April 30, 1976.

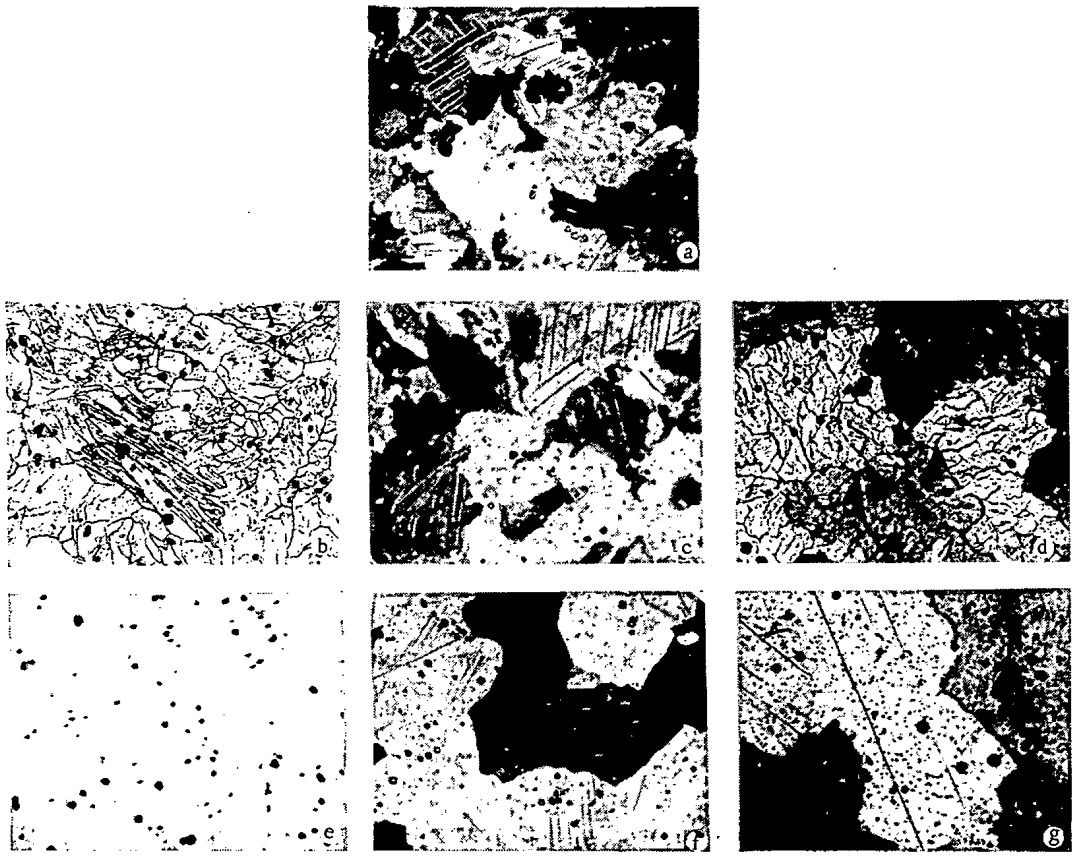

Fig. 1. Structure of hardened and annealed uranium (×300): a) γ hardening and β hardening (soaking for 30 min at 740 and 950°C, respectively); c) γ hardening, 950°C, 30 min; c, d) γ hardening + α annealing, 600°C, 4 h; e) β hardening, 740°C, 30 min; e, g) β hardening + α annealing, 600°C, 4 h; etching: a, c, f) for α grain; b, e) for net; d, g) for net and α grain.

the case of cross hardening was carried out in a bichromate bath. The duration of the heating was reckoned from the time at which the required temperature (700 or 800°C, respectively) was reached on the specimen surface; accordingly, thermocouples were fastened onto the specimens. Recrystallization annealing of hardened specimens took place at 600°C for 4 h. The α grains were exposed by electrolytical etching of electropolished sections at 40 V in a solution containing one part chromic acid to three parts acetic acid. The net substructure of the impurity was exposed by chemical etching in a boiling mixture of equal volumes of nitric and acetic acid.

The recrystallization was studied on the basis of data from metallographic analysis concerning variations in grain size and shape.

Experimental Results and Discussion. Studies of the microstructure of specimens of uranium after hardening and annealing at 600°C for 4 h (Figs. 1a, c, and f) show that the recrystallization processes in γ- and β-hardened uranium do indeed proceed at different rates: β-hardened uranium completely recrystallizes in that time whereas in γ-hardened uranium recrystallization has practically not started.

Possible slight differences in the grain and subgrain size and shape and in the magnitude and the internal stresses can scarcely account for the significant difference in the recrystallization rate of γ- and β-hardened uranium. However, etching for "net" shows that there are appreciable differences in the character of the impurity distribution in γ- and β-hardened uranium (Figs. 1b and e). Only quite large, uniformly distributed inclusions are observed in β-hardened uranium. In the main, these are carbides or hydroxycarbonitrides, formed during the recrystallization process [1, 9, 10]. In addition to such inclusions, γ-hardened uranium has very fine inclusions (primarily carbides) and segregations of impurity atoms, forming a so-called net substructure [6-8].

Impurities behave in different ways in γ- and β-hardened uranium and during the process of recrystallization annealing. Fine, uniformly distributed inclusions as well as large ones were observed in β-hardened

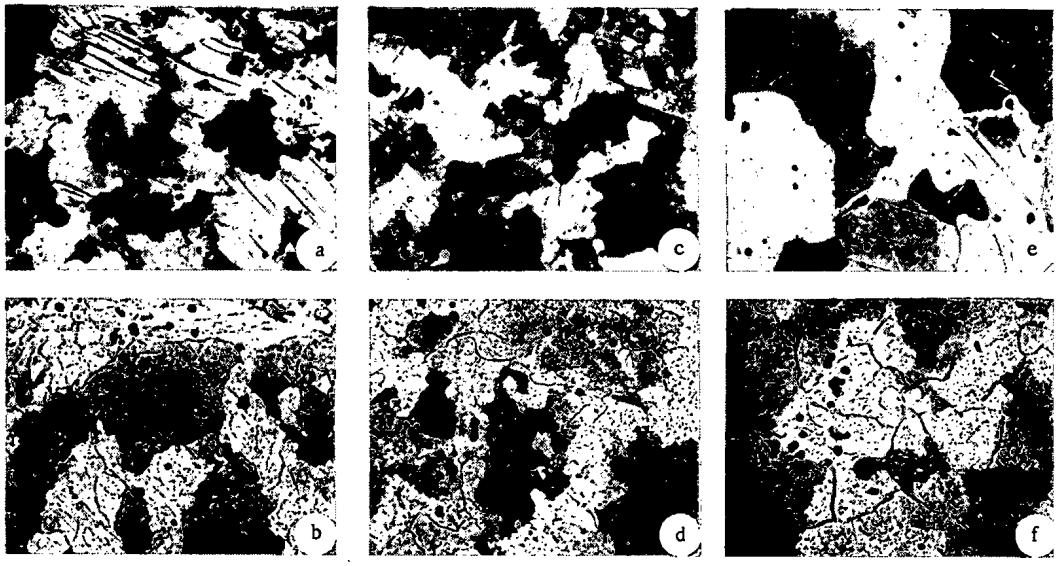

Fig. 2. Structure of uranium hardened from 700°C (γ-hardening + β-hardening) and annealed (α-annealing at 600°C, 4 h); a, b) 30 sec; c, d) 1 min; c, f) 4 min (soaking at 700°C); etching: a, c, e) for α grain; b, d, f) for net and α grain.

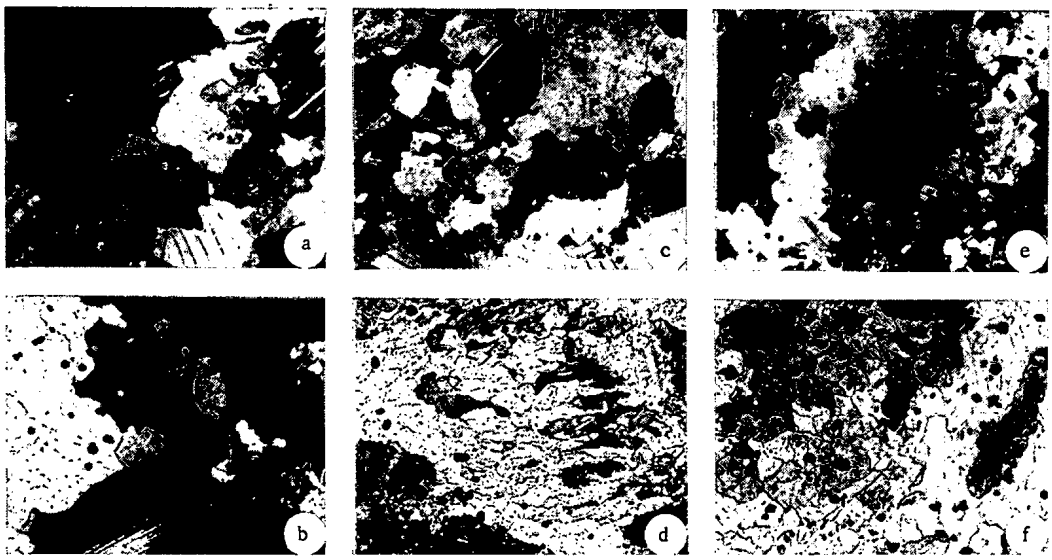

Fig. 3. Structure of uranium quenched from 800° (γ-quenching+β-quenching) and annealed (α-annealing at 600°C for 4 h): a, b) 30 sec; c, d) 1 min; e, f) 4 min (holding at 800°C). Etching: a, c, e) for α-grain; b, d, f) for net and α-grain.

uranium after annealing (Fig. 1f and g). In γ-hardened uranium the original net substructure vanishes during annealing (Fig. 1b) and a large number of inclusions, forming a new net, appear along the boundaries of the α grains and subgrains (Fig. 1c and d).

Owing to the small strains that occur during the phase transformations and cooling in the α-range, recrystallization of the hardened uranium is evidently of a collective nature [5], i.e., individual grains and subgrains grow because of others; it is thus natural to assume that precisely the large numbers of inclusions that are precipitated along the boundaries of α grains and subgrains and that block the motion of these boundaries make recrystallization in γ-hardened uranium more difficult than in β-hardened uranium.

Experiments with crossed hardening from the γ and β phases have been carried out to determine how the character of the impurity distribution in hardened uranium affects its capacity for recrystallization. These experiments showed that heating of γ-hardened uranium for a short time in the β range, followed by hardening, sharply increases the capacity of uranium for recrystallization (Fig. 2a, c, and e), the increase depending on the heating time in the β range.

In the course of the heating in the β range, the original net substructure of the γ hardening is replaced by a new net (Fig. 2b, d, and f); this new net is formed by inclusions that are stable at the β-phase temperature and changes little in the process of crystallization annealing. Even after short 30-sec heating in the β range, there is a sharp drop in the number of inclusions formed during the subsequent recrystallization annealing along the boundaries of the α grains and subgrains (Figs. 1d and 2b). As the heating time is lengthened the number of these inclusions falls off even more (Fig. 2d and f). Thus, a definite correlation exists between the capacity of hardened uranium for recrystallization and the number of inclusions formed along the boundaries of the α grains and subgrains during annealing. The number of inclusions depends on the character of the impurity distribution and the stability of the net substructure in the hardened state.

Brief heating of β-hardened uranium in the β range with subsequent hardening, by contrast, appreciably reduces the capacity of uranium for recrystallization (Fig. 3a, c, and e), this reduction also depending on the duration of the heating in the γ range. The investigations have shown that a net substructure characteristic of γ-hardened uranium is formed in the process and, with subsequent recrystallizing annealing, a net of inclusions is formed along the boundaries of the α grains and subgrains (Fig. 3b, d, and f). One can see clearly that the number of these inclusions along the boundaries of α grains and subgrains grows as the duration of the heating in the γ range increases. Evidently, the quantity of impurities that goes over into the γ-solid solution increases, approaching the equilibrium concentration, and after hardening and annealing these impurities can form inclusions of the other phase along the boundaries of the α grains and subgrains.

Thus, once again a connection is seen between the capacity of hardened uranium for recrystallization and the character of its net substructure and, on the other hand, the number of inclusions formed along the boundaries of α grains and subgrains during annealing. This confirms the assumption that the character of the impurity distribution in hardened uranium has a predominant influence on its recrystallization.

LITERATURE CITED

1. A. P. Holden, Physical Metallurgy of Uranium [Russian translation], Metallurgizdat, Moscow (1962), p. 147.
2. F. G. Foot, Metallurgy of Nuclear Power Engineering and the Effect of Irradiation on Materials [Russian translation], Metallurgizdat, Moscow (1956), p. 89.
3. S. Push and B. Butcher, in: Proceedings of the Symposium – Reactor Technology, Select. Rev. (L. E. Link editor), Oak Ridge, Tennessee (1964), p. 331.
4. A. Smith, J. Nucl. Mater., 26, 341 (1968).
5. S. S. Gorelik, Recrystallization of Metals and Alloys [in Russian], Metallurgizdat, Moscow (1967).
6. A. Robillard, D. Calais, and P. Lacombe, Rev. de Metallurgie, 55, No. 9, 815 (1958).
7. C. Angerman and R. Huntoon, J. Less-Common Metals, 9, No. 5, 338 (1965).
8. A. A. Bochvar et al., At. Energ., 27, No. 3, 193 (1969).
9. G. Ya. Sergeev, V. V. Titova, and K. A. Borisov, Physical Metallurgy of Uranium and Some Other Reactor Materials [in Russian], Atomizdat, Moscow (1960).
10. Ya. M. Sterlin, Uranium Metallurgy [in Russian], Gosatomizdat, Moscow (1962).

APPARATUS FOR THE CALIBRATION OF FILM DOSIMETERS IN ELECTRON RADIATION FIELDS OF HIGH INTENSITY

V. A. Berlyand, V. V. Generalova, M. N. Gurskii, and A. P. Zhanzhora

UDC 621.387.46:541.15

In several technological processes, materials are irradiated with intense beams of 200-700-keV electrons. In such cases one must determine the dose absorbed in 100-500-μ-thick organic material layers. Film dosimeters can be used to measure the absorbed dose in rather thin layers and to determine the dose distribution over the depth of the object irradiated. Overheating by the radiation in the case of high dose rates (up to 10^7 rd/sec), active media (ozone, radiolysis products), and the possible accumulation of space charge in dielectrics [1] can substantially affect the dosimetric characteristics of film detectors. Therefore, when reliable results are to be obtained with film dosimeters, the dosimeters must be carefully calibrated with the aid of an absolute method, a calorimetric method, used under the real conditions of operation of the dosimeters.

The authors of [2-4] have described several calorimeters that are used to calibrate films at electron energies in excess of 1 MeV. Little experimental work has been done on that problem at electron energies below 1 MeV. Some of the work was reported in [5], where the measurements were made at electron energies of 0.3-0.5 MeV. The work by Dmitriev et al. [6] should be noted, because they calibrated polymethylmetacrylate and polyvinylchloride films with the aid of a semiadiabatic total-absorption calorimeter. However, a method of calibrating the detectors was nowhere described in full detail; the errors of the measurements were not analyzed; and the dose rate range in which the calibration was made was either narrow or not indicated at all.

Description of the Calorimetric Apparatus. We developed in our work a calorimetric apparatus (see Fig. 1) and a method of calibrating chemical film dosimeters in high-intensity electron radiation fields. The main component of the apparatus is a calorimeter of the integral thermal flux; the calorimeter is operated under stationary conditions and the electron beam incident upon it is completely absorbed. By using a calorimeter of this type, one can avoid the difficulties resulting from temperature gradients inside the absorber of the calorimeter. In order to reduce the energy losses by bremsstrahlung and by backscattering of electrons, the absorber of the calorimeter was made from materials with a low atomic number and was given the form of a cavity. The absorber of the calorimeter is a combination of components: a graphite vessel with a wall thickness of 1 mm is placed inside a thin-wall aluminum vessel whose external surface is coated with an oxide layer. Calculations have shown that for an absorber of this type and this composition, the bremsstrahlung losses at electron energies of 300 keV do not exceed 0.1%, whereas the losses resulting from backscattering of electrons are below 0.6%. In order to calibrate the calorimeter with Joulean heat, a heating element of manganin wire was inserted into the absorber. The heat flux which originates from the absorber of the calorimeter is proportional to the rate at which under stationary conditions heat is liberated inside the absorber. The heat flux is recorded with a thermopile comprising several thousand differential copper–constantan thermocouples connected in series. A 10-μ-thick aluminum foil prevents the convection of air. In order to reduce the influence of temperature fluctuations in the surrounding medium, a differential scheme is employed: Two identical calorimeters are connected in opposing relationship. During the measurements, one calorimeter is exposed to the electron beam, whereas the other one is shielded by an aluminum shield. The calorimeters are characterized by high thermal conductivity, low heat capacity, and, consequently, a small time constant (τ = 25-27 sec). The calorimeters were calibrated with a heat liberation rate of 10^{-3}-10 W. The sensitivity of the calorimeters was ~40 mV/W. The calorimeters are also electron collectors in the form of a Faraday cylinder. The calorimeters can be used to measure the electron flux and to determine the average electron energy.

Translated from Atomnaya Énergiya, Vol. 42, No. 3, pp. 199-202, March, 1977. Original article submitted May 10, 1976; revision submitted September 14, 1976.

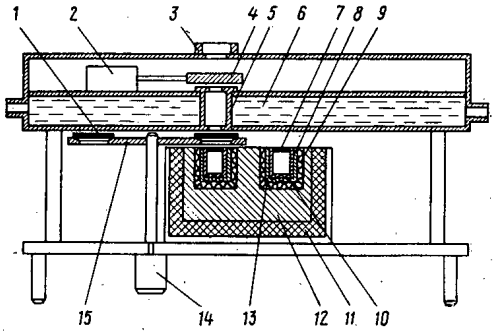

Fig. 1. Scheme of the calorimetric apparatus: 1) detectors; 2) solenoid; 3) electron collector; 4) shutter; 5) collimator; 6) shield with water cooling; 7) aluminum foil; 8) graphite foil; 9) thermopile; 10) heater element; 11) foam plastic; 12) copper block; 13) aluminum vessel; 14) motor; 15) disk-shaped drum.

During the operation of the accelerator, the fluctuations in the density of the energy flux of the incident electrons can exceed 10-15%. It is therefore necessary to continually control the beam of electrons released. An electron collector in the form of a ring was used as the monitor of the electron radiation. A collimator acts as a diaphragm for the electron beam, which thereafter is incident either on the calorimeter to measure the flux density of the electron beam energy or upon the detectors to be calibrated. The detectors are mounted in a disk-shaped drum with 8 openings. The films exposed to the beam are shifted by remote control effected with the aid of a motor. The required exposure to the radiation is obtained with a shutter which is operated by a solenoid. A timer is connected in series with the solenoid. Thus, the time of irradiation can be fixed with rather high accuracy (0.01-0.2 sec). A shield with water cooling is used to protect the entire apparatus from the radiation.

A copper block and a layer of foam plastic reduce the influence of temperature fluctuations in the environment and guarantee uniform temperature conditions in the external shells of the calorimeter.

Calibration of Film Dosimeters. The film dosimeters are calibrated with a substitution method. At the beginning, the flux density φ of the electron radiation energy is determined at a certain point with the aid of the calorimeter. After that, film dosimeters are irradiated under the same conditions and the absorbed dose is calculated. With the calculation method one can account for possible nonlinearities in the dependence of the optical density of the films (or any other film parameters) upon the absorbed dose.

The calculations are made as follows. The relation between the readings of the total-absorption calorimeter and the readings I of the monitor is established by several measurements:

$$\varphi = kI, \tag{1}$$

where k denotes the proportionality factor.

The monitor signal I(t), which changes in the course of film irradiation, is recorded on the tape of an automatic potentiometer. After integrating the function recorded over time, the readings of the monitor can be used to determine the energy transfer of the electron radiation during the irradiation time:

$$F = \int_0^{t_0} \varphi(t)\, dt = k \int_0^{t_0} I(t)\, dt. \tag{2}$$

At the beginning, several individual films are irradiated at given parameters of the accelerator. The exposures are selected so that the entire range of absorbed doses to which the films may be exposed is covered (the range is 2-25 Mrd in the case of cellophane). The energy transfer is determined for each film irradiated and the optical density of the film is measured. The irradiation dose absorbed by the film is evidently directly proportional to the radiation energy transferred.

As a result of these operations one can plot a calibration curve in relative units, i.e., one can plot the relationship between the dose absorbed by the film and some film parameter for which the ratio S/S_0 is conveniently used (S_0 denotes the optical density of the nonirradiated film). The error resulting from the spread of the initial optical densities of the dosimeter films is then reduced (α being the proportionality factor):

$$\alpha D = f(S/S_0). \tag{3}$$

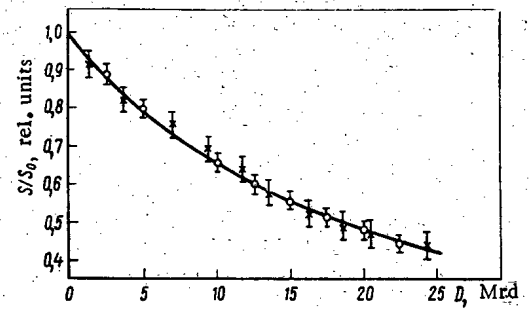

Fig. 2. Calibration curve S/S_0 as a function of the absorbed dose of (×) electron radiation and (○) γ radiation.

The determination of α is the next problem. For this purpose, a set of films which guarantee total absorption of the electron beam is irradiated and measured with a photometer. The coefficient α is obtained from the normalization condition

$$\sum_{i=1}^{n} m_i D_i = E, \tag{4}$$

where m_i denotes the mass of the i-th film of the total-absorption set, with the mass referred to unit area; n denotes the number of films in the set; and E denotes the energy absorbed by the set of films, with the energy referred to unit area. The absorbed energy is equal to the energy transferred minus the energy of the electrons backscattered from the set of films:

$$E = F(1-p), \tag{5}$$

where p denotes the albedo in terms of energy; in the case of cellophane, the albedo is 0.03 at an electron energy of 300 keV [7]. The energy spent on bremsstrahlung can be disregarded. We obtain with Eqs. (3)-(5):

$$\alpha = \frac{\sum_{i=1}^{n} m_i f(S/S_0)_i}{F(1-p)}. \tag{6}$$

Analysis of the Errors Made in the Calibration of Film Dosimeters. The random errors and the systematic error made in the measurements with a calorimeter do not exceed 0.1%. When the flux density of the energy of an electron beam is measured, additional systematic errors arise. A portion of the energy of the electron radiation is carried away by bremsstrahlung and is not recorded by the calorimeter. The error which is made for this reason at an electron energy of 300 keV does not exceed 0.1%. The error which results from the energy fraction carried away by electron backscattering does not exceed 0.3%. The error which is associated with the measurement of the cross section of the beam of electrons incident upon the calorimeter is less than 0.3%. The error which results from a possible deviation of the calorimeter axis from the axis of the electron beam does not exceed 0.6%. The error resulting from electrons scattered in the collimator does not exceed 0.5%. Thus, the total error which is made when the calorimeter is used to measure the density of the energy flux of the electron radiation does not exceed ±1% at the 0.95 confidence level. The coefficient k of Eq. (1), which relates the calorimeter readings and the monitor readings, is obtained from several measurements. For six measurements the error made in the determination of k amounts to ±2% and originates from fluctuations of both the flux density and the electron energy. When the set of films is irradiated, a space charge accumulates, and this may increase the backscattering of the electrons. In order to reduce a possible influence of this effect, the sets of films were wrapped in 10-μ-thick aluminum foil which was grounded. The error resulting from the uncertainty of the coefficient of electron backscattering from the set of film detectors does not exceed 3%. Thus, when the film dosimeters are calibrated, the energy transfer and the energy absorbed by the set are determined with errors of ±2.3 and ±4%, respectively.

The experimental data were processed on a Mir-1 computer with the least-square method; the optimal degree of the approximating polynomial was determined with the Fischer criterion [8].

Experimental Results. Chemical film dosimeters made from cellophane to which thiocyne red had been added (prepared in the L. V. Pisarzhevskii Institute of Physical Chemistry, Academy of Sciences of the Ukrainian SSR) were calibrated on the EOL accelerator. The initial electron energy was 360 keV and the accelerator current ranged from 0.5 to 10 mA. The films were irradiated at a distance of 13 cm from the exit window of the accelerator. The average energy of the incident electrons is 245 ± 15 keV, according to the calculation of

[9], which takes into consideration the absorption of energy by both the foil of the exit window of the accelerator and the air layer. The average energy of the incident electrons was determined as 235 ± 10 keV with the aid of the calorimeter–collector. Within the experimental error limits, this value coincides with the calculations. The maximum rate of the dose absorbed by the films amounted to 1.2 Mrd/sec with these parameters of the accelerator. The calibration curves obtained when the films were irradiated in fields of γ radiation and electron radiation are shown in Fig. 2. The films were calibrated in a photon radiation field with the aid of the calorimeter apparatus described in [10].

The calorimetric apparatus and our method therefore make it possible to calibrate various film dosimeters with proper regard for the nonlinear relationship between the optical density (or any other parameter) and the absorbed dose at electron energies of 0.15-2.5 MeV and at energy flux densities of 10^{-3}-10 W/cm^2. An analysis of the errors of the calibration method, of the random error, and of the systematic error of the optical density measurements performed on the film has shown that cellophane films can be used to measure absorbed doses of electron radiation with an error of ±(15-20%). The apparatus was certified as a measurement standard of the first-class category.

LITERATURE CITED

1. O. B. Evdokimov and N. P. Tubalov, in: Dosimetry and Radiation Processes in Dosimetric Systems [in Russian], Fan, Tashkent (1972), p. 52.
2. W. McLauglin, in: Proceedings of the IAEA Symposium – Large Radiation Sources for Industrial Processes, Vienna (1969), p. 579.
3. H. Eisen, "Electron depth-dose distribution measurement in metals and two-layer slabs," Doctorial Dissertation, Univ. of Maryland (1971).
4. J. Puig, in: Proceedings of the IAEA Symposium – Colloque sur la Radiosterilisation des Produits Medicaux et des Tissus Biologiques, Bombay, Dec. 9-13, 1974, SM-129/18.
5. B. Radak, in: Proceedings of the IAEA Symposium – Dosimetric Techniques as Applied to Agriculture, Industry, Biology, and Medicine, Vienna, April 17-21, 1971, SM-160/31.
6. A. K. Dmitriev et al., in: Dosimetry and Radiation Processes in Dosimetric Systems [in Russian], Fan, Tashkent, (1972), p. 57.
7. V. F. Baranov, Dosimetry of Electron Radiation [in Russian], Atomizdat, Moscow (1974).
8. S. Brand, Statistical Methods in the Analysis of Observations [Russian translation], Mir, Moscow (1975).
9. M. Berger and S. Seltzer, Studies in the Penetration of Charged Particles in Matter, Washington, D. C. (1964).
10. V. A. Berlyand, V. V. Generalova, and M. N. Gurskii, At. Energ., 38, No. 4, 253 (1975).

SPATIAL DISTRIBUTION OF d – d NEUTRONS

D. V. Viktorov and T. S. Tsulaya

UDC 539.107.48+521.039

A study has been made of the spatial distribution of neutrons from D(d, n)^{3}He in relation to angle of emission.

The specific fluence f from a circular target (radius R) at point ($l\cos\alpha, l\sin\alpha$, L) in space is represented as

$$f(\gamma,\ l,\ \alpha,\ L)=(1/2a_0\pi R^2)\,(I_0+a_1I_1+a_2I_2), \tag{1}$$

where

$$\left.\begin{aligned} I_0&=\frac{1}{2\pi}\int_0^{2\pi}\int_0^1 K(\vartheta,\ \theta)\,\frac{x\,dx\,d\omega}{\rho_0^2};\\ I_1&=\frac{1}{2\pi}\int_0^{2\pi}\int_0^1 K(\vartheta,\ \theta)\cos^2\theta\,\frac{x\,dx\,d\omega}{\rho_0^2},\\ I_2&=\frac{1}{2\pi}\int_0^{2\pi}\int_0^1 K(\vartheta,\ \theta)\cos^4\theta\,\frac{x\,dx\,d\omega}{\rho_0^2} \end{aligned}\right\} \tag{2}$$

and the dimensionless symbols are

$$r=Rx;\quad \rho=R\rho_0;\quad l=Rl_0;\quad L=RL_0. \tag{3}$$

Here a_0 is a normalization vector, ρ is the distance from a point on the target ($r\cos\omega$, $r\sin\omega$, 0) to the exposure point, r and ω are polar coordinates in the target plane, while the parallel deuteron beam incident on the target lies in the oxz plane and at an angle γ to the ox axis, and ϑ and θ are the angles of incidence of the deuterons in the laboratory system and in the center-of-mass system, respectively [1]:

$$\left.\begin{aligned} \cos\vartheta&=\frac{1}{\rho}\,(l\cos\alpha\cos\gamma+L\sin\gamma-r\cos\gamma\cos\omega);\\ \rho^2&=r^2+l^2-2rl\cos(\omega-\alpha)+L^2;\\ \cos\theta&=-\delta\sin^2\vartheta+\cos\vartheta\sqrt{1-\delta^2\sin^2\vartheta};\\ K(\vartheta,\ \theta)&=\frac{d\cos\theta}{d\cos\vartheta}=2\delta\cos\vartheta+\frac{1-\delta^2(1-2\cos^2\vartheta)}{\sqrt{1-\delta^2\sin^2\vartheta}};\\ \delta^2&=\frac{m_n/m_{^3\mathrm{He}}}{1+2Q/E}<1; \end{aligned}\right\} \tag{4}$$

m_n and $m_{^3He}$ are the masses of a neutron and ^{3}He, E is the kinetic energy of the deuteron in the laboratory system, and Q is the energy released in the reaction.

Series expansion in terms of the small parameter δ provides formulas for the specific flux of (1) with a computational error not exceeding 0.1%.

A program has been written in the "Engineer" autocode and a series of calculations have been performed with a Minsk-2 computer; the dependence of f on the parameters γ, l, α, and L is presented for the case E = 0.206 MeV (a_1 = 1.27; a_2 = 0.26 [2]) and R = 0.7 cm via graphs, which show marked anisotropy.

The theory is compared with experiment in terms of the specific fluence averaged over the volume of the detector:

$$\bar{f}=\frac{1}{V}\int\int\int f\,dV. \tag{5}$$

Translated from Atomnaya Énergiya, Vol. 42, No. 3, pp. 203-206, March 1977.

The observed $\bar{f}$ were determined by an activation method at a small distance from the target in the neutron generator; the reactions were $^{111}Cd(n, n')$, ^{111m}Cd and $^{31}P(n, p)^{31}Si$, and the deuterons accelerated to 0.180 MeV fell on the target at $\gamma = 35°$. The detectors (cadmium foil and plastic scintillators containing dispersed calcium phosphate) were coaxial with the target and parallel to the plane of the latter; the neutron energy was 2.76 MeV. The neutron source in the first reaction was a standard titanium target, while in the second case it was packed copper wool.

The measured $\bar{f}$ were in reasonable agreement with the theoretical values.

LITERATURE CITED

1. L. I. Schiff, Quantum Mechanics, McGraw-Hill (1965).
2. J. Marion and J. L. Fowler, Fast Neutron Physics, Part 1, Wiley (1963).

(No. 899/6906. Original article submitted January 20, 1976; complete text 0.65 authors' folios, 5 Figs., 3 Tables, 12 Refs.)

CALCULATIONS ON THE ENERGY DEPOSITED IN THE SHIELD OF A FAST POWER REACTOR

V. A. Karpov, B. V. Koloskov, V. I. Matveev, and M. F. Troyanov

UDC 621.039.52

The shield of such a reactor has a complicated shape; e.g., the core in the BN-350 reactor was hexagonal in the measurement period after the physical commissioning [1, 2]. A computational analysis is presented via the VIKAR and KENT two-dimensional program [3], which involves solving the diffusion equation for hexagonal geometry, and it has been found that the differences in reaction rate, e.g., for fission of ^{238}U, are large in the high-enrichment zone with regard to directions at an angle in the wall and at the middle of the wall, while in the first layers of the blanket (15-20 cm) the ratio of the fission rates at a given radius is about 2.

Table 1 compares the theoretical and observed fission rates for ^{235}U and natural uranium observed during the physical commissioning of the BN-350; the calculated distribution of the fission rate for ^{235}U agrees satisfactorily with the measured value (within 5 and 10% for the core and blanket, respectively, [1]). However, the calculations for hexagonal geometry for natural uranium agree much better with experiment for the core and blanket than do results for the one-dimensional case.

TABLE 1. Comparison of Observed and Calculated Fission Rates for ^{235}U and Natural Uranium (directed to a corner of the core)

R, cm	^{235}U							Natural uranium					
	one-dimensional calc.	VIKAR 9 groups	KENT 2 groups	experiment*				one-dimensional calc.	VIKAR 9 groups	KENT 2 groups	experiment*		
0	1	1	1		1			1	1	1		1	
+29,5	0,936	0,964	0,951	0,957	0,969	0,979		1,02	0,920	0,938	0,967		0,948
−29,5†	0,936	0,948	0,936	0, 85	—	—		1,02	0,905	0,927		0,963	
49,2	0,755	0,812	0,837		0,814			0,991	0,903	0,900		0,964	
+59,0†	0,662	0,693	0,712	0,624	0,675	0,672	0,679	0,945	0,850	0,879	0,831	0,784	0,878
−59,0	0,662	0,672	0,695		0,646			0,945	0,825	0,858	0,754	0,737	0,792
68,8	0,528	0,554	0,571	0,538	0,571			0,750	0,690	0,708		0,647	
+88,5†	0,270	0,287	0,277	0,268	0,304	0,296		0,141	0,184	0,196	0,147		0,160
−88,5	0,270	0,279	0,271		0,285			0,141	0,178	0,191		0,181	
108,2	0,083	0,094	0,090	0,082	0,080	0,097	0,095	0,029	0,031	0,030	0,034	0,039	0,036
−108,2†	0,083	0,097	0,091		0,094			0,029	0,032	0,031		0,032	

* The different values for a single radius relate to different experiments, which differed in power level, irradiation time, amount of detector material, etc.
† Distance reckoned in the opposite direction from the center of the reactor.

Therefore, if the shape of the core in a fast reactor differs appreciably from a regular cylinder, the distributions of the various components responsible for the energy release, particularly fission of ^{238}U, may vary substantially with direction. In that case, it is necessary to perform calculations for hexagonal geometry, since one-dimensional models or two-dimensional cylindrical geometry can result in substantial errors in the energy release in the blanket. The observed and theoretical distributions found for the BN-350 indicate that the VIKAR and KENT programs give agreement with experiment, and the characteristics of the blanket can be determined by means of a small number of groups (2-4). The same conclusion has been drawn elsewhere [3] for the core.

LITERATURE CITED

1. V. V. Orlov et al., At. Energ., 36, No. 2, 97 (1974).
2. A. Leipunski et al., Nuclear Power Plant BN-350, Supp. to ANS-100, Detroit (1965), p. 15.
3. V. A. Karpov et al., At. Energ., 38, No. 4, 213 (1975).

(No. 896/8769. Original article submitted April 26, 1976; complete text 0.5 authors' folios, 1 Fig., 4 Tables, 7 Refs.)

THEORY OF NEUTRON-ACTIVATION MEASUREMENTS IN BOREHOLES

G. S. Vozzhenikov and Yu. B. Davydov

UDC 550.835

The distribution of the induced γ radiation along the axis of a borehole of any radius has been determined on the assumption that the material in the borehole differs in properties from the surrounding rock, in particular with regard to neutron and γ-ray transport. It is assumed that the filling differs from the surrounding rock in containing a uniformly distributed tracer, which is produced by nuclear reactions induced by thermal or fast neutrons, the products producing γ rays of a particular primary energy.

Certain restrictions have been imposed in solving this problem; it has been assumed that the angular distribution of the neutrons or γ rays is isotropic and also that the energy losses in single elastic collisions are small. This means that the multigroup diffusion approximation can be used, which simplifies the treatment considerably.

Calculations have been performed on the flux of induced γ rays due to the long-lived isotope of copper and to ^{28}Al produced by $^{63}Cu(n, \gamma)^{64}Cu$; $^{28}Si(n, p)^{28}Al$ by thermal and fast neutrons respectively; the independent variable is the radius of the flooded borehole, the parameter of the curves being the distance from the activation point, and the calculations being for copper-bearing sulfide ores of various grades differing in density and water content.

The following conclusions are drawn. The flux of γ rays from the ^{64}Cu at first increases with the radius, but then decreases; the local peak is due to competition between processes. On the one hand, the flux due to the rapid fast-neutron moderation in the water increases substantially, and such thermal neutrons activate the copper. On the other hand, the induced γ-ray flux itself is absorbed in the borehole. If the diameter is small, the increasing flux of thermal neutrons predominates, but at large diameters the γ-ray absorption becomes predominant. The induced activity in quartzite decreases monotonically as the borehole radius increases. The fall in the activity is due to the rapid moderation of the fast neutrons and absorption of the induced γ rays from ^{28}Al in the flooded borehole.

Figure 1 shows the induced ^{64}Cu and ^{28}Al activities for a central probe; the activation medium was copper-bearing sulfide ore and quartz sand of thickness such that the γ-radiation flux tended to a limit, as did the neutron moderation. The induced activity was recorded with a universal scintillation counter in conjunction with an AI-128 multichannel analyzer. Good agreement was obtained between the observed and calculated functions $\Phi(h)$, where h is the thickness of the layer of water between the borehole wall and the body of the probe. The function $\Phi(h)$ for thermal neutrons differs considerably from that for fast ones, as has previously been observed by Vozzhenikov (in: Proceedings of the Sverdlovsk Mining Institute, Aspects of Prospecting Geophysics, Issue 41 [in Russian], Sverdl. Knizh. Izv. (1962)). The peak observed as a function of borehole diameter for

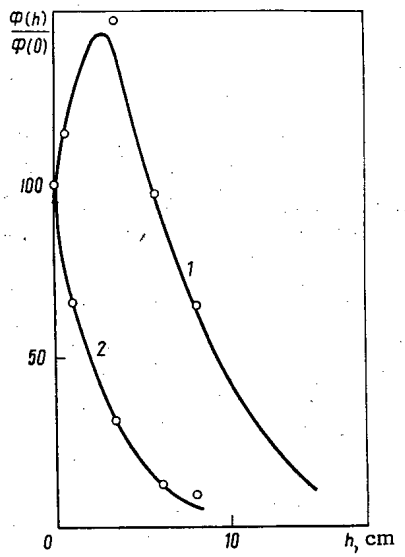

Fig. 1. Comparison of calculations and experiment for induced activity of: 1) ^{28}Al; 2) ^{64}Cu for a probe placed centrally in a flooded borehole.

the (n, γ) reaction (^{64}Cu) and the marked fall in $^{28}Si(n, p)^{28}Al$ as h increases would appear to indicate that it is essential to consider the rock porosity in interpreting neutron-activation measurements in boreholes.

(No. 897/8830. Original article submitted June 8, 1976; complete text 0.65 authors' folios, 3 Figs., 4 Refs.).

THE DOSE DISTRIBUTION FOR A THIN NEUTRON BEAM IN A TISSUE-EQUIVALENT MEDIUM

N. S. Budnikov and D. B. Pozdneev

UDC 577.3:539.12.04+539.125.52

A study has been made of the dose distribution in a tissue-equivalent phantom simulating muscle, the beam being provided by a point unidirectional source (thin beam) for primary energies of 14, 10, 7, 5, 3, 1, and 0.1 MeV.

The first-collision dose has been calculated analytically, while the doses from the second and all subsequent collisions have been calculated by Monte Carlo methods. The latter have also been used to calculate the transport of the resulting photons through the phantoms.

The details of the dose distribution are explicable in terms of the interactions between the neutrons and the material in the phantom.

(No. 900/8771. Original article submitted April 30, 1976; complete text 1.1 authors' folios, 1 Fig., 30 Refs.).

EFFECTS OF ANNEALING ON THE PROPERTIES OF WELDED JOINTS BETWEEN URANIUM AND ZIRCONIUM OR TITANIUM ALLOYS

V. R. Tatarinov, V. P. Ashikhmin, and V. S. Krasnorutskii

UDC 621.791.762.1:(669.822+669.295)+(669.822+669.296)

Measurements have been made on the mechanical parameters and structure of joints made by resistance welding for rods of diameter 6.5 mm between uranium and titanium or zirconium, which have been examined in the initial state and after annealing for various periods at temperatures between 450 and 600°C. Tests were made on welds between uranium (99.8% purity) and technically pure titanium grade BT1-00s, and also with low-alloy titanium (Ti + 2.2% Al + 2.5% Zr) and zirconium (Zr + up to 0.5% Cu + up to 0.5% Mo). Annealing reduces the strength and plasticity. The rate of softening increases with the annealing temperature, and the fall in strength or plasticity tends to a certain limit characteristic of each metal pair. For instance, joints between uranium and BT1-00s gave tensile strengths reduced after 2000 h of annealing at 550°C from $44 \cdot 10^7$ to $25.5 \cdot 10^7$ N/m^2, with no further change.

Metallography showed that the changes in properties in welded joints of uranium–titanium and uranium–zirconium types due to annealing are the result of the formation and growth of transitional zones, which contain the intermetallides U_2Ti and UZr_2 as solid solutions. The densities of these deposits of distinct intermetallide phase increase continuously until a continuous layer of the intermetallide is formed, which appears to represent an obstacle to further expansion of the diffusion zone.

Metallographic examination of fractures in welded joints after prolonged annealing shows that the failure occurs along films of intermetallide, which thereby determine the mechanical characteristics of the joints after prolonged annealing at 500-600°C.

(No. 901/8792. Original article submitted May 10, 1976; complete text 0.5 authors' folios, 5 Figs., 2 Tables, 2 Refs.).

ANISOTROPY OF DOSE SENSITIVITY IN SEMICONDUCTOR DETECTORS OF VARYING CONSTRUCTION USED FOR DOSIMETRY OF IONIZING RADIATION

V. A. Manchuk

UDC 53.089.5:539.1.074

Semiconductor detectors of nuclear radiation with an electron-hole junction possess a number of advantages which are the reason for their promising use in the dosimetry of x-ray and γ radiation [1-3]. One of the most important parameters of a dosimeter that determines its field of application to a considerable extent is the dependence of its sensitivity on the orientation of the detector axis with respect to the direction of propagation of the radiation. The present work presents the results of a study of the dependence of dose sensitivity on the angle of incidence of x-ray and γ radiation for several types of semiconductor detectors operating in the short-circuit current measurement mode.

In dosimetric practice, it is often necessary to make measurements in fields of scattered radiation where it is not possible to pick out a predominant direction of propagation for the quanta and to orient the sensor of the detector in the best manner with respect to this direction. Hence the attempt of experimenters to produce a dosimeter with minimal anisotropy of its readings is understandable. This parameter depends on a number of factors, and primarily on the type of detector, the shape of its sensitive region, and the structural features of the detector and its packaging. The ideal geometric shape of a detector is a sphere, but the manufacture of semiconductor detectors with a spherical (or globular) sensitive region is an extremely difficult technical problem.

This paper describes test results for several laboratory and commercial models of semiconductor detectors of varying construction. One of them was a surface-barrier silicon detector with a sensitive surface in the form of a hemisphere 2 mm in diameter joined to a cylinder 3 mm high. The technology of its preparation is given in [4]. A second sensor was made of two gold–silicon detectors of planar construction connected in parallel with the sensitive surfaces facing in opposite directions. Detectors $4 \times 8 \times 1$ mm in size were manufactured from silicon with a specific resistance of $6 \cdot 10^3$ Ω-cm. The choice of such a system was dictated by consideration of the comparative simplicity of its manufacture. Commercial models of semiconductor detectors were tested in addition to the specified detectors prepared under laboratory conditions. There are well-

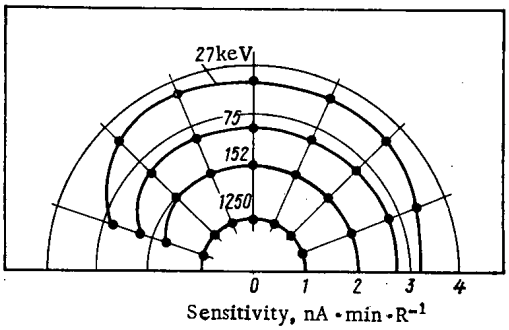

Fig. 1. Dependence of dose sensitivity of a spherocylindrical detector on angle between beam direction and detector axis.

Translated from Atomnaya Énergiya, Vol. 42, No. 3, pp. 207-208, March, 1977. Original article submitted September 15, 1975.

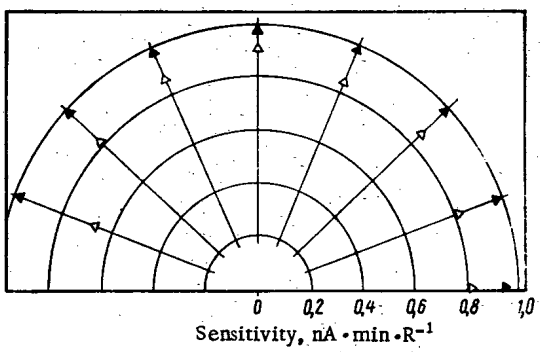

Fig. 2. Spatial characteristic of spherocylindrical detector measured after compensation for "energy dependence:" △) 27 keV; ▲) 1250 keV.

known attempts of a number of investigators [5, 6] to use detectors of commercial manufacture in the dosimetry of x-ray and γ radiation, the main purpose of which was radiometric and spectrometric measurements [7]. However, the spatial properties of such detecors were not discussed.

In the present work, type DDS-5/2A diffusion-drift silicon detectors with a sensitive region 5 mm in diameter and 2 mm thick were tested. The ratio of the dimensions of the sensitive region for such a detector correspond to the requirement for isotopy to a greater degree than in the majority of other known commercial modifications. In addition, for purposes of comparison, a detector model differing from the DDS-5/2A only in the thickness of the sensitive region, which was 0.22 mm, was tested.

The specified detectors were placed in the field of a standardized beam of x-ray and γ radiation. Measurements of the short-circuit current generated by the radiation were made for various orientations of the detector axis with respect to the direction of the beam and for photon energies of 0.03-1.25 MeV. The measurements were used to construct curves for the dependence of the current, normalized to the exposure dose rate, on the angle between the axis of the detector and the direction of the beam. The dependence obtained for the spherocylindrical detector is shown in Fig. 1. As is clear from Fig. 1, the detector current varies with photon energy, which is associated with the significant "energy response" characteristic of silicon detectors with respect to the exposure dose. Compensation of the "energy response" to a value not more than ±10-15% was achieved by means of sample metal filters predominantly of lead and copper.

Definitive measurements made it possible to establish that the DDS-5/2A detector was isotropic with respect to dose sensitivity within a solid angle of 1.7π while the analogous detector 0.22 mm thick was isotropic only within the solid angle 0.6π. Radial anisotropy was strongly expressed in the composite detector. Thus, a reduction in sensitivity by 40% of the maximum value was noted for photons with energies of 0.03-0.07 MeV. The use of detectors with thicker sensitive regions in combination with special filters made it possible to reduce the anisotropy. The spherocylindrical detector has the best spatial properties. As shown in Fig. 2, the dose sensitivity falls within the limits 0.8-1.0 nA · min · R^{-1} within the angle $0-0.75\pi$. Taking the axial symmetry of the detector into consideration, this means the isotropy of its sensistivity covers a solid angle of 3.3π.

Thus, data were obtained for the spatial properties of DDS-5/2A detectors that will make it possible to make a sounder choice of these detectors in the future for specific dosimetric studies. The measurements performed demonstrated the comparatively good isotropy of a spherocylindrical detector which, together with high spatial resolution, furnishes the prerequisites for its application to the solution of a broad group of problems in the dosimetry of x-ray and γ radiation, including measurements in fields with a high dose-rate gradient characterized by a significant contribution from scattered radiation or created by a set of distributed sources.

LITERATURE CITED

1. A. N. Krongauz et al., Semiconductor Detectors in the Dosimetry of Ionizing Radiation [in Russian], Atomizdat, Moscow (1973).
2. R. Parker and B. Morlye, in: Proceedings of the IAEA Symposium – Solid State and Chemical Radiation Dosimetry in Medicine and Biology, Vienna, Oct. 3-7, p. 167.
3. A. A. Petushkov and V. A. Manchuk, Med. Radiol., No. 11, 52 (1971).
4. A. A. Petushkov, V. A. Manchuk, and Yu. F. Pryakhin, Prib. Tekh. Eksp., No. 1, 51 (1975).

5. E. L. Stolyarova, S. N. Volodin, and V. V. Samerov, Vopr. Dosim. Zashch., No. 11, 168 (1970).
6. Yu. M. Larioshin et al., Med. Radiol., No. 10, 70 (1971).
7. R. S. Reznikov and Yu. P. Sel'dyakov, Commercial Semiconductor Detectors [in Russian], Atomizdat, Moscow (1975).

DISPERSIVENESS OF RADIOACTIVE AEROSOLS AT THE NOVOVORONEZH NUCLEAR POWER STATION

S. S. Chernyi, V. P. Grigorov, V. I. Stepchenkov, and V. N. Kirichenko

UDC 621.039.58:541.182.2

Information about the dispersiveness of aerosols is required for rational organization of an air-cleaning system and for ensuring representative sampling of the aerosols. Unfortunately, there is practically no information about the dispersiveness of aerosols at nuclear power stations. In this paper, a study is made of the dispersiveness of radioactive aerosols in the main ventilation systems of the third and fourth units at the Novovoronezh Nuclear Power Station (Table 1).

A six-cascade impactor (sixth cascade is an AFA-RMP filter) was used as a measuring instrument. The backings of the impactor were covered by a thin layer of AFA-B filter (Petryanov tissue of mass 10-20 mg). The efficiency for "adhesion" of aerosol particles to such backings is satisfactorily high [1]. The flow rate of air passing through the impactor was 10 liters/min. Samples were collected over a period of 5-6 days; the β activity of aerosol particles collected on the backings was determined by means of standard radiometric equipment after a holding time of 1 day.

It is well known that the size distribution of particle activity is most often described by the log-normal distribution

$$\varphi(\lg\delta)=\frac{1}{\sqrt{2\pi}\lg\sigma_g}\exp\left[-\frac{(\lg\delta-\lg\delta_g)^2}{2\lg^2\sigma_g}\right], \quad (1)$$

where δ is the diameter of an aerosol particle; δ_g is the average geometric diameter of the particle; σ_g is the rms deviation of $\log\delta$ from $\log\delta_g$. The log-normal distribution is completely determined by the parameters δ_g and σ_g. The determination of these parameters was also a purpose of this study.

The method described in detail in [2] was used to analyze the results. An impactor separates aerosol particles into separate dispersive fractions in accordance with their aerodynamic diameters.

The aerodynamic diameter δ_a of the particles is determined by the condition

$$\rho_0\delta_a^2=\rho\delta^2, \quad (2)$$

where ρ is the density of the particle material, g/cm^3; ρ_0 is unit density, which is 1 g/cm^3.

Results of the studies of radioactive aerosols in ventilation systems (see Table 1) showed that the distribution of particle mass and activity with respect to aerodynamic size is rather well described by a log-normal law. The averaged parameters for the distributions are given in Table 2 along with values for mean mass concentrations. The parameters of the distributions of particle mass and activity with a respect to size do not agree, which is evidence of the association of radioactive materials with fractions of a given dispersiveness.

The change in the ratio of relative activity of individual dispersive fractions of aerosols with sample holding time after collection is of interest.

An analysis of the data obtained indicates that a constant ratio between the activities of individual dispersive aerosol fractions is established after a sample holding time of 5 h. It is also clear that a

Translated from Atomnaya Énergiya, Vol. 42, No. 3, pp. 208-209, March, 1977. Original article submitted March 9, 1976; revision submitted November 3, 1976.

TABLE 1. Main Ventilation Systems of Units and Sampling Points

Ventilation system	Purpose	Aerosol filters present	Sampling points
Stack	Discharge of air into the atmosphere	No	—
B-1	Ventilation of central hall for units III and IV		Collector
4B-2	Ventilation of sealed, unserviced areas of unit IV	Yes	Before aerosol litters
B-3	Ventilation of semiserviced areas of technical equipment in units III and IV		
4B-4	Ventilation of electric motors of main circulating pump and main restricted areas of unit IV		

TABLE 2. Aerosol Distribution with Respect to Aerodynamic Size

Ventilation system	Parameters of log-normal distribution				mean mass concn., mg/cm^3
	particle activity		particle mass		
	$\delta_{a\,g}$, μ	$\sigma_{a\,g}$	$\delta_{a\,g}$, μ	$\sigma_{a\,g}$	
Stack	3,9	2,0	0,5	3,5	0,042
B-1	3,8	2,3	1,1	2,3	0,086
4B-2	1,4	2,3	1,0	3,0	0,017
B-3	1,2	2,2	1,0	1,9	0,048
4B-4	0,9	2,6	0,9	2,9	0,069

*Samples were collected over a period of 10 days for the determination of the parameters of the particle mass distribution with respect to size.

significant portion of the short-lived radionuclides with half-lives less than 1 h is associated with aerosol particles having a diameter less than 1 μ. A similar pattern is also observed in the 4B-4 system. For the other ventilations systems studied, this phenomenon is observed to an extremely insignificant extent and changes do not occur in the ratios between the activities of individual dispersive aerosol fractions.

The authors thank M. A. Baranov, V. I. Kazakov, and S. M. Pankova for help rendered during the study.

LITERATURE CITED

1. A. A. Rusanov and S. S. Yankovskii, in: Impactors for Determination of Dispersiveness of Industrial Dusts [in Russian], Ser. Commercial and Sanitary Purification of Gases, Izd. TsNIITÉNeftekhim, Moscow (1970), p. 30.
2. O. M. Zaraev, B. N. Rakhmanov, in: Scientific Papers of the Institutes for the Protection of Labor [in Russian], No. 71, VTsSPS, Profizdat, Moscow (1971), p. 53.

TITANIUM ALLOYS AS STRUCTURAL MATERIALS FOR LIQUID METAL RADIATION LOOPS

D. M. Zakharov

UDC 669.295.018:669.87

The successful development of radiation loops requires investigations of the resistance of structural materials in liquid metal γ carriers. Titanium alloys are prospective structural materials. The resistance of the titanium alloys VT1-1, VT-6, and VT-14 in liquid indium and in an indium–gallium alloy of 20.5 wt. % indium at 350°C were studied in [1, 2]. Corrosion rates were measured in static tests which lasted 400 h or less.

In the present paper we report on a continuation of the previous studies: corrosion rates are measured in prolonged static tests of samples at 350 and 420°C, and the effect of atmospheric oxygen on the corrosion rate is estimated.

The passivation and testing procedures, data on the materials used, the chemical analysis etc. are given in [1, 2].

The corrosion rate is calculated from the equation

$$K = 0.1\,(V\rho_1 c)/(S\rho_2 t),$$

where K is the corrosion rate in mm/h, ρ_1 and ρ_2 are, respectively, the densities of the liquid metal medium and the solute in g/cm^3, c is the concentration of the solute in wt. %, and t is the duration of the test in hours. The parameter V/S is the ratio of the volume of the liquid metal medium to the surface of the sample. The experimental data obtained are listed in Table 1 which shows for comparison the results of [1] for short tests. In all cases the system consisting of structural material and liquid metal medium was not evacuated. The following conclusions can be drawn from Table 1.

1. The corrosion rate of titanium alloys in liquid indium is practically independent of passivation. Under identical temperature conditions the corrosion rates of various titanium alloys are nearly the same. As the length of the test is increased the concentration of titanium C_{Ti} in liquid indium increases insignificantly, and the corrosion rate of titanium alloys tends to decrease. The corrosion rate is not increased when the temperature of the test is raised to 420°C.

2. At 350°C in the indium–gallium alloy medium the corrosion rate K of passivated titanium VT1-1 is 25 times lower than that of a nonpassivated sample. This results from the protective effect of the TiO_2 oxide film which, however, develops only in the short tests (400 h). Under the prolonged action of the indium–gallium alloy (up to 1000 h and more) the oxide film is destroyed and the corrosion rate is increased appreciably.

3. Passivation does not have an appreciable effect on the solubility of the VT-6 and VT-14 titanium alloys in the indium–gallium medium. This may be due to the low oxidizability of the alloyed titanium and to other causes [1, 2].

Increasing the duration of the test of the VT-6 and VT-14 samples to 1000 h has practically no effect on the titanium content in the indium–gallium alloy.

4. The solubility of titanium alloys in the indium–gallium medium is higher than in indium, but in all the cases examined the titanium content is considerably below the maximum solubility at the corresponding temperatures [2].

In order to estimate the effect of atmospheric oxygen on the corrosion rate of titanium alloys, tests were performed on passivated and nonpassivated VT1-1 and VT-14 samples in special samples at a residual pressure of $5 \cdot 10^{-3}$ mm Hg. The results of the tests are shown in Table 2.

Translated from Atomnaya Énergiya, Vol. 42, No. 3, pp. 210-212, March, 1977. Original article submitted April 12, 1976.

TABLE 1. Concentration of Titanium in Indium and in Indium–Gallium Alloy, and Corrosion Rate of Titanium Alloys

Liquid metal medium	Nonpassivated sample						Passivated sample						Duration of test, h
	VT-1; V/S=2		VT-6; V/S=4		VT-14; V/S=4		VT-1; V/S=2		VT-6; V/S=4		VT-14; V/S=4		
	350	420	350	420	350	420	350	420	350	420	350	420	
	°C												
Indium–gallium alloy	0,8* / 5,6	—	0,43 / 6,0	—	0,38 / 5,3	—	0,03 / 0,21	—	0,38 / 5,3	—	0,29 / 4,4	—	400[1]
	0,7 / 1,94	—	0,8 / 4,47	—	0,4 / 2,24	—	0,3 / 0,84	—	0,94 / 5,2	—	0,21 / 1,22	—	1000
Indium	0,067 / 4,4	—	0,03 / 3,8	—	0,014 / 1,8	—	0,026 / 1,7	—	0,015 / 1,9	—	0,028 / 3,7	—	50[1]
	0,13 / 0,42	—	0,07 / 0,45	—	0,093 / 0,6	—	0,1 / 0,32	—	—	—	—	—	1000
	0,17 / 0,16	0,15 / 0,14	0,1 / 0,19	0,24 / 0,45	0,18 / 0,33	0,23 / 0,43	0,1 / 0,1	0,1 / 0,1	0,17 / 0,31	0,16 / 0,3	0,14 / 0,26	0,16 / 0,3	3500

*Here and in Table 2 the numerator is $C_{Ti} \cdot 10^2$ wt.%, and the denominator is $K \cdot 10^6$ mm/h.

TABLE 2. Titanium Concentration and Corrosion Rate of Titanium Alloys in Indium and in an Indium–Gallium Alloy in Vacuum Tests at 350°C

Liquid metal medium	Nonpassivated sample		Passivated sample		Duration of test, h
	VT-1; V/S = 2	VT-14; V/S = 4	VT1-1; V/S = 2	VT-14; V/S = 4	
Indium–gallium alloy	0,05 / 0,14	0,1 / 0,56	0,026 / 0,073	0,06 / 0,35	1000
Indium	0,026 / 0,025	0,075 / 0,14	0,03 / 0,03	0,075 / 0,14	3500

In evacuated and unevacuated ampuls the corrosion rate of titanium alloys in prolonged tests does not depend on passivation (Tables 1 and 2), but is appreciably lower in evacuated ampuls. This effect of atmospheric oxygen can be accounted for by thermodynamic considerations. According to data in [3], over a wide range of temperatures titanium has an appreciably larger affinity for oxygen than do gallium and indium, since the change in the Gibbs free energy in the formation of TiO_2 (rutile) is much smaller than in the formation of Ga_2O_3 and In_2O_3, the most stable gallium and indium oxides. Therefore, the titanium in liquid indium and in the indium–gallium alloy is able, under certain conditions, to attach the dissolved oxygen. Thus, in unevacuated ampuls at a high temperature an oxide film is formed on the surface of the indium and the indium–gallium alloy, and simultaneously oxygen is dissolved in the liquid metal. Under these conditions various processes can develop which lead to the formation of TiO_2: the intense reduction of gallium and indium oxides by dissolved titanium, the interaction of dissolved titanium with dissolved oxygen, etc., which ultimately decreases the concentration of dissolved titanium in the liquid metal medium and thus stimulates the further solution of titanium alloys with an increase in the total titanium content (dissolved titanium and combined titanium of the dioxide) in the melt.

In the evacuated ampuls, these processes for forming TiO_2 are weaker, and therefore the titanium concentration is lower.

It should be noted that in testing the titanium samples a characteristic grayish-bronze film is formed on the surface of the indium and the indium–gallium alloy only in the unevacuated ampuls. The x-ray structural analysis of the film indicates that it is complex in composition, and definitely establishes the presence of the

TiO_2 phase with the rutile structure, which agrees with the reasons stated for the intense oxidation of titanium in liquid indium and the indium–gallium alloy in unevacuated samples. The presence of TiO_2 in the surface film is explained by the low density of TiO_2.

From experience with the construction and use of radiation loops it is known that under strictly equivalent conditions an indium–gallium alloy is more fluid when circulating in titanium pipelines than in 1Kh18N9T stainless steel pipelines. This results from the fact that over a wide range of temperatures the change in the Gibbs free energy is larger in the formation of Fe_2O_3 than in the formation of the oxides Ga_2O_3 and In_2O_3 [3], and therefore in stainless-steel pipelines gallium and indium will be oxidized as a result of the reduction of the Fe_2O_3 film which is always present on a steel surface. It is known [4] that gallium and indium oxides are easily wetted by an indium–gallium alloy, and therefore with an increase in the oxide content a pasty viscous mass composed of oxides and alloy appears, greatly impairing the fluidity of the γ carrier. On the contrary, titanium can reduce the gallium and indium oxides contained in the liquid metal; i.e., in titanium pipelines an indium–gallium alloy will be cleansed of gallium and indium oxides which are present or produced.

Thus, titanium alloys have very diverse favorable properties as structural materials for radiation loops. The negligible dissolving of titanium alloys does not give rise to problems of the contamination of the γ carrier. An important role is played by the decrease in oxide content of a γ carrier circulating in titanium pipelines, and this contributes to an increase in fluidity. Here it should be stated that there are serious doubts about the expediency of preliminary passivation of titanium alloys, in particular, the VT1-1 alloy used in radiation piping. First of all passivation is effective only for a short contact with γ carriers, and secondly the presence of a passivating film has the undesirable effect of lowering the ability of titanium to reduce gallium and indium oxides.

The authors thank S. P. Yatsenko for all-around assistance, and Z. P. Danelyan for help with the experiments.

LITERATURE CITED

1. D. M. Zakharov et al., At. Energ., 35, No. 3, 202 (1973).
2. S. P. Yatsenko et al., Fiz.-Khim. Mekh. Mat., 10, No. 2, 51 (1974).
3. U. D. Peryatin, V. P. Mashirev, and N. G. Ryabtsev, Thermodynamic Properties of Inorganic Materials [in Russian], Atomizdat, Moscow (1965).
4. D. M. Zakharov, At. Energ., 39, No. 4, 290 (1975).

USE OF PERTURBATION THEORY FOR EXPERIMENTAL STUDY WITH A PULSED NEUTRON SOURCE

V. Ya. Pupko, V. A. Tarasov, and A. K. Sharapov

UDC 621.039.519.4

Along with the extensive use of perturbation theory for the effective neutron multiplication coefficient (k_{eff}), perturbation theory for the eigenvalue of the quasistationary transport equation for prompt neutrons,

$$-(\alpha/v)\varphi = -[\Omega, \nabla\varphi(\mathbf{r}, E, \Omega)] + \hat{\Sigma}\varphi + \hat{Q}\varphi \quad (1)$$

is extremely effective in connection with the development of pulsed methods for measurement of the neutron-physics characteristics of systems.

The operators $\hat{\Sigma}$ and $\hat{Q}$ are of the well-known form where $\hat{Q}$ characterizes neutron production. The real eigenvalue of the equation of least modulus can be measured experimentally. It is the asymptotic damping decrement for the density of prompt neutrons after injection of a neutron pulse into a system, where the density of neutrons in the system decreases exponentially in time [1, 2].

Translated from Atomnaya Énergiya, Vol. 42, No. 3, pp. 212-214, March, 1977. Original article submitted April 30, 1976.

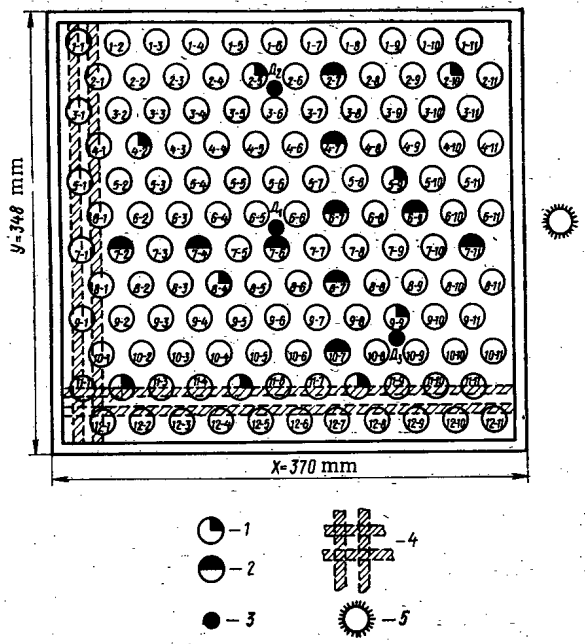

Fig. 1. Loading chart and arrangement of experimental points: 1) group of nine cells for measurement of perturbations in a subcritical reactor; 2) measurement points for distributions in a critical reactor; 3) detectors; 4) expanders for measurement of lateral leakage factors; 5) target of neutron generator.

Perturbation theory for α, in contrast to perturbation theory for K_{eff}, can be applied to multiplying and nonmultiplying systems. With the aid of this theory, it is convenient to measure such parameters as lifetime and generation times of prompt neutrons, the coupling between change in system composition and change in system size, the average neutron diffusion coefficient, the cross section for a 1/v absorber, etc. It was shown [2] that the solution of the nonstationary neutron transport equation can be obtained by expanding its solution in terms of the eigenfunction of the quasistationary Eq. (1), which makes it possible to be able to find the solution of that equation. The constants and method of calculation for that equation should, in principle, be determined in more accurate fashion from the results of studies of nonstationary neutron flow; this is conveniently done by means of pulsed experiments. The perturbation theory for α yields a system of functionals which can be used for this purpose.

The present work presents measurement results for several functionals, evaluates measurement accuracy as a function of the subcriticality of a system, and verifies the theoretical relations in perturbation theory.

Perturbation theory for α was described in [3, 4]; several problems of the experimental studies based on it were described in [5, 6] and in the compilation [2]. It was found that for a variation of the medium constants $\delta\Sigma = \Sigma' - \Sigma$, the variation of the decrement was

$$\delta\alpha = -\frac{(\varphi^+, \delta\hat{\Sigma}\varphi) + (\varphi^+, \delta\hat{Q}\varphi)}{(\varphi^+, 1/v\varphi)}, \tag{2}$$

and for a geometrically similar variation in the dimensions of the system

$$\delta\alpha = \frac{\delta R}{R}\frac{[\varphi^+(\Omega, \nabla\varphi)]}{(\varphi^+, 1/v\varphi)}, \tag{3}$$

where R is a characteristic dimension of the system. Here, $\varphi(\mathbf{r}, E, \Omega)$ is a solution of Eq. (1); $\varphi^+(\mathbf{r}, E \cdot \Omega)$ is a solution of the adjoint equation and the parentheses denote integration over all variables.

We introduce some definitions [7]. The limit of the sum over the volume of the system of the perturbation $\delta\alpha$ resulting from the replacement of the material of density ρ_0^* in a volume $\Delta V \to 0$ by a void is η – the total effectiveness index for system index for system material with respect to α. From Eq. (2) we have

*ρ_0 is the density of a mixture of different nuclei, the ratios between which are unchanged.

TABLE 1. Results from Measurements of Perturbations of the Damping Decrement

Quantity determined	Reactor height, cm		
	27,0	19,2	12,8
K_{eff} *	1,0064	0,8654	0.6714
α, sec^{-1}	312±2	4050±40	8715±200
η, sec^{-1}	24850±300	17850±1000	9950±2000
$(\eta+\alpha)/3$, sec^{-1}	8390±100	7300±300	6220±700
ω, sec^{-1}	8380±100	7540±200	5870±400
T, μsec	29,3±0,3 (30,3) *	30,1±0,7	53,3±6,0
l, μsec	29,1±0,3	27,8±0,6	36,4±3,0
$\langle \nu DB^2 \rangle$, cm^{-1}	12580±150	10950±500	9300±1000
Measurement error, %	1—1,2	2,5—5,6	10—20

*Calculated data taken from [5, 6].

$$\eta = \lim_{\substack{V \\ \Delta V \to 0}} \sum (\Delta\alpha)_\rho = -\frac{1}{\rho_0} \frac{\int_{\rho_0}^{0} \delta\rho \, [(\varphi^+, \hat{\Sigma}\varphi) + (\varphi^+, \hat{Q}\varphi)]}{(\varphi^+, 1/v\varphi)}. \quad (4)$$

Assuming that shielding of the system material is small, the dependence on ρ in the numerator of Eq. (4) disappears. In that case

$$\eta = \frac{(\varphi^+, \hat{\Sigma}\varphi) + (\varphi^+, \hat{Q}\varphi)}{(\varphi^+, 1/v\varphi)} = -\rho_0 (\partial\alpha/\partial\rho)_V. \quad (4a)$$

The neutron leakage factor with respect to α is determined from the variation of the decrement for geometrically similar variations in the dimensions of the system:

$$\omega = -\lim_{\Delta V \to 0} V_0 (\Delta\alpha/\Delta V) = -V_0 (\partial\alpha/\partial V)_\rho.$$

V_0 is the original volume of the system. In the general case [7],

$$\omega = \frac{1}{3} \frac{[\varphi^+ (\Omega, \nabla\varphi)]}{(\varphi^+, 1/v\varphi)}. \quad (5a)$$

Between η and ω there is the relation

$$\omega = \frac{1}{3}(\eta + \alpha). \quad (6)$$

For poisoning of a system by a 1/v absorber, $\delta\Sigma = \delta\rho_a(\sigma_{kT} v_{kT}/v)$, hence we have from Eq. (3)

$$\delta\alpha = \delta\rho_a \sigma_{kT} v_{kT}, \quad (7)$$

which makes it possible to determine the cross section of a 1/v absorber at the neutron energy kT.

With replacement of the fuel by an equivalent absorber ($\delta\hat{\Sigma} = 0$, $\delta\hat{Q} = Q$) [4, 5], we have

$$\lim_{\Delta V \to 0} \sum_V (\delta\alpha)_{e \cdot a} = \frac{(\varphi^+, \hat{Q}\varphi)}{(\varphi^+, 1/v\varphi)}. \quad (8)$$

Equation (8) makes it possible to determine the average prompt-neutron generation time $T = (\varphi^+, 1/v\varphi)/(\varphi^+, \hat{Q}\varphi)$. The average prompt-neutron lifetime $l = (\varphi^+, 1/v\varphi)/[\varphi^+, (\Omega, \nabla\varphi)] - (\varphi^+, \hat{\Sigma}\varphi)$ can be determined from the relation [1, 2]

$$\alpha = (1/l) - (1/T). \quad (9)$$

In the diffusion approximation [4],

$$\eta + \alpha = 3\omega = -2(\varphi^+, D\nabla^2\varphi)/(\varphi^+, 1/v\varphi). \quad (10)$$

For a system without a reflector,

$$\eta + \alpha = 3\omega = 2\langle \nu DB^2 \rangle. \quad (11)$$

The averaging is performed with a weight $(\varphi^+, 1/v\varphi)$.

The measurements were made in a heterogeneous uranium–water reactor without reflector in the shape of a parallelepiped having fuel elements of highly enriched uranium 10 mm in diameter arranged with a 32-mm

spacing [5] (see Fig. 1). Subcriticality was varied by variations in the height of the reactor. The equipment used and the method for determination of α were similar to those described earlier [2, 5, 6].

The results of the measurements are presented in Table 1. To determine the effectiveness index, we measured the perturbation resulting from the replacement of the volume of an equivalent cell by a void with subsequent summation over the volume of the reactor. The replacement was performed with consideration given to the symmetry of the reactor with respect to a single cell in a critical reactor or with respect to a group of several cells in the subcritical state of the reactor (see Fig. 1). The leakage factor was measured by sequential variation of the dimensions of the reactor along the three directions. In this case, $\omega = (1/3)(\omega_X + \omega_Y + \omega_Z)$ for a parallelepiped assuming separation of variables, where $\omega_{X,Y,Z}$ are the leakage factors along the individual directions defined as $\omega_X = -X(\partial\alpha/\partial x)_\rho$ for changes in the X dimension, etc. A measurement with removal of a complete cell, i.e., fuel and moderator simultaneously, takes into account shielding of system materials within a cell in accordance with Eq. (4).

A mixture of boron and aluminum oxide powders was used as an equivalent absorber. The correction for the discrepancy between the cross section of this material and that of the fuel, which is 0.035, was taken from [5]. The reactor was poisoned with boric acid in both the critical and subcritical states. For boron, $\sigma_{kT} = 738 \pm 20$ b.

The experimental data confirms the theoretical relation (6). This fact opens up additional possibilities for experimental studies, for example, to measure the total effectiveness index of the materials with respect to changes in the size of the system. The results point to the possibility of measuring the functionals in the perturbation theory for α and a number of neutron-physics parameters of systems at varying subcriticalities.

LITERATURE CITED

1. Proceedings of the IAEA Symposium – Pulsed Neutron Research, Karlsruhe, May 1-14, 1965, Vols. I and II.
2. V. V. Orlov and É. A. Stumbura (editors), in: Theoretical and Experimental Problems of Nonstationary Neutron Transport [in Russian], Atomizdat, Moscow (1972).
3. E. Pendlebury, Proc. Phys. Soc., A68, 474 (1955).
4. V. Ya. Pupko, Preprint FEI-103, Obninsk (1968).
5. B. I. Kolosov et al., At. Energ., 32, 579 (1972).
6. E. A. Stumbur et al., in: Transactions of the Power Physics Institute [in Russian], V. A. Kuznetsov (editor), Atomizdat, Moscow (1974), p. 138.
7. V. Ya. Pupko and R. M. Strutinskii, in: Transactions of the Power Physics Institute [in Russian], V. A. Kuznetsov (editor), Atomizdat, Moscow (1974), p. 174.

X-RAY SPECTROMETER WITH AN Si(Li) DETECTOR

M. Vidra

UDC 535.853

In the usual charge-sensitive preamplifiers used to amplify signals from a semiconductor detector, a resistance which connects the gate of the field-emission transistor (FET) and the output of the preamplifier is used to set the dc mode at the input of the FET. In addition to Johnson noise ($du_n = 2kTKdf$), however, this resistance contributes an extra noise component which drops like $1/f^{\alpha}$ with increase in frequency. The cause of this extra noise is the imperfect structure of the resistance.

A preamplifier has been described [1] in which the resistive feedback was replaced by an electro-optical feedback. Preamplifier noise was significantly reduced because of elimination of the resistance in the gate circuit and through the reduction in distributed input capacities. Another form of nonresistive feed back was described in [2]. To compensate for the detector current (i.e., inverse current and the current induced by recorded radiation), they used both the gate current of the FET and its dependence on the voltage between the source and drain (the gate current rises exponentially as the voltage between these electrodes increases). The noise does not exceed 100 eV in such preamplifiers using Si(Li) detectors with a sensitive surface having an area of 12 mm^2. When making measurements, quasi-Gaussian shaping of electrical signals was used with a time constant of several tens of microseconds.

In the preamplifier of the spectrometer, drain feedback was used, which is somewhat simpler than the electro-optical feedback and permits the achievement of identical results. Electrical signals from the detector (Fig. 1) were fed into the gate of the FET (type 2N/4416) and then into the input of the amplifier (A_1). Feedback of the ac component was accomplished through the capacity $C_f = 0.15$ nF. A signal was taken from the ouptut of A_1 for control of the drain–source voltage U_{d-s}. An integrator was used to eliminate oscillations in the drain–source voltage control circuit.

With an increase in detector current, because of radiation for example, the average value of the voltage at the output of A_1 rises and the U_{d-s} voltage is correspondingly increased. The rise in this voltage produces an increase in the gate current of the FET. The reverse process occurs with a drop in detector current. In this way, equilibrium between detector current and data current is ensured; the preamplifier is in an operating state at all times. The rest of the spectrometer is constructed in the standard manner.

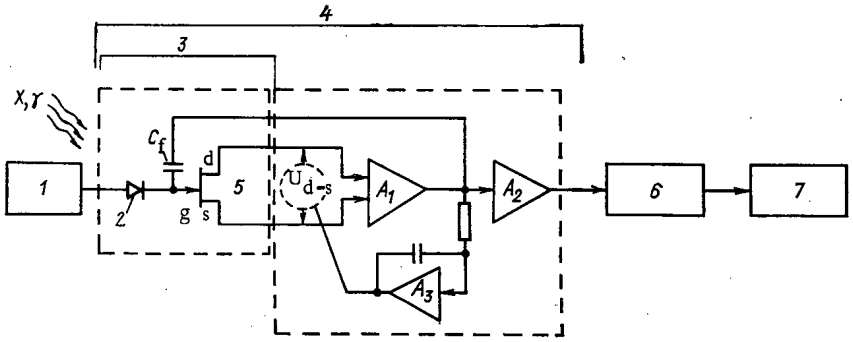

Fig. 1. Block diagram of the spectrometer; 1) detector supply; 2) detector; 3) cooled portion of preamplifier with detector; 4) preamplifier; 5) FET; 6) pulse-shaping amplifier; 7) multichannel pulse-height analyzer; d) drain; s) source; g) gate.

Institute of Nuclear Research, Rzhezh, Czechoslovakia. Translated from Atomnaya Énergiya, Vol. 42, No. 3, pp. 214-215, March, 1977. Original article submitted May 10, 1976.

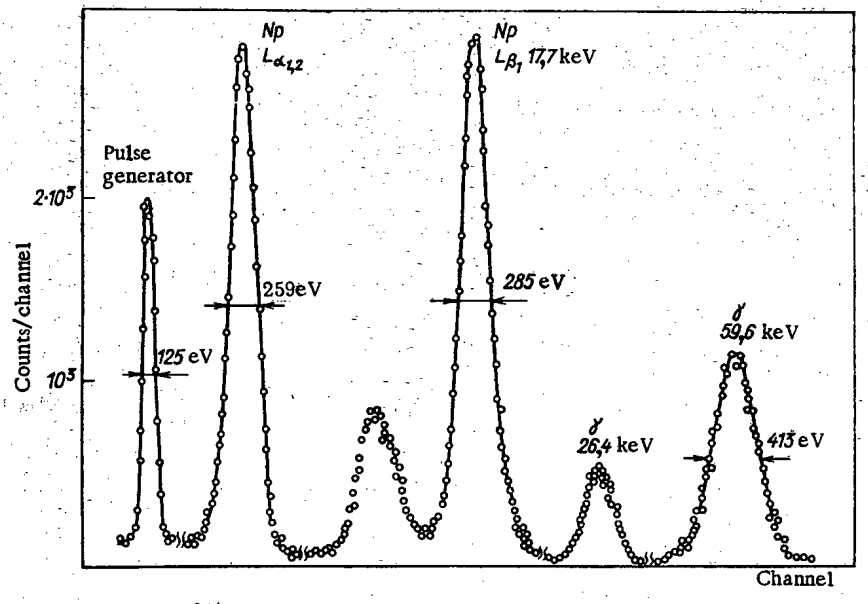

Fig. 2. ^{241}Am spectrum (pulse-shaping time, 9 μsec, detector voltage, 300 V).

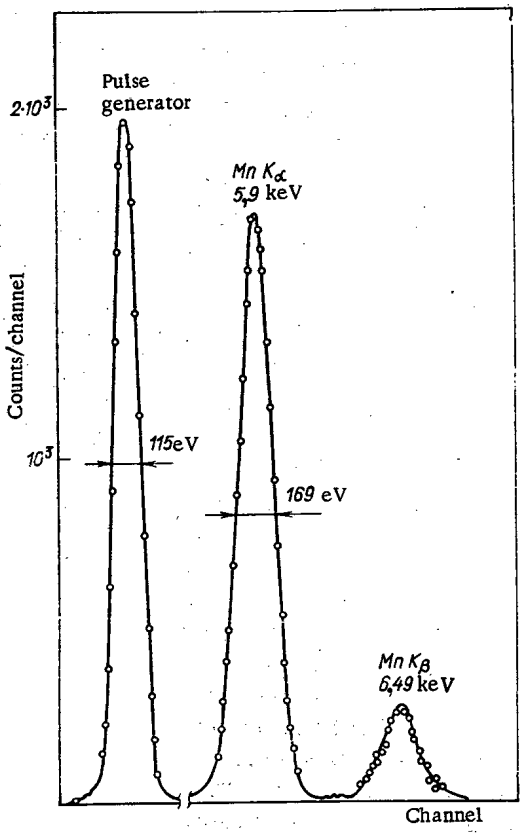

Fig. 3. ^{55}Fe spectrum (pulse-shaping time, 14 μsec, detector voltage, 300 V).

For radiation detection, an Si(Li) detector was used which had a sensitive region 5 mm in diameter and a compression layer 3 mm thick. Like results were obtained with detectors manufactured in Czechoslovakia and East Germany. The detector, together with the FET and elements of the feedback circuit, was placed in a cryostat with a beryllium entrance window 200 μ thick.

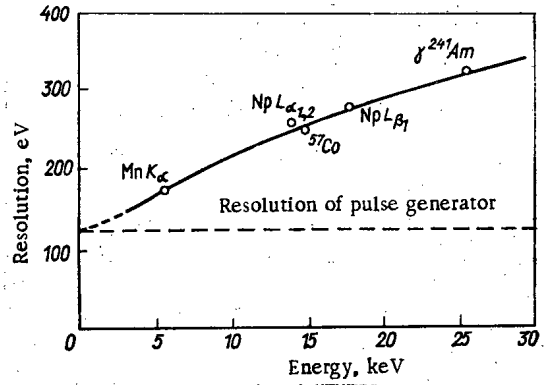

Fig. 4. Energy dependence of spectrometer energy resolution.

A portion of the radiation spectrum from ^{241}Am is shown in Fig. 2 (energy region is ≈ 11-60 keV). The ^{55}Fe spectrum obtained with the use of this detector is shown in Fig. 3. An instrumental resolution of 169 eV was obtained at 5.9 keV (Mn K_α line). An approximate dependence of energy resolution on radiation energy is shown in Fig. 4 for pulse-shaping with a time constant of 8 μsec.

LITERATURE CITED

1. F. Goulding et al., Nucl. Instrum. Methods, 71, 273 (1969).
2. E. Elad, Nucl. Sci., NS-19 No. 1, 403 (1972).

FLOW CHARACTERISTICS FOR HOT WATER AT AN INITIAL PRESSURE OF 22.8 MPa ESCAPING INTO THE ATMOSPHERE

D. A. Khlestkin, V. P. Kanishchev, and V. D. Keller

UDC 621.039.58:621.311.25:530.91

Analysis results for emergencies occurring through leakage in the first loop in a nuclear power station are very much dependent on the values assumed for the water flow rate and the composition of the water–steam mixture.

Calculations on critical flow rate are currently based on trends derived from experimental systems; measurements have been reported [1] for the specific critical flow rate for values of the initial parameters up to the critical level (T = 647.15°K, p = 22.5 MPa). The results presented here represent an extension of earlier measurements, and they refine the values for critical flow rate at temperatures near the saturation point, far from the boiling point and at critical and supercritical initial parameters. The measurements were made with equipment previously described [1]. The measurements were supplemented by means of a check thermocouple to indicate the water temperature at the inlet; the tests involved isobaric increase in the water temperature at the inlet. Each working condition was maintained until all the parameters had stabilized. The configuration of the working parts was as before. Cylindrical pipes with sharp inlet edges were used, with diameters of 3.6 mm and a ratio l/d of length to diameter of 0.5, 1,5, or 6.0. The flow factors for the working parts were determined for water at room temperature with an initial temperature of 3-4 MPa, which were measured for L = l/d of 0.5, 1.5, and 6.0. Here μ_p was 0.723, 0.683, and 0.61, respectively. The results were worked up in terms of

Translated from Atomnaya Énergiya, Vol. 42, No. 3, pp. 216-218, March, 1977. Original article submitted May 28, 1976.

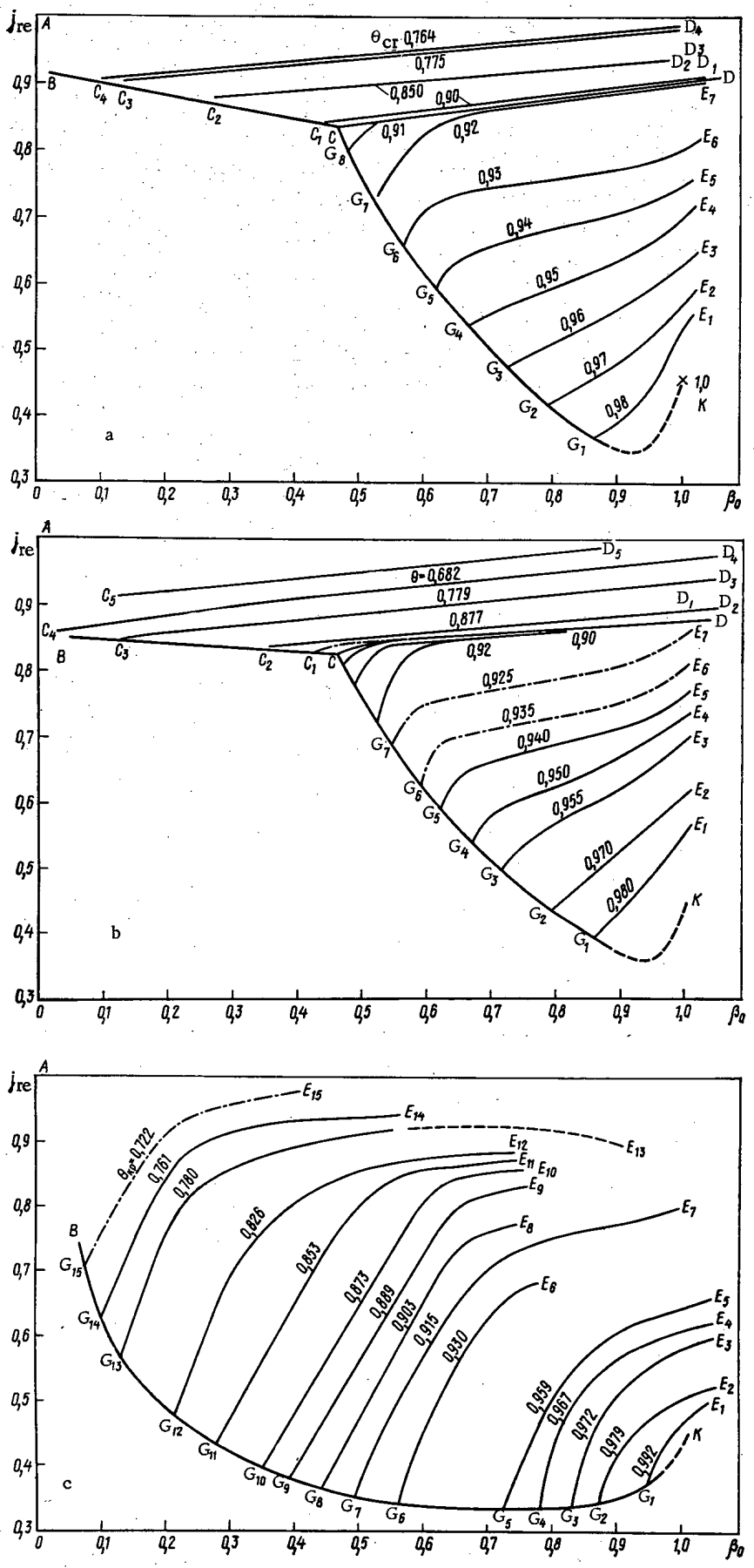

Fig. 1. Relative specific flow rate on leakage to the atmosphere as a function of initial pressure for L = 0.5, μ_h = 0.723 (a); L = 1.5, μ_h = 0.683 (b); L = 6, μ_h = 0.61 (c).

j_{re} against β_0, where $j_{re} = j_{ex}/j_h$, in which j_{ex} is the experimentally measured specific flow rate, while j_h is the specific hydraulic flow rate as determined from the equation $j_h = \mu_h\sqrt{2(p_0 - p_{co})/v}$, where p_0 is the initial water pressure, p_{co} is the counterpressure, and v is the specific volume of water under the initial conditions; $\beta_0 = p_0/p_{cr}$, where p_{cr} is the pressure at the critical point of water. Figure 1 shows the results as $\theta_{cr} = T_0/T_{cr}$ (the relative initial temperature ahead of the working section), where $T_{cr} = 647.3°$ K is the critical point of water.

The following are the reasons for using these relative coordinates: graphical representation indicates the regions of metastable and equilibrium flows, while it is possible to compare the measurements for various initial conditions, and also it is possible to define the flow rate more precisely for the most characteristic state.

Figure 1 shows the relative maximal and critical specific flow rates for pipes having L = 0.5, 1.5, 6.0, respectively; these curves are derived by smoothing numerous measurements, whose maximum coefficient of variation was ±5%. Curves BCK (parts a and b) and BK (part c) correspond to escape of water having the saturation temperature at the inlet to the pipe. Lines C_iD_i and G_iE_i (where i = 1, 2, ...) are isotherms. The further an isotherm from the saturation line, the greater the deviation from the boiling point at the inlet for the particular initial pressure. The relations of L of 0.5 and 1.5 go with the result for L = 6 to reveal characteristic features for the flow in short and relatively long pipes. These features have been observed in less pronounced form previously [1, 2].

Parts a and b of Fig. 1 show that there are two clearly defined major zones. The zone above line BCD represents substantially metastable flow, while DCK corresponds to a considerable reduction in the metastability, and the flow approaches the equilibrium state as the critical point K is approached. The metastable-flow region occurs only for only relatively low-temperature water in the case of L = 6.0, and there is no clear boundary. The flow of water at its saturation point is close to equilibrium at almost all initial pressures. For $\beta_0 \geq 0.85$, the flow characteristics for water near its saturation point for short pipes are almost the same as those for L = 6.0, because in this range the pressure along the spinodal liquid cannot exist. It has previously been supposed [1] that a completely metastable flow occurs for $\beta_0 < 7.0$ MPa, but this is inaccurate. More careful examination has shown that water having the saturation temperature does not pass through the pipe with 100% metastability in this range. Parts a and b of Fig. 1 show that the range BC lies about 15% below the 100% metastability line, which is theline parallel to the abscissa and starting from point A. Our experiments did not produce completely metastable flows under all conditions. The refined flow characteristics for L = 6 indicate that equilibrium flow occurs in this case for $\beta_0 \geq 0.62$ MPa. For instance, it has been reported [3] that the specific flow rate for saturated water is 2.69 kg/m^2 · sec for homogeneous equilibrium model at $P_0 = 14$ MPa. The observed value for these conditions is in the range 2.67-3.0 kg/m^2 · sec.

Therefore, the extended and revised relationships for the specific flow rate should be used in conjunction with the empirical curves reported previously [1].

LITERATURE CITED

1. B. K. Mal'tsev, D. A. Khlestkin, and V. D. Keller, Teploenergetika, No. 6, p. 61 (1972).
2. V. S. Aleshin, Yu. A. Kalaida, and V. V. Fisenko, Abstracts for the Third All-Union Conference on Heat Transfer and Hydraulic Resistance [in Russian], Leningrad (1967).
3. V. A. Zysin (editor), Boiling Adiabatic Flows [in Russian], Atomizdat, Moscow (1976).

MEASUREMENT OF THE RATIO BETWEEN THE CAPTURE AND FISSION CROSS SECTIONS OF ^{239}Pu

V. P. Bolotskii, M. V. Polozov, A. N. Soldatov, and S. I. Sukhoruchkin

UDC 546.799.4:539.172.4.162.2

In order to find the ratio α between the capture and fission cross sections of ^{239}Pu up to 30-keV energy, this quantity has been repeatedly measured in the IBR-30 pulsed fast reactor [1, 2]. In this article we give the final results of the measurements made by the group at the Institute of Theoretical and Experimental Physics (ITÉF). Control values of α obtained before 1972 were published in [2]. The data in [2] are not included in the results of this present article (Tables 1 and 2).

In contrast with the measurements made at the ITÉF up to 1970 [3], we increased the number of detectors to eight, introduced separate registration of γ quanta of different energies in order to allow for possible variations in the shapes of the γ spectra, improved the energy resolution more than tenfold (16 nsec/m), obtained a large number of independent exposures for statistical processing, and made the measurements with a specimen with a much reduced impurity content of other isotopes.

The measurements were made on the 250-m time-of-flight base of the neutron spectrometer of the Laboratory of Nuclear Physics of the Joint Institute for Nuclear Research (LNP JINR) with neutron bursts of about 4 μsec. Fast fission neutrons and capture and fission γ quanta were registered by detectors based on stilbene crystals 7 × 7 cm in size with pulse-shape separator circuits [2]. The flux of incident neutrons was measured by a battery of proportional counters containing enriched boron (SNMO-5). Shielding from neutrons scattered by the specimen was effected by a layer of enriched boron (85% enriched, 2 cm thick), and low-energy γ quanta from the radioactive specimen were attenuated by a layer of lead 1 cm thick. For protection from γ quanta and

TABLE 1. Results of Measurement of α for ^{239}Pu

Energy range, keV	Specimen 0.64 g/cm² thick	Specimen 1 g/cm² thick	Mean from measurement made in 1973-1974
0,1—0,2	0,88	0,94	0,93±0,13
0,2—0,3	0,89	0,93	0,92±0,08
0,3—0,4	1,21	1,16	1,17±0,08
0,4—0,5	0,53	0,60	0,59±0,04
0,5—0,6	0,66	0,76	0,75±0,11
0,6—0,7	1,58	1,43	1,46±0,18
0,7—0,8	0,94	1,01	1,00±0,10
0,8—0,9	0,74	0,79	0,78±0,11
0,9—1,0	0,77	0,76	0,76±0,12
1—2	0,82	0,85	0,85±0,07
2—3	0,97	0,97	0,97±0,11
3—4	0,77	0,66	0,68±0,12
4—5	0,81	0,88	0,87±0,07
5—6	0,83	0,84	0,84±0,09
6—7	0,78	0,72	0,73±0,13
7—8	0,69	0,75	0,74±0,07
8—9	0,56	0,56	0,56±0,09
9—10	0,36	0,50	0,47±0,10
10—15	0,44	0,49	0,48±0,08
15—20	0,35	0,35	0,35±0,10
10—20	0,40	0,42	0,413±0,071
20—30	0,32	0,36	0,35±0,062

Translated from Atomnaya Énergiya, Vol. 42, No. 3, pp. 218-221, March, 1977. Original article submitted June 7, 1976.

TABLE 2. Comparison of Results in [2, 3, 5] with Present Authors' Data

Energy range, keV	Present authors	[3]	[2]	[5] Gwin	[5] Weston	[6]
0,1—0,2	0,93±0,13	0,88±0,03	0,93±0,14	0,87±0,015	0,871±0,052	0,845±0,077
0,2—0,3	0,92±0,08	1,07±0,04	0,98±0,14	0,94±0,010	0,927±0,056	0,912±0,094
0,3—0,4	1,17±0,08	1,23±0,05	1,15±0,16	1,16±0,014	1,15±0,069	1,15±0,099
0,4—0,5	0,59±0,04	0,45±0,05	0,62±0,13	0,44±0,013	0,426±0,026	0,483±0,058
0,5—0,6	0,75±0,11	0,75±0,05	0,78±0,13	0,72±0,040	0,718±0,043	0,704±0,069
0,6—0,7	1,46±0,18	1,72±0,13	1,58±0,20	1,54±0,040	1,488±0,089	1,673±0,133
0,7—0,8	1,00±0,10	0,94±0,09	1,02±0,15	0,97±0,017	0,890±0,053	0,973±0,087
0,8—0,9	0,78±0,15	0,78±0,09	0,85±0,13	0,82±0,025	0,790±0,047	0,778±0,101
0,9—1,0	0,76±0,12	0,71±0,08	0,93±0,14	0,70±0,026	0,675±0,041	0,717±0,077
0,1—1,0	0,91±0,09	—	0,89	0,86	0,86	—
1—2	0,85±0,07	1,02±0,06	0,95±0,14	0,84±0,013	0,802±0,048	0,927±0,093
2—3	0,97±0,11	1,23±0,08	1,08±0,15	1,00	0,972±0,058	1,108±0,103
3—4	0,68±0,12	0,96±0,11	0,77	0,72±0,066	0,738±0,043	0,895±0,086
4—5	0,87±0,07	0,83±0,10	0,84	0,87±0,040	0,831±0,050	0,821±0,079
5—6	0,84±0,09	—	0,81	0,82±0,046	0,807±0,048	0,867±0,084
6—7	0,73±0,13	—	0,69	0,79±0,040	0,745±0,045	0,816±0,086
7—8	0,74±0,07	0,67±0,07	0,73	0,64±0,022	0,642±0,038	0,629±0,073
8—9	0,56±0,09	—	0,63	0,54±0,022	0,537±0,032	0,575±0,064
9—10	0,47±0,10	—	0,65	0,55±0,022	0,606±0,036	0,617±0,067
1—10	0,748±0,048	0,82±0,07	0,80	0,77	0,76	—
10—20	0,413±0,071	—	—	0,48±0,022	0,486±0,029	0,466±0,05
20—30	0,350±0,062	—	—	0,35±0,018	0,332±0,066	0,373±0,04

Note. In the second column, all the errors except for the range between 1 and 10 keV are statistical.

TABLE 3. Ratios of Variable Background to Total Count in Radiation Channel (0.7 MeV < E_γ < 2.5 MeV) and Fission Channel for Various Neutron Energies

Energy range, keV	Radiation channel	Fission channel	Energy range, keV	Radiation channel	Fission channel
0,1—0,2	0,03	<0,02	3—4	0,26	0,09
0,2—0,3	0,03	<0,02	4—5	0,29	0,10
0,3—0,4	0,05	<0,02	5—6	0,33	0,13
0,4—0,5	0,06	<0,02	6—7	0,39	0,14
0,5—0,6	0,05	<0,02	7—8	0,43	0,15
0,6—0,7	0,08	0,03	8—9	0,49	0,14
0,7—0,8	0,09	0,02	9—10	0,51	0,13
0,8—0,9	0,09	0,03	10—15	0,54	0,16
0,9—1,0	0,10	0,03	15—20	0,60	0,14
1—2	0,18	0,04	20—30	0,60	0,13
2—3	0,20	0,09			

neutrons scattered into the room, the detector system was surrounded by a layer of lead (up to 10 cm thick) and a layer of boron carbide and boric acid up to 0.5 m thick.

During the measurements a boron filter 1 g/cm^2 thick (to exclude recycled neutrons) and an aluminum filter 3 cm thick were placed in the neutron beam. The transmission of the neutron flux by the aluminum filter agreed with the attenuation of the effect in the fission channel at the site of this filter (at an energy of 35 keV) but did not agree with the attenuation in the radiation channel if account was taken of the background measured by the lead simulator. Therefore, the background measured with the stimulator in the radiation channel was multiplied by a factor which was calculated afresh for each exposure so as to obtain agreement in both channels. The validity of this procedure can be checked by means of the value of α at energies above 10 keV. To monitor the background level we made special exposures in which we used manganese, aluminum, and vanadium filters. Table 3 lists the ratios of the variable background to the total count in the radiation and fission channels in the same energy range as those used in the determination of α.

The measurements in the radiation channel were made in three ranges of γ-quantum energy. Each range was processed separately, and α was calculated from the expression

$$\alpha = a\frac{\Sigma(N_{\gamma_i}/N_i\sqrt{E_i})}{\Sigma(N_{n_i}/N_i\sqrt{E_i})} + b,$$

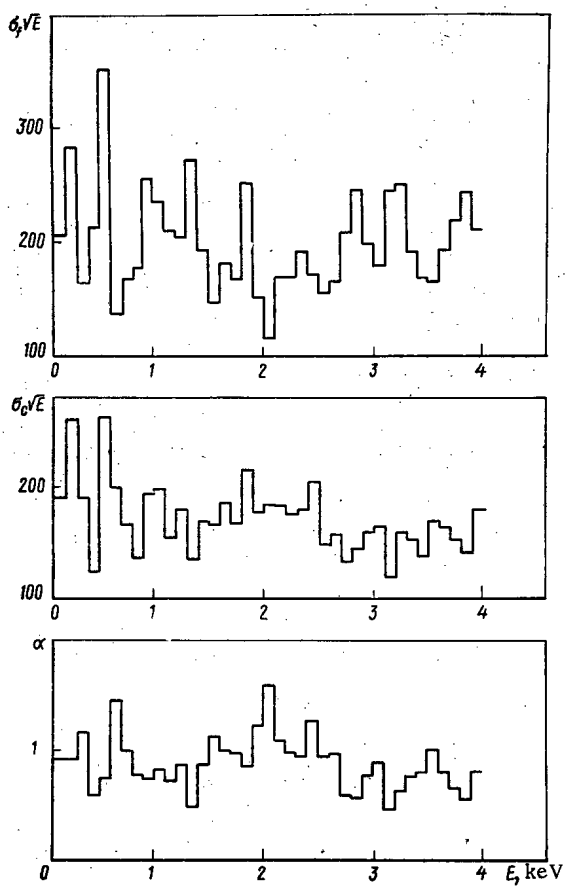

Fig. 1. Capture cross section σ_c and fission cross section σ_f and their ratio α for ^{239}Pu.

TABLE 4. Influence of γ-Quantum Discrimination on Measured Ratio

Energy range, MeV	Energy of γ quanta, MeV		
	0,4—0,7	0,7—2,5	2,5
0,1—0,2	0,92±0,12	0,93±0,13	0,74±0,21
0,2—0,3	0,83±0,11	0,92±0,08	0,67±0,19
0,3—0,4	1,05±0,18	1,17±0,08	0,80±0,53
0,4—0,5	0,57±0,12	0,59±0,04	0,50±0,37
0,5—0,6	0,57±0,12	0,75±0,11	0,58±0,26
0,6—0,7	1,51±0,23	1,46±0,18	1,15±0,74
0,7—0,8	1,04±0,15	1,00±0,10	0,86±0,59
0,8—0,9	0,67±0,15	0,78±0,15	0,41±0,53
0,9—1,0	0,91±0,17	0,76±0,12	0,74±0,57
1—2	0,74±0,11	0,85±0,07	0,73±0,23
2—3	0,93±0,14	0,97±0,11	0,77±0,43
3—4	0,81±0,12	0,68±0,12	0,72±0,74
4—5	0,94±0,15	0,87±0,07	0,76±0,52
5—6	0,84±0,15	0,84±0,09	1,28±0,79
6—7	0,76±0,17	0,73±0,13	0,66±0,80
7—8	0,74±0,18	0,74±0,07	1,17±0,98
8—9	0,54±0,20	0,56±0,09	1,0±1,1
9—10	0,69±0,18	0,47±0,10	0,83±0,97

Note. The values in the first and third columns were taken into account in obtaining this final results.

where *a* and b are the normalized constants, $N_{\gamma i}$ and N_{n_h} are the numbers of counts in the i-th channel of the time analyzer for registration of γ quanta and fast fission neutrons from the specimen, N_i is the flux of incident neutrons, and E_i is the energy of the incident neutrons for the i-th analyzer channel. The results were normalized with the known values of α for the resonances at energies of up to 50 eV [4]. For the γ-quantum

TABLE 5. Control Values of α for ^{235}U and Ratio of Fission Cross Sections of ^{239}Pu and ^{235}U

Energy range, keV	α ^{235}U *	Ratio of fission cross sections of ^{239}Pu and ^{235}U †
0,1—0,2	0,65±0,23	—
0,2—0,3	0,47±0,26	0,90‡
0,3—0,4	0,68±0,23	0,74±0,06
0,4—0,5	0,41±0,27	0,65±0,05
0,5—0,6	0,37±0,27	1,02±0,06
0,6—0,7	0,41±0,27	0,38±0,03
0,7—0,8	0,41±0,27	0,42±0,03
0,8—0,9	0,50±0,25	0,64±0,06
0,9—1,0	0,57±0,24	0,62±0,06
1—2	0,43±0,26	0,63±0,02
2—3	0,49±0,26	0,54±0,03
3—4	0,36±0,28	0,61±0,05
4—5	0,34±0,28	0,54±0,05
5—6	0,33±0,28	0,57±0,06
6—7	0,34±0,28	0,59±0,06
7—8	0,39±0,27	0,62±0,07
8—9	0,32±0,28	0,65±0,08
9—10	0,28±0,29	0,60±0,07
10—15	0,29±0,29	0,62±0,03
15—20	0,22±0,30	0,65±0,05
20—30	0,28±0,28	0,69±0,03

* The error in α is mainly due to normalization errors.
† Statistical error is given for ratio of cross sections.
‡ Normalization value.

energy range $0.7 < E_\gamma < 2.5$ MeV, the normalization constants averaged $a = 0.67$, $b = -0.62$, and varied by up to 10% between one exposure and another. For comparison, Table 4 lists the values of α obtained with various γ-quantum energy discrimination values for neutron energies from 0.1 to 10 keV. We see that for the first two γ-quantum energy intervals the values of α agree within their errors. Values were not obtained for neutron energies above 10 keV for the first interval of γ-quantum energies owing to the high constant and variable backgrounds for this discrimination level. For γ-quantum energies above 2.5 MeV the count numbers in the radiation channel were very small (the ratio between the effects in the third and second intervals was 0.04), and therefore the results there could not be obtained with sufficient accuracy. Owing to the great experimental difficulties associated with the measurement of α for the first and third ranges of γ-quantum energies, the results in these are merely qualitative. In the final results we give only the values for the second range of γ-quantum energies. Nevertheless, our measurements permit us to conclude that possible variations in the shape of the capture and fission spectra cannot cause large errors in the values of α.

As a control, we measured the ratio of the fission cross section of ^{239}Pu to the fission cross section of ^{235}U, and also the value of α for ^{235}U. Table 5 lists the control values of these quantities. The data for ^{235}U were normalized in the same way as in [2].

Table 1 gives the results of our measurements of α for ^{239}Pu, made for two different specimen thicknesses in order to check for dependence of α on thickness (the content of other isotopes in the thinner specimen was also lower). We found no appreciable discrepancy between the results obtained from these specimens. The errors, listed in Table 1, were found from the scatter of the data in different exposures. For energy ranges of 0.1-1, 1-10, and 10-30 keV the errors were, respectively, 10, 6, and 18%, and were found from the scatter of the data between different exposures. Table 2 compares our results with those obtained previously by a group at the ITÉF [2, 3] and also with new experimental data [5] and estimates made at the International Atomic Energy Agency (IAEA), Vienna [6], including all the results found up to 1970. These results agree within their errors. The differential data on α so far will be compared and assessed in a separate article.

Figure 1 shows the capture and fission cross sections and their ratio α for ^{239}Pu for neutron energies of 0.1-4 keV, averaged over ranges up to 100 eV. In normalizing the cross sections we used the value 17.65 b for the finite cross sections at 0.1-0.2 keV. This value was found by Belyaev et al. [3] for the same specimen used in our measurements. The energy dependence of the fission cross section, shown in Fig. 1, agrees with the results of Sowerby and Konshin [6], but the energy dependence of α does not entirely agree with their results. The numerical data obtained in this work were sent to the Center for Nuclear Data.

In conclusion, the authors would like to thank their colleagues at the LNP JINR, V. I. Lushchikov, L. B. Pikel'ner, and G. S. Samosvat, for help in organizing the measurements, their colleague at the FÉI, Yu. V. Grigor'ev, for lending them the specimens, and their colleagues of the Neutron Group of the ITÉF, F. N. Belyaev and S. P. Borovlev, for discussing the results and helping to process them.

LITERATURE CITED

1. Yu. V. Ryabov et al., JINR Preprint R3-5113, Dubna (1970).
2. V. P. Bolotskii et al., in: Proceedings of the Conference on Neutron Physics [in Russian], Part 4, Obninsk, Izd. ONTI FÉI (1974).
3. F. N. Belyaev et al., in: Proceedings of the Conference of IAEA – Nuclear Data for Reactors, Vol. 1, Vienna (1970), p. 339.
4. S. I. Sukhoruchkin, At. Energ., 31, No. 3, 245.
5. R. Gwin et al., in: Proceedings of the Fourth Conference on Nuclear Cross Sections and Technology, March 3-7, 1975, Rep. GB-23, Washington.
6. M. Sowerby and V. Konshin, At. Energy Rev., 10, No. 4, 453 (1972).

DENSITY, SURFACE TENSION, AND VISCOSITY OF MELTS OF URANIUM TRICHLORIDE WITH RUBIDIUM AND CESIUM CHLORIDES

V. N. Desyatnik, S. F. Katyshev, S. P. Raspopin, and Yu. F. Chervinskii

UDC 531.756:532.61.133

Owing to the paucity of information [1] on the properties of melts of uranium trichloride with rubidium and cesium chlorides, we have investigated the density (ρ), surface tension (σ), and viscosity (ν) of melts of the $RbCl-UCl_3$ and $CsCl-UCl_3$ systems in wide ranges of temperature and concentration. The density and surface tension were measured by the method of maximum pressure in a gas (argon) bubble, and the viscosity was determined by the method of torsional oscillations of a cylindrical crucible with the melt [2, 3]. The initial compounds were obtained by known methods [1].

In the temperature range investigated, for all the melts of the $RbCl-UCl_3$ and $CsCl-UCl_3$ systems we obtained linear temperature dependence of ρ and σ (Table 1) and an exponential temperature dependence of ν (Table 2) (temperature in °K). The values of ρ, σ, and ν for pure rubidium and cesium chlorides agree closely with the literature data [4, 5].

The molar volumes (V) and their relative deviations from additivity ($\Delta V/V_{ad}$), the adsorption of the surface-active component (Γ), the excess free energy (C^S), entropy (S^S), and enthalpy (H^S) of a monomolecular surface layer of a mole of the substance, the dynamic (η) and molar (μ) viscosities, and the activation energy of viscous flow (E_μ) were calculated throughout the concentration range from the experimental data. Figure 1 gives plots of the experimental and calculated values for 1130°K vs concentration.

Mixing of chlorides of Rb, Cs, and U, the cations of which have different sizes and charges, must be accompanied by predominant formation of complex groups based on the uranium cation, which has a higher polarizing capacity [6]. This must be manifested on the concentration dependences of these properties. In fact, the reactions between the components during mixing are indicated by the marked positive deviations of the molar volumes from the additive values, and the negative deviations of the σ, G^S, and H^S isotherms from linearity [7]. This is also corroborated by the negative deviations (24.6% in the $RbCl-UCl_3$ system and 31.4% in the $CsCl-UCl_3$ system) of the surface tension of the equimolar composition from the ideal values, calculated by means of the Zhukhovitskii–Guggenheim equation [8].

Translated from Atomnaya Énergiya, Vol. 42, No. 3, pp. 221-224, March, 1977. Original article submitted June 21, 1976.

TABLE 1. Density and Surface Tension of Melts of the $RbCl-UCl_3$ and $CsCl-UCl_3$ Systems

UCl_3, mole %	$\rho = a - bT$, g/cm³			$\sigma = \sigma_0 - cT$, mJ/m²			Temp. range, °K
	a	$b \cdot 10^3$	$S \cdot 10^3$	σ_0	$c \cdot 10^3$	$S \cdot 10^2$	
0,0	3,1069	0,8799	1	155,59	64,34	6	1012—1142
15,0	3,4979	0,9404	1	122,69	40,03	3	917—1133
20,0	3,5001	0,8600	2	126,40	44,78	2	1001—1155
25,0	3,6142	0,8569	3	130,10	49,52	2	1036—1183
33,2	3,8281	0,8755	2	121,58	42,04	1	973—1133
37,4	3,9795	0,9055	1	114,77	35,86	2	949—1126
40,1	4,1056	0,9452	1	112,86	34,16	3	867—1130
45,5	4,2272	0,9476	2	108,41	30,13	2	851—1138
50,0	4,4739	1,0578	2	111,42	31,90	3	891—1125
60,0	4,4236	0,7984	1	—	—	—	952—1148
62,1	4,6964	0,9726	3	114,97	33,72	1	963—1128
70,0	4,9532	1,0008	1	122,42	36,34	2	993—1129
80,2	5,3940	1,1541	1	139,37	45,20	1	1048—1198
88,0	5,7054	1,2458	3	162,55	61,20	4	1089—1229
100,0	6,3747	1,5222	2	224,70	95,70	1	1138—1296
				$CsCl-UCl_3$			
0,0	3,7776	1,0716	1	155,50	72,08	6	922—1125
10,0	3,9168	1,0902	1	132,57	56,67	2	906—1129
20,0	3,9805	1,0498	2	119,17	45,75	2	855—1126
25,1	4,0782	1,0707	2	123,10	48,49	4	991—1132
33,2	4,1153	0,9954	2	156,38	78,86	6	1029—1158
34,1	4,1875	1,0431	2	129,93	55,70	2	1037—1132
39,0	3,9566	0,7493	1	115,17	41,78	3	1012—1097
39,8	4,1125	0,8764	1	107,32	35,06	3	965—1135
49,0	4,2937	0,8701	2	—	—	—	919—1127
50,2	4,4837	1,0261	2	105,64	33,85	2	906—1120
58,5	4,5972	0,9324	2	105,06	33,26	4	943—1107
60,1	4,7418	1,0370	2	104,87	31,84	3	937—1129
70,0	4,9738	1,0293	2	115,07	37,42	1	986—1142
75,0	4,8918	0,8671	2	122,58	39,98	3	1049—1227
84,0	5,1311	0,8874	2	142,79	51,63	3	1049—1221
92,2	5,6432	1,1577	2	164,73	59,79	6	1114—1270
94,1	5,9419	1,3533	3	176,22	67,19	2	1112—1298

TABLE 2. Viscosity of Melts of the $RbCl-UCl_3$ and $CsCl-UCl_3$ Systems

UCl_3, mole%	$\lg \nu = A_\nu + \frac{B}{T}_\nu$ (ν, cSt)			$\lg \eta = A_\eta + \frac{B}{T}\eta$ (η, cP)			$\lg \mu = A_\mu + \frac{B}{T}\mu$ [μ, (erg·sec)/mole]			Temp. range, °K
	$-A_\nu$	B_ν	$S \cdot 10^3$	$-A_\eta$	B_η	$S \cdot 10^3$	$-A_\mu$	B_μ	$S \cdot 10^3$	
					$RbCl-UCl_3$					
0,0	1,2413	1032	6	1,1194	1258	13	1,1588	1032	7	1000—1250
10,0	0,9295	657	2	0,7538	872	7	0,7733	657	3	996—1253
16,0	1,1082	893	10	0,8886	1080	32	0,9132	893	16	929—1250
24,9	1,3631	1274	8	1,1058	1458	21	1,1162	1274	13	1034—1251
33,1	1,4887	1432	3	1,1830	1597	14	1,1989	1432	7	991—1256
43,8	1,5390	1463	17	1,1818	1613	65	1,1989	1463	37	926—1250
53,9	1,5896	1501	11	1,1769	1640	36	1,2069	1501	27	935—1253
64,0	1,5640	1569	19	1,1293	1712	66	1,1425	1569	51	978—1256
75,0	1,7264	1796	16	1,2654	1949	63	1,2662	1796	46	1043—1246
88,8	1,8381	1919	14	1,3581	2095	61	1,3338	1919	45	1095—1242
100,0	1,2213	1100	3	0,7387	1310	11	0,6843	1100	9	1128—1278
					$CsCl-UCl_3$					
0,0	1,3764	965	6	1,1375	1157	17	1,1502	965	11	929—1185
10,0	1,3035	916	13	1,0435	1107	32	1,0341	916	24	933—1191
22,0	1,2553	913	4	0,9953	1129	11	0,9392	913	8	1068—1235
33,0	1,5987	1369	8	1,2815	1547	22	1,2437	1369	18	1023—1211
44,0	1,9734	1770	13	1,5800	1896	37	1,5826	1770	31	903—1210
50,0	2,0168	1841	18	1,6263	1987	53	1,6079	1841	45	930—1233
56,0	2,0236	1913	26	1,6025	2048	82	1,5972	1913	69	908—1247
64,0	2,1029	2028	14	1,6655	2169	50	1,6542	2028	40	946—1241
75,0	2,0771	2069	57	1,5996	2198	20	1,5995	2069	17	1062—1253
87,2	1,8156	1866	54	1,3152	2005	23	1,3079	1866	17	1073—1242

Maximum deviation of the molar volumes from additivity is observed in the concentration range corresponding to the congruently melting compound Me_2UCl_5 [1]; this is apparently due to formation of complex uranium groups UCl_5^{2-} in the melt. This deviation increases in going from the $NaCl-UCl_3$ system (5.13% [3]) to the $RbCl-UCl_3$ (9.50%) and $CsCl-UCl_3$ systems (10.97%), indicating intensification of the reactions of uranium trichloride with alkali metal chlorides as the alkali-metal cation radius increases.

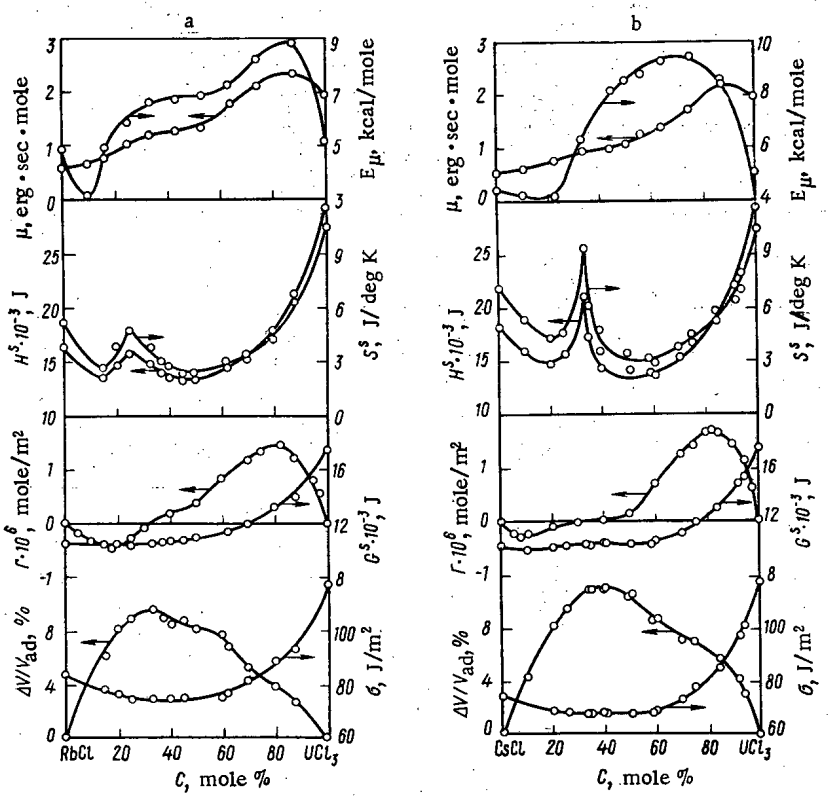

Fig. 1. Physicochemical properties of melts of the $RbCl-UCl_3$ (a) and $CsCl-UCl_3$ (b) systems at 1130°K.

On the σ isotherms in the range 25-50 mole % UCl_3 we observe a minimum due to formation of uranium complexes which exhibit surface activity with respect to both components of the mixture [9]. Adsorption of ions in the surface layer in the concentration region corresponding to compounds Me_2UCl_5 is zero, and the S^S curves display maxima. This indicates that the complex UCl_5^{2-} ions formed when the components are mixed are stable in melts of both systems, which are apparently also surface-active.

Additional information on the change in the structure of the mixtures enables us to investigate the concentration dependence of μ and the activation energy of viscous flow. Thus in the concentration range 0-50 mole % UCl_3, as structural units involved in viscous flow we find elementary rubidium and cesium cations, complex UCl_5^{2-} ions, and a very small amount of UCl_6^{3-}, $RbCl_4^{3-}$, and $CsCl_4^{3-}$ ions [10]. As the uranium trichloride concentration is increased, the complex $RbCl_4^{3-}$ and $CsCl_4^{3-}$ ions disintegrate. Here the viscosity of the melt shows little change, the latter being largely due to a decrease in the number of readily displaceable rubidium and cesium cations. In melts containing more than 50 mole % of UCl_3, the increase in viscosity is due to the appearance of complex uranium cations of type UCl_2^+ in the second coordination sphere. The change in its value and in that of the activation energy of viscous flow in melts containing more than 80-90 mole % of UCl_3 indicates the decomposition of the complex uranium groups into simpler ones.

LITERATURE CITED

1. V. N. Desyatnik, B. V. Dubinin, and S. P. Raspopin, Zh. Fiz. Khim., 47, No. 10, 2726 (1973).
2. A. M. Vokhmyakov et al., Physicochemical Investigations of Metallurgical Processes [in Russian], No. 2, Izd. UPI im. S. M. Kirova, Sverdlovsk (1974), p. 70.
3. V. N. Desyatnik et al., At. Energ., 39, No. 1, 70 (1975).
4. A. G. Morachevskii (editor), Fused Salts [Russian translation], Vol. 1, Khimiya, Leningrad (1971).
5. A. G. Morachevskii (editor), Fused Salts [Russian translation], Vol. 2, Khimiya, Leningrad (1972).
6. B. F. Markov, Thermodynamics of Fused Salt Mixtures [in Russian], Naukova Dumka, Kiev (1974).
7. M. V. Smirnov and V. P. Stepanov, Tr. Inst. Elektrokhim., Akad. Nauk SSSR, Ural. Fil., No. 16, 21 (1970).
8. N. Boardman, A. Palmer, and E. Heymann, Trans. Faraday Soc., 51, No. 2, 277 (1955).
9. O. A. Esin, in: The Structure of a Substance and Spectroscopy [in Russian], Izd-vo Akad. Nauk SSSR, Moscow (1960), p. 111.
10. M. V. Smirnov, Electrode Potentials in Fused Chlorides [in Russian], Nauka, Moscow (1973), p. 201.

SOME YIELD CHARACTERISTICS OF SHORT-LIVED FISSION PRODUCTS IN A SODIUM HEAT-TRANSFER AGENT

I. A. Efimov, Yu. V. Lopatin,
L. I. Mamaev, S. A. Stabrovskii,
and V. S. Filonov

UDC 621.039.548.004.4:621.039.526

The hermeticity control of fuel elements by delayed neutrons is extensively used in fast reactors with a sodium heat-transfer agent [1, 2]. To better evaluate the equipment potential, it is necessary to improve the leakage mechanism of the recorded fission products into the heat-transfer agent.

Experiments on the BR-5 reactor have shown that even in the case of hermetic fuel elements, the leakage behavior can not be explained by the simplest mechanism of escape of the fission fragments into the heat-transfer agent. In particular, the existence of temperature dependences of the instrument readings for the hermiticity control of the fuel elements [3] is not explained. A theoretical analysis of the data of [3] has revealed an exponential dependence of the leakage on the temperature. This may be explained by the effect of the diffusion processes on the leakage; the low activation energy of these processes (14 kJ/mole for isotopes, emerging delayed neutrons, and 27 kJ/mole for inert gases) indicate diffusion into the liquid.

Another experiment carried out on the BR-5 reactor, for studying the behavior of the control instrument using delayed neutrons in the presence of oscillations of the reactor power, is illustrated in Fig. 1. It shows that the relative oscillations of the instrument readings exceed the relative oscillations of the power by a factor of 2.3. On analyzing this result from the point of view of diffusion leakage, we obtain the diffusion coefficient for the fission products equal to $\sim 10^{-10}$ m^2/sec. Such a high value of the diffusion coefficient is also typical for processes in liquids.

In order to explain these results, special experiments were carried out on the BR-10 reactor in the absence of hermetic fuel elements; the readings of the control instruments using delayed neutrons were recorded with varying temperature and flow rate of the heat-transfer agent (Fig. 2). An analysis of the experimental results showed that all the observed effects can be explained by the presence of a viscous turbulent sublayer of sodium flow near the walls. Since the thickness of this sublayer is comparable to the mean free path of the fragments in the heat-transfer agent, the yield of the fission products in the main flow is accomplished by direct escape

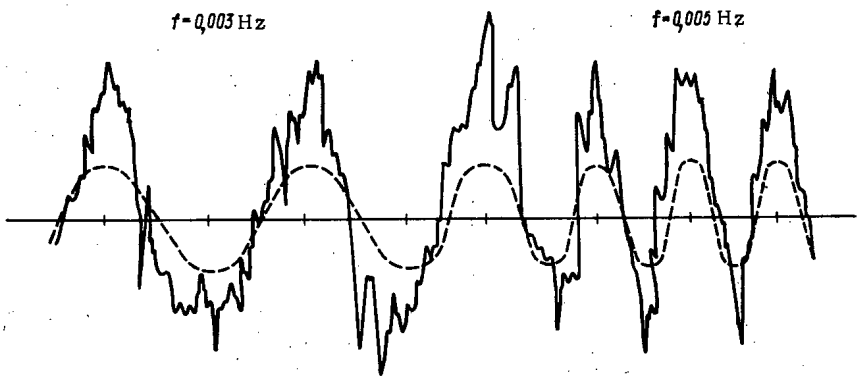

Fig. 1. Oscillations of the readings of the instrument for hermeticity control of fuel elements using delayed neutrons in the presence of power oscillations.

Translated from Atomnaya Énergiya, Vol. 42, No. 3, pp. 224-226, March, 1977. Original article submitted June 21, 1976.

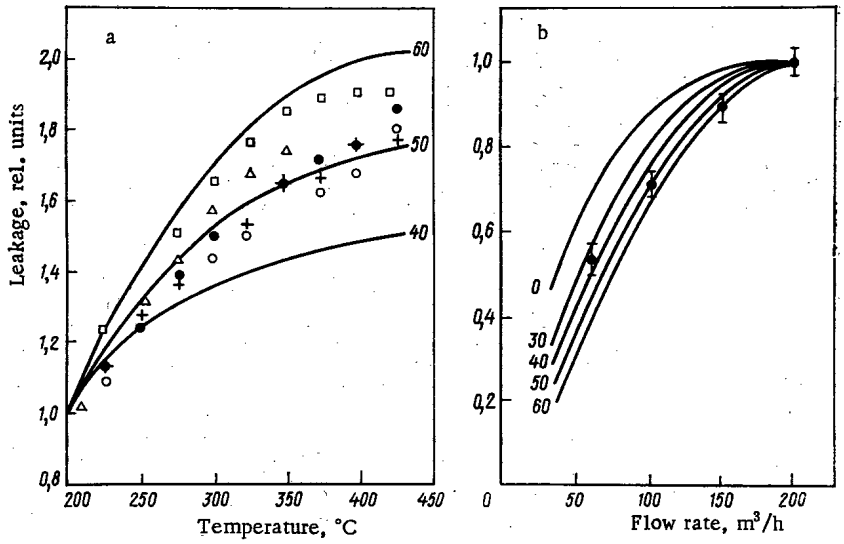

Fig. 2. A comparison of the theoretical computations of the dependence of yield of fission products, emerging delayed neutrons on temperature (a) and flow rate (b) of the heat-transfer agent with experimental data obtained with control instrument using delayed neutrons on the BR-10 reactor in the absence of hermetic fuel elements: △, □) Dec. 24, 26, 1974, respectively; +, ●, ○) Feb. 14, 1975. The numbers on the curves indicate the thickness of the viscous sublayer (μ) at 373°K with the velocity of the heat-transfer agent equal to 3.8 m/sec.

across the sublayer and by diffusion into the sublayer. The change of the diffusion coefficient and the thickness of the sublayer must govern the dependence of the leakage on the parameters of the heat-transfer agent.

Computations were carried out using special one-dimensional differential diffusion equations in which the natural decay of the isotopes was also taken into consideration along with the direct escape and diffusion into the sublayer. The boundary conditions reflected the low concentration of the fragments in the turbulent sublayer and the small probability of an atom getting absorbed at the walls in one collision. It was assumed that the thickness of the sublayer was directly proportional to the viscosity and inversely proportional to the averaged linear velocity of the heat-transfer agent [4]; the data for calculating the temperature dependence of the diffusion coefficient (activation energy 22 kJ/mole) were taken from [5] and the temperature dependences for viscosity and density of sodium were taken from [6]. The computations were done on a computer. The results of these computations for the BR-10 reactor are shown in Fig. 2; a "thick" layer (on the mean free path scale) of a mixture of uranium and sludge deposited on the walls of the active zone was taken as the source of the fission products. A better agreement between the theoretical and experimental data is obtained under the assumption that the thickness of the viscous sublayer is equal to 52 ± 6 μ for the temperature of the sodium equal to 373°K (200°C) and the velocity of the heat-transfer agent in the active zone equal to 3.8 m/sec. Some disagreement between the theoretical and experimental dependences of the leakage on the flow rate is accounted for by the decrease of Reynolds number to critical values at small flow rates.

Based on the model of leakage for hermetic fuel elements, a general model of leakage of fission products in liquid metal heat-transfer agents is developed, which has extensive practical application to full-scale fast reactors.

The model presented earlier explained the anomalous phenomena in the behavior of leakages without casting any doubt on the specialists' opinion about the existence of a linear relationship between the surface area of dehermetization of the fuel elements and the readings of the control instrument of the hermeticity of fuel elements using delayed neutrons.

LITERATURE CITED

1. S. Hackney and J. Wood, in: Proceedings of the IAEA Symposium – Sodium-Cooled Fast Reactor Engineering, Vienna (1970), p. 853.
2. In: Experience of Operation of Fast Reactors in France and Development of Industrial Fast Reactors [in Russian], TsNIIatominform, Moscow (1975), p. 35.

3. I. A. Efimov, L. I. Mamaev, and V. S. Filonov, "Testing the hermeticity of fuel elements in the BR-5 reactor," At. Energ., 31, No. 6, 567 (1971).
4. V. G. Levich, Physicochemical Hydrodynamics [in Russian], Fizmatgiz, Moscow (1959).
5. T. Row and R. Davis, Nucl. Safety, 11, No. 4, 315 (1970).
6. V. M. Borishanskii et al., Liquid Metal Heat-Transfer Agents [in Russian], Atomizdat, Moscow (1967).

ELECTRICAL RESISTANCE AND STORED ENERGY IN LOW-TEMPERATURE IRRADIATION OF TITANIUM DIBORIDE

L. S. Topchyan, I. A. Naskidashvili, V. V. Ogorodnikov, V. V. Petrosyan, and L. M. Murzin

UDC 154-162:539.16.04

The borides of metals are effective absorbers and also possess a high melting point, great hardness, and chemical resistance in corrosive media [1-3]. To predict the stability of metal-boride products in a reactor one must make a careful study of the nature of the radiation damages. The type of radiation-induced defects formed, their subsequent annealing or transformation into more complex configurations, as well as the fission fragments of the $^{10}B(n, \alpha)^{7}Li$ reaction determine the operating life of structures made of metal borides, among which titanium boride exhibits the highest radiation stability [4-6]. However, products made of titanium boride break down under the action of reactor radiation before its absorption capacity is exhausted.

The character and degree of radiation damage depend not only on the dose but also on the irradiation temperature [4, 5]. During high-temperature irradiation, along with thermally activated relaxation of internal stresses, helium interstitial atoms are observed to leave the boride matrix by diffusion, thus increasing the effective radiation stability of the material. A decrease in the radiation temperature, which prevents the defects from being partially annealed and is conducive to their accumulating, should lead to a significant growth of internal stresses in the lattice and an increase in the crack initiation and growth rate. Therefore, low-temperature irradiation provides an opportunity to study the role of primary defects and (η, α)-reaction products and radiation damage to borides.

The present paper gives an account of the results of research done on hot-pressed TiB_2 samples (Table 1) in a process of irradiation at 15 and 110°K in the cryogenic channels of a nuclear reactor by measuring the electrical resistance as well as by determining the stored energy during annealing of irradiated samples. The procedure for the irradiation and investigation was described earlier [7, 8].

As is seen from the data obtained (Fig. 1) at 15°K (curve 1) and 110°K (curve 2) the electrical resistance varies monotonically with a subsequent abrupt jump. An increase in the irradiation temperature from 15 to 110°K shifts the beginning of the jump in electrical resistance as a function of the radiation dose by more than twofold.

This effect can be assumed to be associated with the formation of microcracks because of large internal stresses which, in turn, are the consequence of the buildup of radiation defects and fission fragments.

The results of irradiation at 15 and 110°K show that the first jump (points A and B on the dashed curve) occurs at the same ratio in both cases, $\Delta\rho/\rho_0 = 1.2$, i.e., at a particular concentration of defects produced during irradiation process.

Samples were simultaneously irradiated in two different containers, aluminum and cadmium. The cadmium container intercepted part of the thermal neutrons and in this case the electrical resistance was observed to grow monotonically over the entire range of doses studied. The absence of a jump in the electrical resistance on the curve at point C is evidently due to the lower concentration of He and Li in the diboride lattice.

Translated from Atomnaya Énergiya, Vol. 42, No. 3, pp. 226-228, March, 1977. Original article submitted July 13, 1976.

TABLE 1. Calorimetric Data on Release of Stored Energy in Titanium Diboride

Sample batch No.	Mode of irradiation	Irradiation temp., °K	Thermal-neutron fluence, neutrons/cm²	Fast-neutron fluence, neutrons/cm²	Overall heat release, cal/g
I	Without shield	115	$1,2 \cdot 10^{18}$	$1,2 \cdot 10^{18}$	22,7—0,5
II	Without shield	130	$1,4 \cdot 10^{17}$	$1,5 \cdot 10^{17}$	7,0—0,3
III	With cadmium shield	130	—	$1,5 \cdot 10^{17}$	1,4—0,1

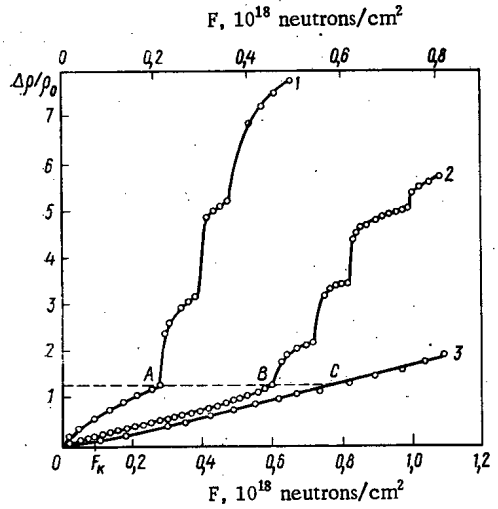

Fig. 1. Increment in electrical resistance vs irradiation dose: 1, 2) irradiation at 15 and 100°K, respectively; 3) irradiation at 100°K in a cadmium shield; ρ_0 is the electrical resistance of TiB_2 prior to irradiation at 15 to 110°K, respectively; F_K is the integrated radiation dose after which the TiB_2 was analyzed.

To study the nature of radiation defects which emerge in titanium diboride samples under various irradiation conditions (Table 1), the stored energy was measured calorimetrically by annealing the irradiated samples in a special differential low-temperature calorimeter [9]. The resulting thermograms (Fig. 2) show that after irradiation of TiB_2 samples with a fluence of $1.2 \cdot 10^{18}$ neutrons/cm² at 115°K, heat is released at the rate of 22.7 cal/g in the temperature range 170-320°K. Reduction of the fluence by a factor of ten causes a threefold decrease in the heat release and irradiation in a cadmium shield causes a fivefold reduction.

Each of the thermograms has three peaks of heat release, changes in the irradiation conditions altering only the height and not the location of the peaks on the temperature scale. This means that in the process of irradiation defects of an identical nature are formed in all cases and only their concentration varies. Studies of their resistance show that defects accumulate at a higher rate at an irradiation temperature of 15°K than at 110°K. This indicates partial annealing at 110°K. Thus, it is seen that an irradiation temperature of 110°K is clearly above the temperature range in which stage-I annealing of radiation defects is observed, this stage being due to the recombination of close-lying and correlated Frenkel pairs as well as the migration of free interstitial atoms. Apparently, the peaks recorded above 160°K (Fig. 2) correspond to stage-II annealing of radiation defects in TiB_2. It should be noted that the samples studied (Table 2) are not distinguished by high purity and, hence, impurities which are present may be traps for radiation defects and for interstitial atoms

TABLE 2. Composition and Properties of Titanium Diboride

Chemical comp., mass %			Ti/B ratio	Pressing temp., °K	Grain size, μ	Porosity, %	Bending strength, kgf/mm²	Electrical resistivity at 300°K, μΩ·cm
Ti	B	C						
68,5	29,5	0,8	1,95	2400	до 40	7	29,0	25

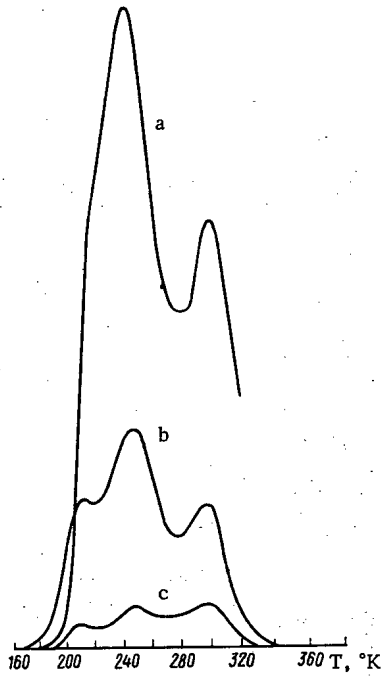

Fig. 2. Thermograms of annealing of irradiated samples: a, b) T_{irr} = 115 and 130°K, respectively, and F = $1.2 \cdot 10^{18}$ and $1.4 \cdot 10^{17}$ thermal neutrons/cm^2, respectively; c) T_{irr} = 130°K, and F = $1.5 \cdot 10^{17}$ fast neutrons/cm^2, with irradiation in a cadmium shield.

as well. It is possible that in the range from 160 to 360°K as a result of thermal activation the interstitial atoms may be highly excited out of the impurity traps with subsequent annealing at various sinks.

LITERATURE CITED

1. G. V. Samsonov, Boron and Its Compounds and Alloys [in Russian], Izd. Akad. Nauk Ukr. SSR, Kiev (1960).
2. Absorbing Materials for Nuclear Reactor Control [in Russian], Atomizdat, Moscow (1965).
3. Properties of Reactor Materials and the Effects of Reactor Damage, London (1962), p. 457.
4. V. V. Ogorodnikov et al., At. Energ., 23, No. 4, 341 (1967).
5. G. V. Samsonov et al., At. Energ., 24, No. 2, 191 (1968).
6. V. V. Ogorodnikov, L. M. Murzin, and A. G. Krainii, in: Radiation Effects on Variations in Mechanical Properties of Structural Methods and Methods of Studying Them [in Russian], Naukova Dumka, Kiev (1976).
7. É. D. Andronikashvili et al., Soobshcheniya Akad. Nauk. Gruz. SSR, No. 34, 45 (1964).
8. L. A. Vadachkoriya et al., At. Energ., 26, No. 3, 288 (1969).
9. V. V. Gerasimov et al., Izv. Tomsk. Politekhn. Univ., No. 170, 108 (1968).

MEASURING THE TEMPERATURE OF THE NEUTRON GAS WITH SOLID-STATE TRACK DETECTORS OF FISSION FRAGMENTS

A. M. Bogomolov, A. D. Molodtsov, and L. Ya. Tikhonov

UDC 621.039.519

To date the spectral parameters of a field of thermal neutrons are measured mainly with activation detectors which cannot always be used in critical low-flux systems.

The goal of our work was to develop a method of measuring the temperature of the neutron gas with the aid of modern solid-state track detectors. The high sensitivity of this type of detector, their possible use in the case of low neutron fluxes and long irradiation times, the small disturbance which they cause in the neutron field, and the information storage over an almost unlimited time make the solid-state track detectors very promising in measurements to be performed on experimental critical assemblies working with low power.

In integral measurements of the neutron gas temperature, the ratio of reaction rates in absorbers is determined; the cross section of one of the absorbers has a resonance in the thermal range, whereas the cross section of the other absorber obeys the 1/v law. In calculating the temperature, the theoretical model by Westcott was used to describe the field of thermal neutrons [1].

The energy distribution of the neutron flux of a thermal reactor can be represented as a sum of a Maxwellian component and an epithermal component:

$$\Phi(E)=\Phi_t[E/(kT)^2]\exp(-E/kT)+\Phi_e[\Delta(E/kT)/E], \quad (1)$$

where Φ_t and Φ_e denote the total flux of the thermal and epithermal neutrons, respectively; and $\Delta(E/kT)$ denotes the function of the transition region; the function depends upon the lower limit of the spectrum of the epithermal neutrons.

According to the Westcott formalism, the reaction rate R in a thin indicator (self-shielding can be ignored) is expressed by the relative flux nv_0 and the effective reaction cross section $\hat{\sigma}$ as follows:

$$R = nv_0\rho\hat{\sigma}=\rho\int_0^\infty n(v)v\sigma(v)\,dv,$$

where ρ denotes the number of nuclei in the indicator; v_0 = 2200 m/sec; and n denotes the total neutron density.

When we use the representation (1) for the spectrum, we find

$$\hat{\sigma}=\sigma(v_0)[g(T)+rS(T)],$$

where g(T) and S(T) denote parameters depending upon the neutron temperature and taking into consideration the deviation of the cross section from the 1/v law in the thermal and epithermal regions; and r denotes a parameter which characterizes the ratio of the epithermal and thermal components of the neutron flux.

We used in the experiments a thin foil of a plutonium–aluminum alloy with a ^{239}Pu thickness of less than 4.5 mg/cm^2 (resonance at 0.296 eV) as the absorber with a resonance in the thermal range; we used a thin indicator layer of ^{235}U (thickness < 0.15 mg/cm^2) as a 1/v absorber; the layer had been obtained by electrical vacuum sputtering of the uranium upon a thin (< 100 μ) aluminum substrate. The ratio of the fission reaction rates was measured in the neutron spectrum under consideration with the aid of a ~100-μ-thick olivine glass while the indicator was simultaneously irradiated in contact with the detector.

Translated from Atomnaya Énergiya, Vol. 42, No. 3, pp. 228-229, March, 1977. Original article submitted August 11, 1976.

TABLE 1. Coefficients of Self-Shielding of Neutrons

Element	F_t	F_r	G	h
Pu	0,97	0,937	—	—
U	1	1	1	0,005

TABLE 2. Results of the Measurements

Parameter	F-1 reactor	Critical assemblies
B	0,839±0,006	1,195±0,005
R_{Cd}	23,8±0,2	43,7±0,3
r	0,0665±0,0005	0,0333±0,0002
T, °K	(343±14)	(326±13)
$\hat{\sigma}_{29}/\hat{\sigma}_{25}$	1,63±0,01	1,50±0,01

With proper regard for the self-shielding of the neutrons by the indicators, the ratio of the reaction rates in the indicator layers of ^{239}Pu and ^{235}U can be expressed as:

$$\frac{N_{29}}{N_{25}}=\frac{[\xi\rho\sigma(v_0)]_{29}\,[g_{29}(T)\,F_t^{29}+rS_{29}(T)\,F_r^{29}]}{[\xi\rho\sigma(v_0)]_{25}\,[g_{25}(T)\,F_t^{25}+rS_{25}(T)\,F_r^{25}]}, \tag{2}$$

where N_{29} and N_{25} denote the density of the tracks resulting from ^{239}Pu and ^{235}U; the densities are proportional to the reaction rates; ξ denotes the efficiency with which the fission fragments are recorded; and F_t and F_r denote the coefficients of self-shielding of the thermal neutrons and of the resonance neutrons.

The constant $[\xi\rho\sigma(v_0)]_{29}/[\xi\rho\sigma(v_0)]_{25}$ was determined from calibration measurements in the thermal column of the F-1 reactor in which the neutron spectrum is completely thermalized (cadmium ratio in excess of 10^3, according to dysprosium; r = 0) and the neutron temperature corresponds to the temperature of the moderator [2]:

$$\frac{[\xi\rho\sigma(v_0)]_{29}}{[\xi\rho\sigma(v_0)]_{25}}=\frac{N_{29}^t}{N_{25}^t}\,\frac{g_{25}(T)}{g_{29}(T)}\,\frac{F_t^{25}}{F_t^{29}}=B\frac{F_t^{25}}{F_t^{29}}.$$

The second equation for calculating the temperature was obtained from measuring the cadmium ratio of the ^{235}U indicator layer:

$$R_{Cd}=\frac{N_{25}}{N_{25_{Cd}}}=\frac{g_{25}(T)\,F_t^{25}+rS_{25}(T)\,F_r^{25}}{r\{S_{25}(T)\,F_r^{25}G-g_{25}(T)\,W_{25}F_r^{25}G\sqrt{T/T_0}+[g_{25}(T)\,F_t^{25}/K]\sqrt{T/T_0}\}+hg_{25}(T)\,F_t^{25}}, \tag{3}$$

where G and h denote the transmission coefficients of resonance neutrons and thermal neutrons by the cadmium shield, respectively; and

$$W=\frac{\sqrt{\pi}}{2}\,\frac{1}{\sigma(v_0)\,g(T)}\int_0^{\infty}\left[\sigma(E)-\sigma(v_0)\sqrt{\frac{E_0}{E}}\right]\frac{\Delta(E/kT)}{E}\,dE$$

is a correction for the deviation of the cross section from the 1/v law at the lower boundary of the epithermal spectrum, E_b, to the energy of the cadmium limit, E_{Cd} (E_0 denotes the energy corresponding to a neutron velocity v_0 = 2200 m/sec at T_0 = 238°K); and k denotes a coefficient taking into consideration both the thickness and the form of the cadmium shield. Measurements were made both at the center of the uranium–graphite F-1 reactor and in the active zone of the critical assembly with water as a moderator (an uranium indicator of smaller dimensions was used in the measurements made on the critical assembly). The indicators were irradiated in the F-1 reactor for 5-10 min at a power of ~10 W. The coefficients of self-shielding and transmission of neutrons by the 0.5 mm thick cadmium were determined by calculation (see Table 1).

Equations (2) and (3) were graphically solved with the parameters g(T) and $S_4(T)$ listed in the tables of [1]. The detectors were visually inspected with an MBI-15 optical microscope.

The neutron gas temperature (343 ± 14°K) measured at the center of the F-1 reactor with the aid of the solid-state track detectors is in good agreement with the temperature obtained at that point by activation measurements (350 ± 10°K) [3]. The results were used to calculate the relative (nv_0) and total ($\Phi = \Phi_t + \Phi_e$) fluxes of the neutrons at the center of the F-1 reactor:

$$nv_0 = \frac{N}{(\xi\rho)\,\bar{\sigma}t};$$

$$\Phi = \frac{N_t}{(\xi\rho)\,\sigma(v_0)\,g(T)\,(\sqrt{\pi}/2)\,(\sqrt{T_0/T})\,F_t t}.$$

$$\Phi_e \approx r\Phi_t.$$

The absolute value of $\xi\rho$ was determined from calibration measurements in a known flux of thermal neutrons and t denotes the time of irradiation. The contribution to the reaction intensity which originates from the thermal component N_t of the flux was estimated with the formula

$$N_t = N\,[1-(F_{Cd}/R_{Cd})],$$

where F_{Cd} denotes the coefficient accounting for the capture of neutrons having an energy between E_φ and E_{Cd} by cadmium; the coefficient was calculated with the formula

$$F_{Cd} = 1 + \frac{(\sqrt{\pi}/2)\,\sigma(v_0)\,g(T)\,WF_r + 2\sigma(v_0)}{\left[F_r \int_{E_{Cd}}^{\infty} \sigma(E)\,(dE/E) + (F_t - F_r)\right]} \cdot \frac{g(T)\,F_t\,(\sqrt{E_0/E_b} - \sqrt{E_0/E_{Cd}})}{g(T)\,\sigma(v_0)\,(\sqrt{E_0/E_{Cd}})}.$$

The values of the reduced neutron flux and the total neutron flux [$nv_0 = (0.79 \pm 0.06)\cdot 10^{10}$ and $\Phi = (0.82 \pm 0.08)\cdot 10^{10}$] referred to the nominal power of the F-1 reactor (24 kW) are in good agreement with the value measured for the neutron flux with the activation technique [$(0.85 \pm 0.15)\cdot 10^{10}$ neutrons/cm^2·sec].

LITERATURE CITED

1. C. Westcott, AECL-1101 (1960).
2. W. Fox, AEEW-R (1964), p. 342.
3. S. S. Lomakin et al., in: Design of Nuclear Instrumentation [in Russian], Tr. SNIIP, No. 12, Atomizdat, Moscow (1972), p. 230.

A LIGHT FLASH EXCITED BY A γ-QUANTUM PULSE WITHOUT DIRECT VISIBILITY OF THE SOURCE

A. V. Zhemerev, Yu. A. Medvedev, and B. M. Stepanov

UDC 621.039.555

In this work we consider the characteristics of a light flash which is produced by the unscattered radiation of light excited by a pulsed γ-quantum source without direct visibility of the source and estimate the limit distances over which the unscattered light signal can be recorded.

The luminescence spectrum of air exposed to γ radiation consists of systems of bands in the spectra of both the nitrogen molecule and the nitrogen ion and extends over the entire visible and infrared spectrum, with a maximum appearing at the wavelength ~4000 Å [1]. When the distance between the source and the receiver is of the order of hundreds of kilometers, one must consider the real geometry of the medium, i.e., the spherical shape of the earth. One must therefore think of the possible geometrical obscuration of various regions of luminescent air, with the luminescence generated by γ radiation.

Figure 1 serves to illustrate the geometry of the problem. An isotopic, monochromatic point source of γ radiation is located at point 1 at the altitude h above the surface of the earth; an uncollimated detector of the light radiation is situated at point 2; Ω denotes the angular distance.

Assume that the energy $\dot{E}(r, t)$ absorbed per unit volume at the distance r from the γ source per unit time is known and that also the law governing the luminescence of a unit volume under the influence of an instantaneous pulse (δ pulse), $K\delta t$, of γ quanta is known. The time dependence of the intensity of the light flux at point 2 is given by the formula of [2] (the self-absorption is disregarded):

$$I(t)=\frac{\eta}{4\pi}\int\limits_{V_0}\frac{dv}{R^2}g(\mathbf{r})\int\limits_{r/c}^{t-R/c}K_\delta(t-t'-R/c)\dot{E}(r, t'-r/c)\,dt', \tag{1}$$

where η denotes the efficiency of de-excitation (ratio of the fluorescent energy in the optical range to the absorbed energy of γ quanta). The integration is performed over a volume V_t which is bounded by the surface of

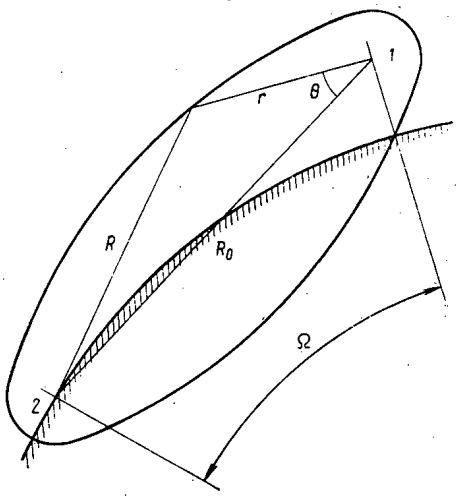

Fig. 1. Geometry of the problem.

Translated from Atomnaya Énergiya, Vol. 42, No. 3, pp. 230-231, March, 1977. Original article submitted August 11, 1976.

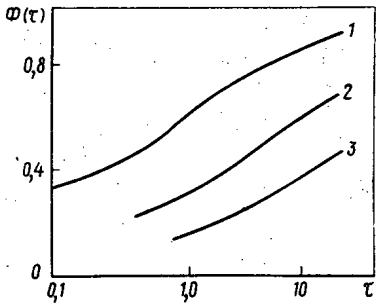

Fig. 2. The function $\Phi(\tau)$: 1) B = 0.5; 2) B = 2; 3) B = 5.

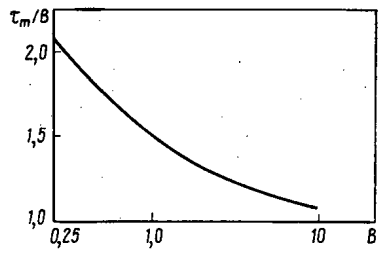

Fig. 3. Time required for reaching the maximum of the light flash.

the response-lag ellipsoid r + R = ct; points 1 and 2 are the foci of the ellipsoid. By contrast to [2], the factor g(r) appears in Eq. (1); the factor accounts for the possible geometrical obscuration of the various regions of the ellipsoid of the response lag. In a spherical coordinate system with the center at point 1 and a z axis parallel to R_0, g(r) has the form

$$g(\mathbf{r}) = \begin{cases} 1 & \text{for } r\,(\Omega/2\cos\theta + \sin\theta\cos\varphi) > R_e\Omega^2/2 - h; \\ 0 & \text{for } r\,(\Omega/2\cos\theta + \sin\theta\cos\varphi) \leqslant R_e\Omega^2/2 - h. \end{cases}$$

Let us consider the case in which the altitude is small relative to the radius R_e of the earth and $\Omega \ll 1$.

The absorbed energy can be expressed with high accuracy in the form of [2, 3]:

$$\dot{E}(r, t) = \mu\varepsilon N_0 f(t) \exp(-\mu r)/4\pi r^2,$$

where ε denotes the energy of the γ quanta; μ denotes the absorption coefficient of the γ quanta; N_0 denotes the total number of γ quanta emitted by the source; and f(t) denotes the time dependence of the γ source, with $\int_0^\infty f(t)dt = 1$ and f(t < 0) = 0; the law governing the de-excitation of the unit volume is $K_\delta(t) = \alpha e^{-\alpha t}$, where α^{-1} denotes the time of radiative decay of the excited states of the molecules; this time is $\sim 10^{-8}$ sec [4].

Let us consider the case in which the parameter $\beta = R_3\Omega^2/2 - h$ is positive (no direct visibility of the γ source). We use the δ function as the law for the fluorescence $K_\delta(t)$. Indeed, the characteristic times of the problem, $(\beta c)^{-1}$ and $(\mu c)^{-1}$, are for ε ~ 1 MeV and $\mu^{-1} \approx 300$ m [3] greater than the time α^{-1} and the de-excitation law slightly influences the time-dependent characteristics of the light flash.

At large distances ($R_0 \gg \mu^{-1}$) from the instantaneous source of the γ quanta [f(t) = δ(t)], the light flux (1) is given by the formula $r\cos\theta + R \approx R_0$ (an approximation is used for the equality):

$$I(t_1) = \eta \frac{\mu\varepsilon c N_0}{8\pi^2} \int_{\theta_1}^{\theta_2} \frac{\exp\{-\mu r(\theta)\}}{R^2} \arccos\left\{\frac{1}{\sin\theta}\left[\frac{\beta}{r(\theta)} - \frac{\Omega}{2}\sin\theta\right]\right\} \sin\theta\, d\theta, \qquad (2)$$

where

$$r(\theta) = ct_1\,(R_0 + ct_1/2)/[ct_1 + R_0(1 - \cos\theta)],$$
$$t_1 \equiv t - R_0/c;$$

and θ_1 and θ_2 denote the roots of the equations $r(\theta)(\Omega/2\cos\theta + \sin\theta) = \beta$. Since Ω is small, Eq. (2) can be simplified:

$$I(t_1) = \eta \frac{\mu\varepsilon c N_0}{8\pi^2 R_0^2} \int_0^{2\,\mathrm{arctg}(ct_1/\beta)} \exp\left(-\frac{\mu c t_1}{1-\cos\theta}\right) \arccos\left(\frac{\beta}{ct_1}\,\mathrm{tg}\,\frac{\theta}{2}\right) \sin\theta\, d\theta.$$

The value of $(\beta/ct_1)\tan(\theta/2)$ varies more slowly than the exponential and therefore can be taken before the integral sign and assumed to be equal to some average value $(\pi/2)\Phi(\tau)$. We obtain after integration:

$$I(\tau) = \eta \frac{\mu\varepsilon c N_0}{16\pi R_0^2}\,\Phi(\tau)\,[\exp(-\tau u)/u - \tau E_1(\tau u)], \tag{3}$$

where $\tau = \mu c t_1$ denotes the dimensionless time; $\mu = (B^2/\tau^2 + 1)$, $B = \mu\beta$; $E_1(x)$ denotes the integral exponential function [5]; and $\Phi(\tau)$ is a function which slowly varies with time. The functions $\Phi(\tau)$ which were obtained by numerical integration of Eq. (2) for various B are shown in Fig. 2. The quantity $I(\tau)$ first increases sharply, approximately like $\exp(-B^2/2\tau)$, reaches a maximum at times τ_m which are given by the formula

$$B^2 \exp(-\tau_m u) = \tau_m^3 u^2 E_1(\tau_m u)$$

(the $\tau_m(B)$ dependence is shown in Fig. 3), and thereafter decreases approximately like $\exp(-\tau/2)$.

The result shows that, in principle, one can determine the parameter B from the time-dependent characteristics of the pulse of unscattered light.

At a distance exceeding the distance of direct visibility $(\sqrt{2hR_3})$, the light flux decreases approximately like $\exp(-B)$, and therefore, at large B values the unscattered light signal is exponentially attenuated.

The maximum distances over which recordings can be made are given by the quantity $R_m \approx [2(h + B_m\mu^{-1})R_e]^{1/2}$, where the value of the parameter B_m is smaller than 10 and depends upon the ratio of the useful signal to the background light signal.

The light signal received comprises quanta that have experienced one or several collisions. However, the contribution of these quanta over distances not exceeding R_m is insignificant in the initial time period (of the order of several microseconds), because the characteristic time of the change in the scattered light radiation is given by the path length of the light quanta in air and amounts to ~100 μsec.

LITERATURE CITED

1. D. Westervelt, E. Bennet, and A. Skumanich, in: Proceedings of the Fourth International Conference on Ionization Phenomena in Gases, Vol. 1 (1959), p. 225.
2. A. V. Zhemerev and Yu. A. Medvedev, At. Energ., 29, No. 4, 287 (1970).
3. A. V. Zhemerev et al., At. Energ., 35, No. 6, 438 (1973).
4. A. Johnson and R. Fouler, J. Chem. Phys., 53, No. 1, 65 (1970).
5. G. Korn and T. M. Korn, Manual of Mathematics, McGraw-Hill (1967).

A HIGH-CURRENT INJECTOR OF A LINEAR ELECTRON ACCELERATOR

V. A. Vishnyakov, V. M. Grizhko,
I. A. Grishaev, B. G. Safronov,
and G. L. Fursov

UDC 621.384.644.3

In [1, 2] the construction features and the characteristics of a single-section laboratory linear electron accelerator were discussed for an electron energy of 20 MeV at a 1.6-μsec pulse length and a 50-Hz pulse frequency. At present this accelerator is operating in the regime with a current pulse length of 11 μsec. An old klystron amplifier operating in the self-oscillator regime [3] with a 25-Hz pulse frequency and a 12-MW hf power is used as the hf power source. The stability at the top of the klystron voltage pulse with a 220-kV amplitude is 2.2% for an 11-μsec length and 0.5% for an 8-μsec length.

The cathode of the electron gun is made of lanthanum hexaboride. The stability at the top of the high-voltage pulse fed to the gun is 1.5%.

The current of the accelerated beam is measured by induction-type transit sensors calibrated with the use of a Faraday cylinder. The sensitivity of the sensors is 9 V/A. The shape and the amplitude of the current pulse from the sensor is displayed on an oscillograph screen. Also, a special electronic circuit transforms the pulse signals from the sensors into dc current, which permits relative measurements of the current by a needle-type instrument and recording of the form of the energy spectrum on the film of a ÉPP-09 recorder after passing through a magnetic analyzer.

The vacuum of $(2\text{-}3) \cdot 10^{-7}$ mm Hg in the system is obtained with three AIN-50 and four TÉN-30 pumps [4].

The energy spectrum obtained for a 720-mA current is shown in Fig. 1; the shape of the current pulse is shown in Fig. 2. The halfwidth of the spectrum, which comprises 4.2%, agrees with the calculation for a 1-6-μsec pulse length [2]; the energy at the peak intensity is 12 MeV.

The insertion of a buncher at the output of the electron gun increased the current in the pulse to 1 A.

The horizontal and vertical emittances of the beam of accelerated electrons are shown in Figs. 3 and 4; the dependence of the energy of the accelerated electrons and the electron efficiency on the load current is shown in Fig. 5.

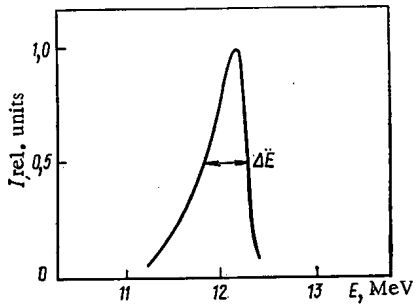

Fig. 1. Spectrum of the accelerated electrons (ΔE = 0.5 MeV).

Translated from Atomnaya Énergiya, Vol. 42, No. 3, pp. 231-233, March, 1977. Original article submitted August 23, 1976.

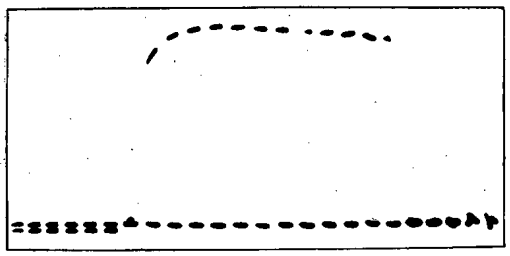

Fig. 2

Fig. 2. Oscillogram of the current pulse.

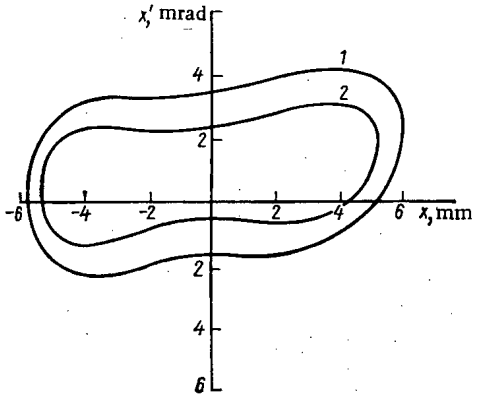

Fig. 3

Fig. 3. Horizontal emittance of the beam: 1) 90% current involved in emittance of 20.6 mm·mrad; 2) 50% in 9.8 mm·mrad.

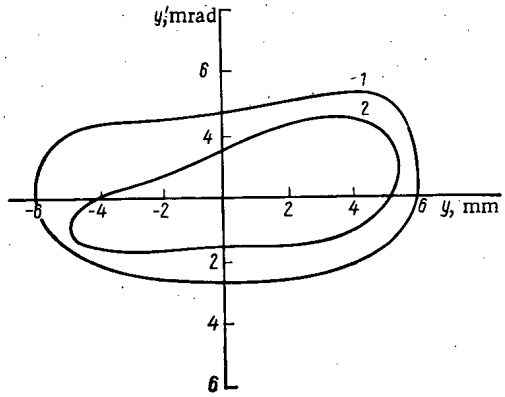

Fig. 4

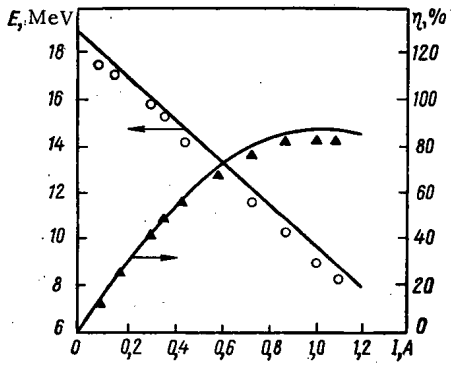

Fig. 5

Fig. 4. Vertical emittance of the beam: 1) 90% current involved in emittance of 20 mm·mrad; 2) 50% in 9.2 mm·mrad.

Fig. 5. Dependence of energy (○) and electron efficiency (▲) of the accelerator on current load. Continuous curves) computed; dots) experimental results.

The availability of a new klystron oscillator offers the possibility of increasing the mean current to 1 mA and the energy to 20 MeV at this current load due to the inclusion of an accelerating section. The bremsstrahlung of 10^5 rad/(min·mA·m) and photoneutron yield of $2 \cdot 10^{13}$ neutrons/(sec·mA) permit us to conduct radiation investigations effectively and to solve other problems requiring high levels of radiation.

LITERATURE CITED

1. V. A. Vishnyakov et al., in: Problems of Atomic Science and Technology [in Russian], High-Energy Physics Series, No. 1(1), Kharkov (1972), p. 19.
2. V. A. Vishnyakov et al., ibid, No. 4(6), Kharkov (1973), p. 11.
3. G. G. Oksyzyan et al., ibid, No. 4(4), Kharkov (1973), p. 67.
4. I. A. Grishaev et al., in: Problems of Atomic Science and Technology [in Russian], Physics and Technology of High Vacuum Series, No. 1(4), Kharkov (1975), p. 92.

HIGH-TEMPERATURE REACTIONS BETWEEN Zr + 1% Nb AND COMPACTED URANIUM DIOXIDE

G. P. Novoselov, É. V. Komarov, and B. G. Pastushkov

UDC 542.942.3

Compacted UO_2 reacts only slightly with zirconium and zircalloy at 700°C [1, 2], but more appreciably at 1100-1600°C [3, 4]. However, nothing has been published on the interaction of UO_2 with Zr + 1% Nb alloy on brief heating to higher temperatures.

We have evaluated certain features of the solid-state reaction on specimens of Zr + 1% Nb alloy in the form of tablets of diameter 8 mm and thickness 2 mm, which were used with pressed and sintered tablets of UO_2 of diameter and height 13 mm, density 10.3 g/cm^3, and open porosity 1-5%. When the contact surfaces had been ground, the alloy specimen was placed on the UO_2 briquette and the assembly was loaded into an alumina crucible, as alumina is incompatible with UO_2 up to 1800°C [5]. These assemblies were heated in argon or technical nitrogen (total impurities 0.1%) at atmospheric pressure to 1600 or 1750°C at rates of 30 and 150 deg/min, the high temperature being maintained for 4 h.

When the UO_2 – (Zr + 1% Nb) assembly was heated in nitrogen to 1600°C at 30 deg/min, a brownish film was formed on the contact surface of the alloy, which was readily removed with nitric acid. No attachment of the alloy to the UO_2 was detected. The uranium content in the alloy was 0.03 wt. %. Heating at 150 deg/min produced a stronger film, which was not removed even by prolonged boiling in nitric acid. In that case the uranium content of the alloy was 0.18 wt. %.

The microstructures indicated that the higher heating rate favored the formation of zirconium nitride, and also produced local melting in the alloy on account of the exothermic reaction between the zirconium and nitrogen. The microhardness was 2000 kgf/mm^2 for droplets of diameter 0.1-0.2 mm, which is close to the value for zirconium nitride. These results agree with previous conclusions on the effects of heating rate on nitriding [6].

No such effect was found on heating on assembly in argon to 1600°C; the uranium contents of the alloy were 0.14 and 0.22 wt. % for slow and rapid heating respectively. In the case of molten Zr + 1% Nb in argon at 1750°C, the melt wetted and penetrated the UO_2 briquette, and the solidified alloy contained 11.0 wt. % uranium and was inseparable from the briquette.

These experiments show that UO_2 is only slightly reduced at 1600°C in technical nitrogen; zirconium begins to react with nitrogen above 750°C and with UO_2 above 1100°C, so one supposes that a film of zirconium nitride is present on the surface of the alloy when the reaction with UO_2 starts, this film being compatible with UO_2 [7].

The argon atmosphere at 1600 and 1750°C produced considerable transfer of uranium into the alloy, which shows that the UO_2 was reduced. Higher temperatures produce more extensive reaction in the UO_2 – (Zr + 1% Nb) system [8].

LITERATURE CITED

1. C. Weber, Prog. Nucl. Energy, Ser. 5, 2, 295 (1959).
2. A. R. Kaufmann (editor), Nuclear Reactor Fuel Elements, Wiley, New York–London (1962).
3. T. T. Torlie et al., Nucleonics, 23, No. 4, 58 (1965).
4. C. O. Smith, Materials in Nuclear Reactors, Addison-Wesley (1967).

Translated from Atomnaya Énergiya, Vol. 42, No. 3, p. 233, March, 1977. Original article submitted September 3, 1976.

5. R. B. Kotel'nikov et al., in: High-Temperature Nuclear Fuel [in Russian], Atomizdat, Moscow (1969), p. 400.
6. K. I. Portnoi, Yu. V. Levinskii, and S. E. Salibekov, Poroshk. Metall., No. 12, 36 (1965).
7. W. B. Blumenthal, The Chemical Behavior of Zirconium, Krieger, New York (1958).
8. U.K. Patent No. 977566 (1963).

SEMINAR ON EQUIPMENT AND OPERATION OF REACTOR SYSTEMS OF VVÉR TYPE

G. L. Lunin

This seminar was held in March, 1976, in Neuglobsow, GDR, and was attended by over 60 specialists from COMECON member-nations, representatives of the COMECON Secretariat, and representatives of Interatomenergo. The seminar operated in two sections: the first dealt with the commissioning, operation, and safety of nuclear power stations, while the second dealt with physics and chemistry. In all there were 56 papers on the construction of power stations containing VVÉR (water-cooled–water-moderated) reactors, including initial commissioning, staff training, organization of repair and reloading, and researches designed to extend knowledge in the design and operation of VVÉR reactors.

Surveys on nuclear power station operation and nuclear fuel use were presented by workers from Bulgaria, the GDR, and the USSR; a paper entitled "Ten years of nuclear power in the GDR" (A. Schönher, W. Brune, and W. Winkler) dealt with the development stages in nuclear power from the Reinsberg nuclear power station containing a VVÉR-70 reactor to the Bruno Leuschner power station in Greifswald, which has a VVÉR-440 reactor. F. Ya. Ovchinnikov et al. (USSR) presented major results on the operation of four units in the Novovoronezh nuclear power station, together with economic parameters and surveys of major repairs. Particular attention was directed to methods of equipment diagnosis, especially vibrational acoustic and neutron-noise techniques. Some mention was made of the operation of the first unit in the Kozlodui nuclear power station, and also of commissioning of the second unit (K. Kuzmanov et al., Bulgaria), and also of some features of the operation of the high-power Kola nuclear power station in a closed power system (L. M. Voronin et al., USSR).

The utilization of nuclear fuel was considered in several papers; much interest was aroused by the paper by H. Akkerman (GDR), which presented results on researches extending over many years on the fuel cycle in power stations containing VVÉR reactors. The working efficiency was considered, and also a method of improving fuel use under variable-load conditions at the end of the reactor cycle, when the reserve reactivity of the VVÉR has deteriorated considerably. One way of improving the utilization of fuel in a VVÉR reactor is based on the temperature and power-level effects for the reactivity that occur on interchanging the rods, which was discussed by V. M. Tsybenko (USSR). The paper by H. Suschowsk (GDR) dealt with major principles for optimizing the choice of VVÉR fuel-loading cycles by computer.

Interest was also aroused by papers on the physical commissioning of the Nord-1 nuclear power station (L. Kirchmayer, GDR), and also by researches on the cores of VVÉR-440 reactors during physical commissioning (G.Ya. Aidrianov et al., USSR), and on power-reactor noise (A. Grabner et al., GDR).

The participants also devoted much attention to radiation safety in nuclear power stations containing VVÉR reactors; the following aspects were considered in the 15 papers on this topic:

1. The radiation environment during power-station commissioning with a view to providing staff safety and testing shielding performance;

2. analysis of staff exposure during power-station operation;

3. accumulation of corrosion products on surfaces; and

4. the effects of the power station on the environment.

Interesting data were presented on staff exposure during operation of the Nord power station by W. Schreiter et al. (GDR); the Reinsberg station has been operated over eight fuel cycles, and during this time the

Translated from Atomnaya Énergiya, Vol. 42, No. 3, pp. 234–235, March, 1977.

external radiation dose to the staff was 200 rem/cycle, the mean individual dose being 0.4 rem/yr. At the Bruno Leuschner station, the mean individual dose for 1973-1975 was 0.14 rem/yr.

The major conclusions were presented in several papers from the GDR and USSR on the effects of power stations containing VVÉR reactors on the environment; it was stressed that power stations with this type of reactor represent one of the cleanest sources of energy during normal operation. Escapes of radioactive products to the environment at the Kola, Novovoronezh, Reinsberg, and Bruno Leuschner stations have been only at few percent of the permissible level, while the maximum exposure of individuals in the locality was less than the maximum permissible level by four orders of magnitude, viz., a few percent of the natural background.

Fuel-rod monitoring in VVÉR reactors was discussed in two papers; the survey by K. Herold and H. Chirna (GDR) dealt with existing methods of monitoring rod sealing in a working reactor and during recharging; various topics for research on monitoring improvement for the core as a whole were proposed, as well as means of monitoring cassettes during reloading.

There was an excursion to the Nord power station at the end of the conference.

THIRTY-FIRST MEETING OF THE COMECON STANDING COMMISSION ON ATOMIC ENERGY

Yu. I. Chikul

This meeting was held during November, 1976, in Riga (USSR), and it dealt with measures in the nuclear-power field implied by the decisions taken at the Thirtieth Meeting, and also by the Executive Committee of the Council. Papers were presented on scientific and engineering collaboration between COMECON members on the utilization of nuclear energy for peaceful purposes in 1971-1975, with suggestions for the main lines of collaboration up to 1990, as well as developments in the field of common standards and specifications for nuclear instrumentation for laboratory and industrial purposes made during 1971-1975.

The Commission discussed the forecasts for the major trends in radiation technology and engineering up to 1990.

The meeting also discussed the state of the art in multilateral international specialization and cooperation in the production of isotopes and the use of radioisotope methods and radiation technology in various branches of the economy of member countries. Particular attention was paid to improved performance in the Interatom instrument international joint economic enterprise.

The Commission also discussed the organization of studies on topics 1-2 "Construction and Commissioning of power units with water-cooled–water-moderated reactors of output 1000 MW" and 1-3 "Research and design studies on the construction and operation of high-power fast reactors," which were included in the agreed plan for multilateral integrated studies in 1976-1980, which involves an agreed division of the work between the member countries.

The meeting also confirmed plans for the work of the Commission during 1977-1978, and also studies in the field of standardization for 1977.

The appropriate recommendations or decisions were made on all the topics considered by the Commission.

COLLABORATION NOTEBOOK

The Eighth Meeting of the Radiation-Safety Standing Committee was held September 20-24, 1976, in Erevan. This meeting discussed topics arising from surveys at the conference on "The provision of radiation safety in nuclear power-station operation," especially those related to collaboration up to 1985 between member-nations in the area of radiation safety and the detailed implementation of working plans, for which purpose a report was discussed that dealt with comparison of individual γ-ray dosimeters performed in 1976 in the GDR. The comparison showed that the error of measurement was quite acceptable in most instances. It is proposed in 1977 to perform a comparison of individual dosimeters intended for mixed x-ray and γ-ray fields.

The meeting also discussed and agreed a report entitled "Analysis of methods and instruments for individual dosimetry used in COMECON member-nations during normal operation and emergency situations in nuclear power stations." This surveyed the individual dosimeters used in the various countries, and also defined the levels of individual dosimetric monitoring at nuclear power stations and on research reactors, with presentation of suggestions and conclusions on this topic. The analysis led to the recommendation that Interatominstrument should examine the scope for designing and producing indiivdual dosimeters.

The meeting also made preparations for a symposium to be held in May 1977 in Czechoslovakia on "New methods in individual dosimetry," at which it was proposed to discuss suggestions for future collaboration on individual dosimetry, including comparison of individual-dosimetry methods for mixed γ-ray and neutron fields.

The meeting also accepted "Recommendations on the organization of medical support to staff working with radioactive substances and ionizing-radiation sources," and it further considered reports on researches on the radioactivity of the Danube and the Baltic during 1975, with suggestions for joint research expeditions from member countries.

The meeting also agreed on drafts for collaboration plans for member countries in the area of radiation safety for 1977-1978.

■

The Thirteenth Meeting of the Interatominstrument Council was held November 16-19, 1976, in Warsaw, Poland with the chair taken by the General Director of the Electronics and Light-Current Engineering Undertakings, K. Vancl; the meeting dealt with division of labor and cooperation in the production of equipment, as well as the lines for collaboration in this area in 1977. During the meeting, the first agreement on multilateral international specialization in the production of nuclear-engineering components was signed. Therefore, the Council requested the director of Interatominstrument to implement the publication of catalogs of specialized equipment in 1977.

Also, there was a discussion on a report prepared by Interatominstrument, "Proposals for the main lines of collaboration in forecasting research and design studies," and the Director of Interatominstrument was requested to define the details of such collaboration with interested members.

There was also a discussion of economic aspects in the narrow sense, which was based on "Results and development prospects from branches of Interatominstrument in economic agreement in relation to self-sufficiency," and the Council made decisions designed to improve the major performance features of Interatominstrument in service and design improvements, especially with regard to equipment covered by economic agreements.

After careful consideration, the Council confirmed the working plans for the organization for 1977 and also the main lines of the annual plans of the branches for engineering support, as well as a program for the operation of the organization for 1977-1980.

The Director of the organization for the next five-year period up to February 28, 1982, was again chosen as Z. Twardon, while a reorganization commission would operate up to the end of 1978. K. Vancl was chosen as the President of the Council for 1977.

The Council also agreed a preliminary agenda for the Fourteenth Meeting, which is to be held in Czechoslovakia in May 1977.

The meeting of the Council was characterized by a general cooperative atmosphere.

NEW USSR NUCLEAR POWER STATIONS

E. P. Karelin

At end of the first year in the Tenth Five-Year Plan, a major achievement in Soviet power engineering occurred: the commissioning of the first units at the Kursk and Armenian nuclear power stations and of the fourth unit at the Bilibinsk power station. The installed power of nuclear stations in the Soviet Union increased by almost 1.5 GW.

The first unit at the Kursk station was run up to power starting on Dec. 19, 1976 (Fig. 1); this was preceded by extensive commissioning studies. The Kursk station has RBMK water–graphite channel reactors of output 1 GW(e), which had been operated successfully at the Leningrad nuclear power station. Extensive use was made of the experience with that power station in constructing the Kursk one.

On Dec. 30, 1976, the turbines in the first unit at the Kursk power station were connected to the central grid; construction of the station continues. It is planned that the second unit should be commissioned in 1978.

The commissioning of the first unit at the Armenian nuclear power station (Fig. 2) represents an important stage in the advance of Soviet nuclear power. A specific feature of the station is that it lies in the region of high seismicity, which has a required large volume of research and design studies to improve the VVÉR-440 standard reactor in order to ensure reliability and safety in the presence of potential seismic loads, and also to provide special building designs.

Fig. 1. General view of the Kursk nuclear power station and of the control room.

Translated from Atomnaya Énergiya, Vol. 42, No. 3, pp. 236-238, March, 1977.

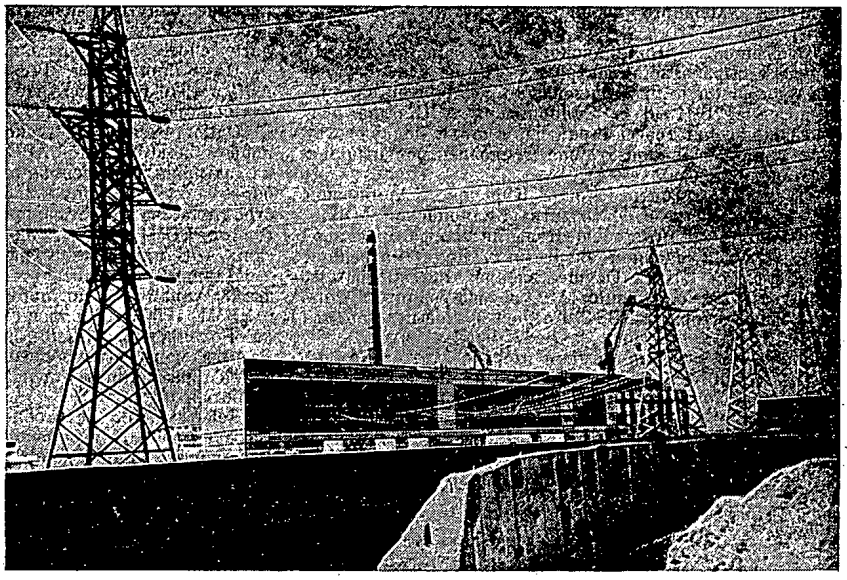

Fig. 2. The water intake of the Armenian nuclear power station.

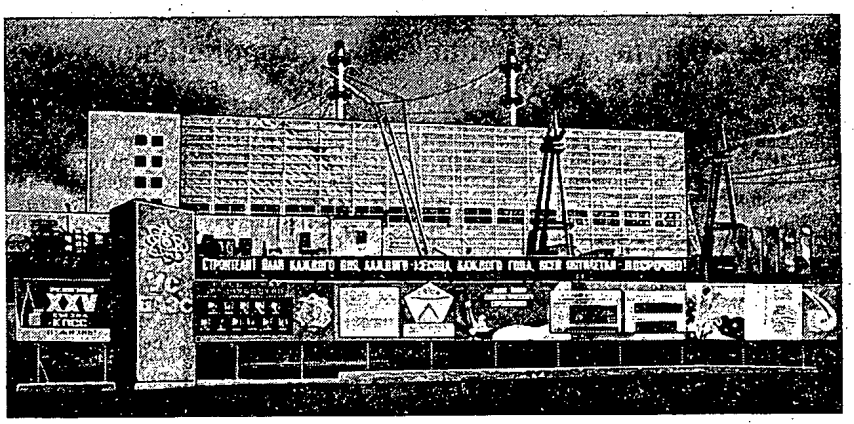

Fig. 3. General view of the Bilibinsk nuclear thermal and electrical station (photo by V. I. Bratchikov).

The reactor was brought to power on Dec. 28, 1976; the commissioning of the first unit at this power station provides substantially improved power supplies to Transcaucasia.

A start was made in 1976 on the construction of the second unit at the Armenian power station; the concrete rafts under the reactor section have been poured, and the framework of the machine hall has been installed, while equipment sections Nos. 3 and 4 have been built.

On Dec. 27, 1976, the last (fourth) unit at the Bilibinsk nuclear power station was commissioned (Fig. 3). The completion of construction is highly significant to the economic progress of the Chukotka area.

A special feature of the Bilibinsk station is that it produces heat for industrial organizations and dwellings in addition to electrical energy; in 1976, this station was connected to the heat grids in the area and became essentially the first fully commercial nuclear thermal and electrical station in the Soviet Union.

The commissioning of the first units at the Kursk and Armenian power stations and the completion of construction at the Bilibinsk power station represent major stages in the extensive nuclear power program envisaged by the Twenty-Fifth Congress of the Communist Party of the Soviet Union; this program envisages the construction of nuclear power stations with VVÉR (water-cooled–water-moderated) reactors or with RBMK (water–graphite channel) reactors.

Also during 1976, a start was made on constructing the fifth unit at the Novovoronezh power station, and further starts were made at the Kalinin, Rovensk, and South Ukrainian power stations, which have VVÉR reactors. Of these advances we may note particularly the fifth unit at the Novovoronezh power station, which has a

VVÉR-1000 reactor of electric-power output 1 GW. The concrete shield has been almost completed, as have construction operations in the machine hall. Much engineering equipment will be installed in 1977.

Work proceeded on the production of the concrete bodies at the Kalinin, Rovensk, and South Ukrainian power stations in 1976.

The commissioning operations on the first unit at the Kursk power station and the construction of the second unit were accompanied by completion of major building operations for the first unit in the Chernobyl power station, while the construction of the second unit continued, both of these having RBMK-1000 reactors. It is planned that the first unit at the Chernobyl power station should be commissioned in 1977.

The commissioning of units with long-standard reactor types (VVÉR-440, VVÉR-1000, and RBMK-1000) has been accompanied by continuing construction of a third unit at the Beloyarsk power station, which has a BN-600 fast reactor. The main equipment in the reactor section has been installed, and preparations are being made for installing the turbines.

The currently operating units in the nuclear power stations of the Ministry of Energy of the USSR (four units at Novovoronezh, two at Kola, three Bilibinsk, and two at Beloyarsk) have all operated reliably during 1976, and they have provided a good match to the power system load graphs.

CONFERENCE OF THE AMERICAN AND EUROPEAN NUCLEAR SOCIETIES

V. A. Sidorenko

This conference was held in Washington, USA, Nov. 14-19, 1976, and it consisted of five plenary sessions and about 75 sectional (technical) meetings. The latter dealt with various scientific–technical aspects of nuclear power, and the meetings were based on invited and submitted papers. Plenary sessions dealt with the following topics: the future of world power, engineering reports on fuel cycles, social aspects of fuel cycles, future systems, and safety in water-cooled reactors.

This joint meeting led the organizers to provide for a discussion of topics of interest to nuclear-power engineers in the USA and European countries.

The conference proceedings show that a major aspect at the present time is to support nuclear power with fuel-reprocessing facilities, particularly spent-fuel reprocessing. At present there is no such reprocessing plant anywhere in the world. President Ford stressed the need to prevent the spread of nuclear weapons, which requires a temporary delay in fuel reprocessing, which can proceed only on a modified basis. However, this should not affect the fast-breeder program, for which large-scale fuel reprocessing will be deferred after 1985. President Ford expressed the view that additional research is required in this area, especially with a view to supporting nuclear power without processing irradiated fuel, e.g., by avoiding the separation of uranium and plutonium in the reprocessed fuel, or else cycles for successive use of partially burned fuel in various reactors, and so on. This approach has led to vigorous protests from some interests in nuclear power; it was reported by the president of companies that have built nuclear power stations in the USA that the major obstacles to advance in nuclear power at the present time come not from society generally but from governmental organizations. Nuclear power has come under suspicion on account of lack of clarity and lack of certainty over certain problems in the fuel cycle.

The first plenary session, which defined the general lines of the conference, was concerned also with papers by R. Simons (ERDA), A. Gireau (French Atomic Energy Commission), and Reza Fallah (Iran).

The Iranian representative made the following points: 1) it is essential to control oil and industrial-goods prices; the rising prices of industrial goods in recent years have led in turn to rising prices for oil, and the process threatens to get out of control; 2) it would be desirable to set up an internal energy-resource bank. The most reliable bank is the Earth itself, but the oil-extracting countries have agreed, while continuing to extract oil, to deposit the product in an international bank in order to be able to utilize their contribution subsequently in economic development. The ERDA representative emphasized that a task of American industry is not only to provide national energy independence but also to develop the enormous markets of Asian countries in order to provide new energy sources. The early estimates made by the United States Atomic Energy Commission on the progress in nuclear power up to the year 2000 were unrealistic. By that time there are expected to be about 300 nuclear power stations, not 1000. A. Gireau gave an extended analysis of the growth trends in energy demand and the development of nuclear power in various countries; he showed that the main rise in demand for all forms of fuel is to be expected in the developing countries rather than in industrially developed ones. These demands at present are not being met. The problem can be solved only by introducing breeder reactors by the year 2000, particularly ones suitable for general use.

Demand and possible supplies of nuclear fuel in the United States are approximately in balance; on the other hand, demand essentially exceeds supply on the international market, particularly in European countries, which accounts for their considerable interest in a closely controlled market for nuclear fuel.

Translated from Atomnaya Énergiya, Vol. 42, No. 3, pp. 238-239, March, 1977.

New methods of uranium enrichment developed in various countries have no advantages with regard to capital investment or energy consumption by comparison with the diffusion method, but they do make separation technology available to countries that could not envisage the diffusion technique. The centrifuge method requires less than a tenth of the electrical energy for the same capital cost. The laser method is considered as a third-generation one (for the end of the century).

Reprocessing of irradiated fuel may involve major developments in centrifuge techniques, which provide high throughput and short contact times between reagents. These are promising methods for processing high-activity fuel after short cooling periods, which is important for fast reactors designed for short fuel doubling times.

Also, plutonium may be reused in thermal reactors. It is anticipated that in future there may be a surplus of uranium when breeder reactors are commissioned, and this could be utilized in thermal reactors. The return of plutonium from exhausted fuel from thermal reactors could result in a uranium economy of about 20%, while the maximum economy from recycling fuel could attain 60% (paper by B. Spinrad, USA).

Much attention was also given to improved fuel utilization in thermal reactors. Edlund (USA) gave a paper on the scope for a plutonium fuel cycle in an ordinary water-cooled–water-moderated reactor, which can be operated in such a way as to provide a breeding factor up to 1.08. Analogous techniques are possible also for heavy-water reactors.

Canadian researchers have considered ways of using thorium in heavy-water reactors, which could allow the nuclear power output to be raised to $200 \cdot 10^6$ MW even though uranium stocks in the country may be restricted, and this level could be supported from domestically produced fuel.

One of the arguments against fuel reprocessing and for reactor designs not requiring chemical reprocessing (improved burnup in ordinary reactors, fused-salt reactors) is based on the desire to restrict the spread of nuclear weapons.

Two aspects may be distinguished in the discussion of safety problems for nuclear power stations:

1. Man is involved at all stages in the utilization of nuclear power, and human errors cannot be entirely eliminated, which must be borne in mind in engineering safety measures;
2. The future of nuclear power in each particular country is very much dependent on accidental circumstances, for instance, major emergences in nuclear power stations in any other country. Every country wishes nuclear power stations to be reliable and safe, not only for that country but also for others. This aspect provides a major basis for general international collaboration on nuclear power station safety.

There was also a plenary session on alternative systems, and a paper was presented on behalf of two countries (the USSR and the USA) engaged in a joint research program on thermonuclear power: for this purpose, E. P. Velikhov presented a paper, which had a very good reception.

The complete texts of the papers from the plenary sessions were published as a single volume; the abstracts of all the others were distributed to the participants.

INTERNATIONAL CONFERENCE ON LIQUID METAL COOLANTS

F. A. Kozlov

This conference was held on May 3-6, 1976, in Champion, Pennsylvania, USA, and was attended by 203 representatives of 11 countires. Most of the papers (out of 124) dealt with sodium as a coolant for fast reactors.

Impurity Sources and Carrier Purification. Much attention was given in these 22 papers to the contamination arising during operation; the initial contamination of the sodium by oxygen extracted from the surfaces of the materials in the Phoenix reactor in France was 2 g/m^2. The subsequent contamination in the second loop was due to hydrogen arising from corrosion, which entered from the third loop at a rate of 0.7 mg/h $\cdot$ m^2 in the initial operating period or about 0.35 in the same units after operation at power for 334 days. The main impurities accumulating in the cold traps were oxygen and hydrogen, which were present as sodium oxides, hydrides, and hydroxides.

The papers from the French workers quoted cases of emergency contamination due to entry of oil from pumps, which greatly hindered subsequent purification of the carrier.

The following impurity levels have been maintained by the use of cold traps: oxygen $(1\text{-}5)\cdot10^{-6}$, hydrogen $(5\text{-}8)\cdot10^{-8}$, and carbon $(0.4\text{-}5)\cdot10^{-6}$.

Transport of Radioactive Corrosion and Fission Products. These eight papers dealt with the formation and transport of the radioactive impurities ^{65}Zn, ^{110}Ag, ^{54}Mn, ^{182}Ta, ^{124}Sb, ^{60}Co in various materials; a study of the behavior of the tritium in sodium has shown that this is deposited in a cold trap by normal crystallization of sodium tritide on cooling and also by exchange between tritium and hydrogen, the latter present as hydride. There was also a detailed discussion of the distribution of radioactive products in the cold trap (from the United Kingdom).

A picture was also given of the accumulating radioactivity in a loop in the Rhapsodie reactor (France). So far, ^{54}Mn has been dominant, but at the end of 1974 the contribution from ^{137}Cs had risen to about 20% and become comparable with that from ^{22}Na.

The weight loss in the stainless steel due to corrosion was more than halved by reducing the oxygen concentration in the sodium from $2.5\cdot10^{-6}$ to $0.5\cdot10^{-6}$; at the same time, the deposition (over 6000 h) of ^{54}Mn was reduced about 30% and that of ^{60}Co by a factor three. Hot-trap purification to oxygen contents of $<10^{-8}$ did not prevent the deposition of radioactive substances.

Monitoring Instruments and Methods. About 30 papers dealt with instruments for monitoring oxygen, hydrogen, and carbon helium in sodium and in protective gases, and also with instruments for monitoring the thermophysical parameters of sodium-cooled reactors. Particular attention was given to direct determination of impurities in circulating sodium. Development work is proceeding on instruments for monitoring oxygen by electrochemical means in cells containing solid electrolytes. The vanadium method of assaying oxygen in sodium has been perfected. Researches on the Na–V–O system at low oxygen potentials have shown that a β phase is formed in vanadium wire no matter what the oxygen concentration in the sodium, and this acts as a barrier to the diffusion of oxygen into α-V. This gives rise to some doubt whether the vanadium method is usable.

Some interest is attached to continuous monitoring of oxygen in sodium by the vanadium method in conjunction with ultrasonic techniques; the ultrasonic absorption alters on immersing a vanadium specimen in sodium, the change being dependent on the oxygen concentration in the vanadium, which itself is governed by the oxygen content of the sodium and the temperature. Electrochemical methods are also being developed for continuous monitoring of the thermodynamic activity of carbon in sodium.

Translated from Atomnaya Énergiya, Vol. 42, No. 3, pp. 239-241, March, 1977.

Although many difficulties have been encountered, it appears possible to build such devices for on-line monitoring of oxygen and carbon in sodium.

Other developments concern detectors for identifying gases leaking into the sodium, induction-type and float level gauges, fast pressure transducers, magnetic flowmeters for pipelines of diameter 400 mm and for pipe sets in the core, gas-bubble detectors, monitors for low levels of helium in sodium, and many other such instruments.

Sodium–Water Steam Generators and the Reaction between Water and Sodium. Over 20 papers dealt with this topic, with particular emphasis on composition stability, mechanical characteristics, and technological features of material for steam generators, safety in such generators, and detection of leaks of water into the sodium.

General Electric (USA) stated that researches had been performed on the mechanical and other properties of 2.25% Cr+1% Mo steel, which has been selected as the main steel for steam generators. The maximum working temperature is 510°C, while the corrosion under heat-transfer conditions may be serveral times that under isothermal ones. Studies are being performed in the USA on nickel-rich steels for sodium–water steam generators.

Extensive researches are being performed on self-propagating leaks; it has been found that the size of the leak channel on the water side increases spontaneously, although the channel is blocked by corrosion products and reaction of the sodium with the water. In some cases, such leaks can seal spontaneously but then reopen and grow. Methods have been developed for detecting such leaks by means of a circulating 5-10% solution of citric acid.

Good agreement between theory and experiment has been obtained on a large sodium–water leak in a large-scale (1:2.5) model for the steam generator in the Monju fast reactor; there was no failure in adjacent tubes for leaks giving 6.7 and 9.7-14.2 kg/sec (the amounts of water were, respectively, 61 and 412 kg).

The hydrogen concentration in sodium has been adopted as the basic means of detecting leaks of water into sodium, for which purpose nickel membranes are used. The flow of hydrogen through such a membrane is monitored by a magnetic-discharge pump or a mass spectrometer.

Researches on solid-electrolyte cells based on thorium and yttrium oxides are being performed only in the USA; a computer analyzes the input from the monitoring instruments and produces a hazard signal. Many studies are on hand on the sources of hydrogen in loops and on the performance of leak monitoring systems, which are performed directly on reactors by injecting hydrogen (Phoenix, PFR, and SCTI) or water (actually performed with SCTI, planned for EBRII). The cold traps are operated continuously in order to maintain the minimum hydrogen background and improve the sensitivity.

Sodium Elimination and Equipment Reuse. Five papers dealt with the nitrogen–steam and alcohol methods, as well as the vacuum-distillation one. The reagent is denatured ethanol, which is the following mixture: 85.8% anhydrous ethanol, 4.3% methanol, 9% isopropanol, and 0.9% methyl isobutyl ketone.

The reaction rate is controlled by means of the temperature. The addition of up to 1.5% acid to the alcohol is considered by General Electric researchers as eliminating alkali corrosion, particularly for components whose temperatures during the reaction exceed the temperature of the alcohol by not more than 7°C. Gaps of width in excess of 0.025 mm can be cleaned in this way.

Dry ice is used in the Federal German Republic before cleaning and during reaction with methanol to improve the cooling and to provide a layer of inert gas over the alcohol.

The nitrogen–steam method is recommended for cleaning large units containing no narrow gaps or slots; the major stages are as follows: the sodium is run off at about 200°C, and the system is reacted with steam at $\leq$ 120°C (up to 4% hydrogen may be present in the gas vented to the atmosphere), washing with water to remove the alkali at 80°C, and drying in nitrogen at 80°C until the dew point falls to –48°C. This technique has not resulted in any occurrence or extension of alkali corrosion.

Corrosion, Friction, Wear, and Seizure. There were about 50 papers on these topics. Particular attention was given to the effects of nonmetallic impurities in sodium (oxygen, carbon, and nitrogen) on the alkali corrosion and mechanical parameters of constructional materials; studies have also been made on mass transport for corrosion products from such materials, and also for carbon and nitrogen, in equipments containing liquid metal coolants.

Measurements have been made over very wide ranges in impurity concentration (oxygen $\sim 10^{-5}$-10^{-8}, carbon $\sim 10^{-6}$-$2 \cdot 10^{-8}$), and also wide ranges in temperature, 220-738°C, working time (up to 60,000 h), and coolant speeds (up to 6 m/sec), for which purpose numerous combined measurements are required. Studies have been made on the effects of the mean coolant temperature and the heat flux, and also on the effects of various processes on the hydraulic resistance in channels in the core. The experiments on mass-transfer for corrosion products have been performed with a special system built on a 1:2.5 scale.

Extensive studies have been performed on friction, wear, and seizure for various materials operating in sodium.

Researches on liquid metals used at high temperatures are continuing in the United States, as are researches on fundamental characteristics of the lithium-impurity system. Researches have been performed on liquid metals as means of accumulating or transforming energy, and also as current collectors for high-power unipolar generators. Measurements have also been made on the transport of sodium vapor through the shielding gas in sodium-cooled fast reactors; fundamental researches have been performed on the combustion mechanism for sodium, reaction between potassium peroxide and excess potassium, the preparation and properties of double oxides of sodium and transition metals, the effects of argon released from solution on heat transfer in the intermediate heat exchanger in a fast reactor, and the performance of thermal insulation operating in argon containing sodium aerosols and vapor.

The conference proceedings showed clearly that researchers in many countries have performed a great variety of studies on the technology of liquid metal cooling, which means that such coolants can now be utilized in power reactors. Engineering design studies have now made it possible to prevent hazardous contamination of the coolant in most forms of reactor operation, or else to suppress the effects of such contamination.

THIRD INTERNATIONAL CONFERENCE ON ZIRCONIUM IN THE NUCLEAR POWER INDUSTRY

B. G. Parfenov

This conference was held in Quebec, Canada, Aug. 10-12, 1976; it was organized by the American Society for Testing Materials in collaboration with the Canadian Nuclear Association and the Committee on Nuclear Metallurgy of the American Institute of Mining, Metallurgy, and Petroleum. The 39 papers dealt with reliability and safety of zirconium as a material for fuel-rod sheaths and channel tubes. In particular, the behavior of zirconium alloys under critical conditions arising from loss of coolant has been examined. The sheath of a fuel rod may fail for thermal reasons under these conditions, or else on account of embrittlement arising from structural changes and absorption of oxygen, as well as on account of melting, accelerated oxidation, and cracking.

Hunt and Foot showed that zirconium alloys deform at temperatures above 1000°C largely in accordance with the structural state, the deformation being largest when the alloy is in the $\alpha + \beta$ two-phase region. A Zr–2.5% Nb alloy considered in Canada as a promising material for fuel-rod sheaths is less rigid than zircalloy at 600-900°C, whereas above 900°C it is stronger than zircalloy. The deformation rate is less by about a factor 100 than that for zircalloy, while the failure occurs at a higher temperature. The reason is that volatile elements and impurities dissolve at such temperatures in the zirconium and produce a greater increase in strength than do inclusions of excess-phase particles. The alloy dissolves 2.5 at. % of alloying elements above 1000°C, whereas zircalloy will dissolve only 0.5 at.%. A mathematical relationship was presented for the temdependence of the strain rates in the α and β states, as well as an expression for the activation energy and an equation for the stresses in isotropic tubes. The activation energy for deformation of Zr–2.5% Nb alloys ranges from 36,700 to 16,000 and then to 23,400 cal/mole as the temperature goes from 700-800 first to 900-1000 and then to 1100-1200°C, respectively.

Translated from Atomnaya Énergiya, Vol. 42, No. 3, pp. 241-244, March, 1977.

TABLE 1. Calculated and Measured Changes in Channel-Tube Size (mm) for Hanford Reactor N

Tube type	Extension ratio	Reduction (%) during cold rolling	On diameter		On length	
			calc.	meas.	calc.	meas.
1	29 : 1	29—30	—0,05	—0,05	35	35,6
2	8 : 1	30—35	0,08	—	24	28,0
3	13 : 1	17—18	0,03	0,13	19,7	18,8
1a	29 : 1	17—18	—0,06	from —0,05 to 0,01	25,8	25,5

Zawatsky and Urbanik considered the oxidation of alloys in high-temperature steam and the diffusion of oxygen under such conditions; the following phase sequence reckoned from the surface arises during oxidation: ZrO_2/α-Zr/β-Zr. The layer of ZrO_2 produced by the oxidation and the underlying layer of α-Zr are very brittle, so they cannot withstand deformation and determine the oxygen embrittlement mechanism. When zirconium is cooled slowly, oxygen diffuses from the β-Zr to the α/β phase interface, which causes the layer of α-Zr to thicken. A two-phase layer composed of the α and β phases is produced at the interface on rapid cooling. The oxidation rate increases around 1500°C, which is evidently due to change in the structure of the oxide from tetragonal to a mixture of tetragonal and cubic forms. There are no major differences in the rate and mode of oxidation of Zr—2.5% Nb alloy and zircalloy. The measurements agree well with computer calculations. It was concluded that this sequence in the layers of oxide and metal, which differ in structure, is governed by the exact test conditions and may allow one to define by metallographic methods the working conditions for fuel-rod sheaths in emergency situations.

The oxidation rates for zirconium alloys in high-temperature steam obey a parabolic law.

Some of the papers dealt with the corrosion of zirconium alloys, particularly uneven corrosion, and the effects of some fission products (in particular cesium) on the oxidation.

Much attention has also been given to the effects of radiation on creep and deformation; a notable feature of most of the papers is that mathematical models have been set up for these processes, which involve comparing theoretical and observed curves which allow one to reduce the volume of measurements and to predict the behavior of zirconium alloys. Franklin and Franz described a model for anisotropic creep in zircalloy under irradiation, which allows one to calculate the reduced shear stress on any slip system. The deformation is described as a function of the texture, state of strain, and test conditions on the assumption that the slip occurs on two intersecting systems, one of which is the $[10\bar{1}0]\ \langle 1\bar{2}10\rangle$ prismatic system. The calculations were performed with new computer program termed SPAC by standard numerical methods.

Dressler et al. have examined the creep in tubes in various initial states at 400 and 320°C for stresses of 10 and 11.3 kgf/mm^2 and have found that cold-deformed tubes show higher creep resistance over short periods (up to 4000-5000 h), whreas recrystallized ones show better resistance over longer periods.

French researchers (Charquette and others) discussed the effects of elevated tin contents (up to 2%), impurities (oxygen up to 0.2% and carbon up to 0.02% by weight), and also intermediate quenching from the β region, on the creep in irradiated sheaths made of zircalloy; it has been found that the circumferential deformation can be reduced by a factor of 2-3.

Interesting evidence was presented by Alexander and others on the size changes in channel tubes in the N reactor at Hanford after 12 years of operation; the zircalloy tubes (1004 in all) of diameter 82.7 mm, wall thickness 6.5 mm, and length 16,150 mm were made in four different ways with different degrees of drawing and hot pressing (from 29:1 to 8:1) and of reduction during cold rolling (from 17-18 to 30-35%). After operation at 202-292°C for 50,000 h, a tangential stress of 6.2 kgf/mm^2, and an axial stress of 5.8 kgf/mm^2 in a neutron flux of $2 \cdot 10^{13}$ neutrons/cm^2 · sec (above 1 MeV), the tubes were found to differ in deformation. The extension of the tubes was proportional to the channel power. The largest extension (0.35%) occurred for tubes stretched considerably during extrusion (29:1) or highly deformed in the cold (by 30-35%), while the extension was least (0.19%) for the other limiting case (8:1) for low degrees of cold strain (17-18%). Intermediate values were found for other forms of processing (Table 1). Tubes showing the maximum axial extension usually showed little change in diameter (sometimes a negative change), while the smallest change in length was accompanied by a considerable increase in diameter.

TABLE 2. Minimal Characteristics of Irradiated Zircalloy-2 Tubes at Room Temperature

Test	Characteristic	After tempering	After annealing
Axial stretching	Yield point $\sigma_{0,2}$, kgf/mm²	39,5	31
	Ult. strength σ_b, kgf/mm²	48,5	41,5
	Extension δ (over 50 mm), %	20	25
Internal pressure	σtan, kgf/mm²	62	59
	δtan, %	10	18
Metallography	Grain size, μ	Mean ≤ 10, maximal ≤ 25, or 22 after 3 days in steam at 400°C, or 38 after 14 days with formation of black lustrous oxide film	
Corrosion	Mass increase, mg/dm²		
Hydride orientation	Number of hydride plates oriented at ≥ 40° to the tube axis, %	⩽ 35	⩽ 40

TABLE 3. Mechanical Parameters of Channel Tubes Made of Zircalloy-2 and Zr–2.5% Nb Alloy at 300°C*

Material	State	Test direction	Yield point $\sigma_{0,2}$, kgf/mm²	Ult. strength σ_b, kgf/mm²	Extension, %
Zircalloy-2	Hot pressing, cold rolling with 20% reduction, stress relief, annealing at 400°C	Axial	31,0	36,5	22
Zr–2,5% Nb	Hot pressing	Axial	36,5	43,4	22
	Hot pressing, cold rolling with 20% reduction	Axial	42,7	48,2	12
		Tangential	—	52,4	12
	Hot pressing, cold rolling with 20% reduction, annealing at 400°C for 72 h	Axial	34,4	46,8	14
		Tangential	—	53,7	13
	Hot pressing (fine structure)	Axial	44,8	51,7	18
	Hot pressing (fine structure), cold rolling with 20% reduction, stress relief, annealing at 400°C	Axial	48,2	58,6	16
	Hot pressing (fine structure), cold rolling, quenching from 870°C, cold rolling, and aging at 500°C	Axial	57,4	62,7	—
		Tangential	61,3	66,1	—

* The specifications for grain size, corrosion rate, and hydride orientation were analogous to those for the irradiated tubes.

The extension and change in diameter are associated with radiation-induced creep and radiation-induced swelling, which themselves are dependent on the texture, dislocation density, temperature, and neutron flux. One result of the swelling is that the length increases (along the working direction), and this increase in the cold-deformed material (the size change at constant volume) occurs at a constant rate at high neutron fluences ($> 3 \cdot 10^{20}$ neutrons/cm² above 1 MeV). Also, the rate increases with the extent of the cold deformation even when the material has been annealed. Estimates have been made of the effects of each factor (radiation-induced swelling and anisotropic creep) on the size change, and it has been found that the texture is very much dependent on the mode of manufacture. Any increase in the degree of drawing or cold reduction increases the number of transversely oriented basic poles.

The diameter change due to the radiation-induced growth may be negative if the proportion of normals to the basal plane lying perpendicular to the axis increases, which may compensate the effects of creep either partially or completely. Electron-probe measurements indicate an increase in diameter at the outlet, which may be due to variations in radiation-induced creep rate due to variation in the coolant temperature along the tube. Laboratory tests on tubes processed in a similar fashion and tested for 45,000 h under identical conditions showed no changes in length and diameter.

One of the models that explain these effects in zirconium alloys involves dislocation glide in response to irradiation; in this model, the strain rate during creep or swelling is proportional to the texture coefficients for the three principal directions. It has been found empirically that the rate is linearly dependent on the neutron flux and that the creep rate is proportional to the load. Therefore, the following formula can be used to determine the size in any direction:

$$\dot{\varepsilon}_d = \dot{\varepsilon}_{gd} + \dot{\varepsilon}_{cd},$$

where $\dot{\varepsilon}_d$ is the strain rate in direction d, $\dot{\varepsilon}_{gd}$ is the rate of growth deformation, and $\dot{\varepsilon}_{cd}$ is the rate of creep deformation:

$$\dot{\varepsilon}_d = G_d K_{gd}(S)\,\Phi + C_d K_{cd}(S)\,\Phi\sigma,$$

where K_{gd} is the rate of radiation-induced growth in direction d for $G = \Phi = 1$, which is a function of the structure S, while K_{cd} is the rate of radiation-induced creep for $C = \Phi = 1$, which is a function of S, where Φ is the fast-neutron flux and σ is stress.

The independent variables K_g and K_c may be derived in order to calculate the changes in size in a tube made in any particular way.

Calculations on the size changes for the Hanford reactor agreed well with the measurements (Table 1); if the initial structure of the tube is known along with the reactor working conditions, it is possible to determine the size change with reasonable precision, and also to estimate the channel reliability and to define a suitable manufacturing technique.

Much attention was also devoted to the interaction between stress and strain on the one hand and radiation damage on the other; e.g., Lee discussed the mechanism of local deformation in neutron-irradiated zirconium alloys in states of two-dimensional strain, which involves sequential displacement of dislocation systems, which are subsequently blocked by radiation-induced defects.

Cheddle pointed out that in 1976 the CANDU reactors consumed 400 tons of zirconium, mainly in the production of tubes costing about 80 dollars per kg, and the demand in 1986 would be about 800 tons. Rigid quality standards have been laid down. Tubes for fuel-rod sheaths should have a uniform fine-grained structure, in which the α-phase grains are oriented in such a way that the normals to the basal planes are nearly radial. This provides the best combination of strength and plasticity, as well as the best orientation for the platy hydride inclusions.

The specifications for the tubes (Tables 2 and 3) impose major restrictions on the pressing, cold-rolling, and annealing techniques. Particularly careful monitoring is required in cold deformation, which determines the uniformity of the properties over the cross section.

Much attention was also given to alloy failure during use; Smith's paper presented a relationship between cracking in tablets in uranium dioxide fuel rods and cracking in zircalloy sheaths. The friction between the tablets and the sheath when the fuel swells results in local strain in the sheath, and appropriate combinations of the coefficients of friction, swelling rate, number of cracks in a tablet, crack growth rate, and other parameters can result in local strain in the shell and cracks expanding towards the outer surface.

The Canadian papers were concerned particularly with hydrogen embrittlement in channel tubes, on account of emergencies arising in the third and fourth units at the Pickering nuclear power station; papers by Simpson, Coleman, and others describe cracking due to hydrides in cold-rolled Zr–2.5% Nb alloy, which results in rapid wall failure. It was supposed that the cracking mechanism involves repeated growth and cleavage of hydride crystals of critical size (over 20 μ). The threshold factor for the stress distribution for crack propagation is about ~5 MPa $\cdot$ m$^{1/2}$. Zircalloy is highly plastic, so this hydride embrittlement is not observed. Also, stress reduction by annealing reduces the cracking probability. Dutton and Pilet described a model that describes quantitatively the slow crack propagation occurring in the region of hydrides in stressed zirconium alloys. They derived a formula for the dissolution of hydrides remote from crack vertices and the deposition on existing hydrides near such vertices. A reactor working temperature of 247°C can result in crack propagation rates as high as $1.5 \cdot 10^{-8}$ m/sec. Conditions for reducing cracking probability have been used in a method of determining the acceptable flaw size for tubes. If the stress is up to 170 MPa, the depth of a flaw should not exceed 0.34 mm, and such flaws can be detected in ordinary monitoring.

During the conference, the Organizing Committee awarded the Kroll medal for research on corrosion mechanisms to B. Cox; this medal is awarded by the Kroll Institution of Reductive Metallurgy and is awarded annually for the best researches on zirconium.

We should also like to record the warm welcome given to the Soviet delegates by the leaders and members of the Canadian group, especially D. Robertson and W. Evans.

IAEA SEMINAR ON DESIGN, MANUFACTURE, AND TESTING OF PACKAGING SYSTEMS FOR SAFE TRANSPORTATION OF RADIOACTIVE SUBSTANCES

A. K. Sedov

This seminar was held Aug. 23-27, 1976, in Vienna and was attended by 139 representatives of 28 countries; 42 papers were read on three main research lines:

I. Researches on Safe Transportation of Radioactive Substances. The paper by A. Greel (USA) presented five-year statistics on emergencies, including ones in shipping nuclear materials. The representatives from the United States in this connection brought forward proposals for yet more severe fire and mechanical tests on such packaging, together with detailed suggestions for test programs.

II. Design and Manufacture of Packaging Systems. The papers on this topic provide a survey of experience in many countries that may serve to define test specifications and identify aspects requiring research. Typical examples here are papers on the design of cheap packaging systems and on multiton systems and containers. Experience in India is here of some interest, where a 70-ton container for shipping agent fuel has been made and tested.

III. Tests. A distinctive feature of the papers on tests was the extensive analysis of design principles for packaging derived from statistical evidence; an example of this approach was presented for type-A packaging systems in the USA, where over 400 individual tests on packaging are performed.

The design of multiton systems has given particular importance to tests on scale models. An example is a statement from the French Atomic Energy Commission that drop tests have been made on an 800 kg model for a 100-ton packaging system for shipping spent fuel, the results being processed by computer to define the deformation. Tests have also been performed on a quarter-scale model for an 80-ton container for shipping radioactive substances, with emphasis on failure at the high pressure level of 500 kgf/cm^2 (Japan).

The tests have included researches on effects related to deformation rate in certain common constructional materials used in shipping and packaging systems for radioactive substances.

Interesting reports were presented from the Oak Ridge National Laboratory on full-scale tests on containers up to 21 tons, which have been dropped from a height of 27 m onto reinforced-concrete sheets of mass 45 tons. A paper from the Federal German Republic was also of considerable interest, since it presented a method of calculation designed to confirm the integrity of packaging systems under fire-test conditions. Tests have been performed on the systems for which the calculations were run.

The seminar also dealt with tests on packaging systems designed to detect radioactive leakage, particularly as regards possible leakage mechanisms for aerosols escaping from damaged packaging, in addition to certain specialized test methods.

The discussions showed that most representatives are entirely convinced of the need to comply with the IAEA Rules and to organize effective means of ensuring that the standards are met by the member countries.

Translated from Atomnaya Énergiya, Vol. 42, No. 3, pp. 244-245, March, 1977.

FIFTH INTERNATIONAL CONFERENCE ON CURRENT TRENDS IN ACTIVATION ANALYSIS

I. N. Ivanov

This conference was held September 13-17, 1976, in Munich (Federal German Republic) as one of a series of conferences held every 4 years, which are the most representative meetings of those researching in this area. The organizing bodies were the German Chemical Society, the Institute of Radiochemistry at Munich Technological University, and the Biophysical Laboratory of the Society for Radiation Protection and Environmental Research. There were 335 registered participants.

The program included plenary lectures, papers by the participants, and discussion of papers taken as read. The meetings were divided into 20 sessions, and most of the papers dealt with fundamental researches in the use of activation analysis in biology and medicine, archeology, art, forensic science, geology, space research, and the environment. In addition, there were researches on materials and industrial applications, and comparisons of accuracy with other analytical methods. Some of the papers dealt with sampling procedures and material standardization.

The program included a visit to the Triga III research reactor near Munich and the Garsching Institute of Radiochemistry of the Technological University.

Advances in activation analysis are closely related to advances in nuclear physics and technology, as well as in radiochemistry. Reactors, accelerators, scintillation counters, and semiconductor detectors are used with multichannel analyzers and computers, and these facilities together have determined the level of studies in this area over the last two decades. It is clear that this close relationship will continue. Activation analysis is now a reasonably mature science, and future development will involve mainly the improvement of characteristics such as accuracy and sensitivity, in addition to extension of the scope for simultaneous determination of numerous elements due to improvements in equipment performance.

Advances in the generation of intense radiation fluxes were dealt with in the paper by Wynerdie of the USA, who dealt with activation analysis employing a neutron generator providing a flux between $5 \cdot 10^{12}$ and $5 \cdot 10^{13}$ neutrons/sec. He stated that such generators will become available in the next 2-4 years.

New facilities in activation analysis are provided by fast-neutron sources provided by charged-particle accelerators; papers by representatives of the Federal German Republic and Belgium reported that neutrons may be generated with a cyclotron by bombarding beryllium with deuterons at 30-50 MeV and 10 μA to increase the sensitivity by a factor of 50-100 by comparison with that available from ordinary neutron sources.

More extensive use is also being made of charged-particle activation and x-ray emission. The bombarding particles are α particles of comparatively low energy (5-15 MeV), while the radiation is recorded by high-resolution silicon devices. X-ray emission has also been recorded in photon activation. For instance, a paper from the Federal German Republic reported that the sensitivity in determining copper can be increased by a factor of 100 in this way.

Studies have also been made on the use of cyclotron-accelerated tritium and heavy ions such as lithium, boron, and fluorine. A paper from France on this topic recorded that high sensitivity is accessible in the determination of light elements in heavy matrices by the use of tritium ions accelerated to 3.5 MeV. A paper from the USA indicated that traces of hydrogen can be detected by heavy-ion bombardment.

Several papers from the Federal German Republic, the USA, and the United Kingdom indicated that there is good scope for analysis based on isotopes and isomers of half-life less than 1 sec; this has become possible because fast pneumatic systems have been constructed, in which the transfer time has been reduced to milliseconds. They have also been used with high-flux sources.

Translated from Atomnaya Énergiya, Vol. 42, No. 3, pp. 245-246, March, 1977.

Much attention was also given to activation analysis applied to industrial analytical problems; the section on materials examination and industrial application had four sessions, at which about 30 papers were read. About 40% of the papers were based on reactor use. Charged-particle accelerators accounted for 20%, followed by neutron generators, isotopic neutron sources, and electron accelerators for γ-activation analysis. This balance between the papers indicates that many difficult analytical problems have so far been handled by means of the strongest radiation sources, which provide sensitivities unavailable from other methods. Only a few papers were presented on studies that ended with the introduction of activation-analysis equipment directly into industrial use. Nevertheless, the interest in this area is considerable.

Particular attention with regard to methods was given to improvements in accuracy, sensitivity, and selectivity; the analysis of high-purity materials has always taken a large place at such conferences, but in the present instance many papers were concerned with the compositions of surface films and the determination of concentration distributions by means of reactors and accelerators operating with protons, deuterons, and other particles. These studies were concerned primarily with industrial applications in the production of semiconductor materials and devices, and also with laser engineering.

Rapid separation of activation products from irradiated specimens can provide high sensitivity in determining certain elements in matrices that themselves become highly active, such as silicon in high-purity metals, where activation with thermal neutrons is appropriate, or again carbon and nitrogen in sodium by x-ray activation (France).

Activation analysis in biomedical areas was represented by 30 papers from the United Kingdom, the Federal German Republic, the USA, Bulgaria, Romania, and other countries. Studies have been made on elemental-composition measurements for living human beings. It seems clear that this approach can provide a realistic diagnostic tool. A paper from the United Kingdom contained suggestions on a method of determining nitrogen from the prompt radiation from thermal-neutron capture, which can be combined with potassium determination from the nautral radioactivity in order to find the ratio of nitrogen to potassium in the body, which is a major characteristic of muscle tissue. A cyclotron was used for this purpose.

A paper from the USA dealt with a method of determining sodium and chlorine by means of 14 polonium–beryllium sources of 50 Ci each. Isotope sources have also been used in the Federal German Republic to determine the calcium–phosphorus ratio, which characterizes the state of bone tissue (in extremities in the human body). A paper by Thomas et al. (USA) described a new analysis method on resonant γ-ray scattering. Very promising experiments were reported on determination of copper in the liver. Many papers also dealt with activation analysis for determining trace elements in body fluids and in vitro.

Activation analysis has been applied to determine drug distributions in the body; a paper from the USA reported a track-counting method for determining lithium contents in the treatment of brain disease.

About 30 papers dealt with activation analysis applied to environmental researches; 12 of these were from the USA and the Federal German Republic. The major line here involved the extension and application of instrumental activation analysis. Most of these studies were performed with neutrons of reactor origin. However, there were some papers in which combinations of neutrons and γ-ray fluxes were employed (analysis of ooze, sediments, and fertilizers). In addition, electron microscopes have been used with x-ray recording in the analysis of marine aerosols.

A paper from Israel presented an interesting method of suppressing background from high-energy β particles in the determination of elements from characteristic radiation; a magnet producing a field of about 4 kOe was employed for the purpose.

Activation analysis has been used in geology and space research mainly on account of the exceptionally high sensitivity, and this also determined the form taken by the analysis: 16 out of the 17 studies used reactor irradiation, most of the irradiations being followed by radiochemical separation. Some papers dealt with the combination of methods, including activation by fast neutrons (14 MeV) and the photoneutron method of determining beryllium. One paper dealt with track methods in the identification of uranium and thorium.

Seven papers dealt with accuracy in activation analysis and comparison with other methods; these reflected practically all areas in activation analysis, neutron, photon, and charged-particle methods.

The conference may be summed up by saying that the period of rapid advance in methods has virtually ended. The traditional areas of application have been defined. The main development trends at the present time may be formulated as follows:

1. extension of the energy range for the activating radiation;
2. increased intensity in radiation sources;
3. increasing use of low-energy charged particles in the analysis of films;
4. utilization of short-lived isotopes in recording induced activity (with half-lives down to 0.1 sec or so); and
5. special systems for fast specimen transport.

In spectrometry, there is an increasing tendency to use characteristic radiation and soft γ radiation in recording induced activity.

It is intended that the next (sixth) conference shall be held in 1980.

SOLAR PROCESSES AND SOLAR NEUTRONS

G. E. Kocharov

The Eighth Leningrad International Seminar was held in September, 1976, and was attended by about 200 researchers, including ones from Hungary, Poland, Czechoslovakia, the USA, and the Federal German republic.

The first session was addressed by G. E. Kocharev, who presented a paper on unsolved problems in solar nuclear astrophysics. Results from 39 cycles of measurement on solar neutrinos indicate that the flux of high-energy solar structure is far below that predicted by the standard theory. Four attempts may particularly be emphasized amongst the numerous ones made to interpret neutrino experiments: highly variable mixing rates within the sun, deviation of particle-pair distributions from Maxwellian, possible combustion of ^{3}He within the sun, and possible discrepancies between the current surface chemical composition of the sun and the composition of solar material when the solar system was formed. The second part of the paper dealt with the latest results on the high ^{3}He levels found in corpuscular fluxes from the sun. Kocharov considered that the most attractive hypothesis here is that the active regions are enriched in ^{3}He on account of influx from under the photosphere, with the particles subsequently accelerated by a mechanism whose performance is proportional to Z^n/A, where Z is particle charge, A is mass number, and $n \geq 2$.

In all, there were six papers on neutrino astrophysics at the first session.

The paper by S. S. Vasil'ev dealt with a quantitative examination of a new and attractive possibility for eliminating the discrepancies between theory and experiment in solar-neutrino recording. The paper discussed the effects of plasma turbulence on the particle distribution. Turbulence can raise the tail of the distribution and thus increase the effective cross sections of reactions that produce the energy, which ultimately results in low fluxes of high-energy solar neutrinos.

The paper by V. A. Krat presented some novel measurements made from the large Soviet solar stratospheric observatory. Photographs reveal granular areas of size 100-200 km, and the data serve to define dynamic features of the temperature gradient, magnetic fields, and movements in various formations on the sun.

A paper by J. Vorpal (USA) presented a detailed analysis of measurements on soft x-ray remission in solar flares; it was pointed out that a flare usually occurs in an entire sequence of loops rather than in a single one.

The most important feature of solar flares (charged-particle acceleration) was discussed in the paper by A. A. Korchak, who drew a strict distinction between the acceleration mechanism and the corresponding model.

Translated from Atomnaya Énergiya, Vol. 42, No. 3, pp. 247-248, March, 1977.

The shape of the spectrum for any charged particle may be explained only if an appropriate acceleration model can be constructed. Detailed discussion of the Fermi model indicates that it cannot be used to explain flare phenomena without major modifications.

B. V. Somov discussed the nonstationary gasdynamic flow of a plasma arising in the atmosphere during phase heating by a high-intensity electron beam accelerated in a flare.

J. Simpson (USA) presented the latest data from the Pioneer 10 and 11 probes; these have revealed new phenomena in interplanetary space due to the interaction between magnetic fields carried by the solar wind and the surrounding charged-particle fluxes at radial distances of more than 10 astronomical units. There are repeated rises in proton-flux intensity at 1-10 MeV, and this raises the problem of where the particles are accelerated, namely on the sun or in interplanetary space. Parallel measurements have been made of the proton and α-particle fluxes at 0.5-2 MeV/nucleon with the IMP-8 (about 1 AU) and the Pioneer 10 and 11 (about 2.5 AU), which together indicate that the acceleration is local, and may occur near the boundaries of jointly rotating interaction regions, where shock waves occur. The second part of the paper discussed the origin of the intensity variation for relativistic electrons around Jupiter, which were first observed in 1973 during the Pioneer 10 flyby. The electron flux as a function of time has been estimated for the range from 1 to 10 AU, which indicates that the main short-term variations (particularly the 25-day ones) are due to modulation effects arising from periodic rotating regions in interplanetary space, not from direct changes in the rate of leakage of electrons from Jupiter's magnetic field or from the electron-acceleration mechanism associated with the region.

Some of the abundance of cosmogenic isotopes in nature and of sun–earth relationships were read at the closing session.

Much interest was aroused by V. A. Dergachev's paper on the determination of cosmic-ray intensities in the past from radiocarbon data; variations in ^{14}C activity observed in annual rings up to 8000 years ago may be due to various astrophysical and geophysical phenomena: 1) changes in the global cosmic-ray flux outside the solar system, 2) variations in galactic cosmic radiation due to solar phenomenon, 3) time variations in the earth's magnetic field, and 4) variations in carbon mixing on account of changes in climatic conditions.

Dergachev pointed out the distribution of the radiocarbon data is similar to that for the solar-spot count; there are two main peaks, which correspond to periods of about 11 and 80 years. However, the amplitudes of the harmonics differ. For instance, the major harmonics in the radiocarbon data correspond to the 80-yr period, whereas those for the sunspots correspond to 11-yr cycles. The radiocarbon and paleomagnetic data also indicate that there are four cycles: ones at 600 and 360 years due to the time variations in the earth's magnetic field, the 80-yr cycle associated with solar activity, and the 36-yr climatic cycle.

Povinc (Czechoslovakia) dealt with the scope for research on solar activity in the past from concentration measurements on cosmogenic isotopes in lunar specimens; the latter (whether mass rock or fragmentary) can be used to estimate the cosmic-ray variations and solar activity. The data would appear to indicate solar-activity variations in the past.

Much interest and lively discussion arose from B. M. Vladimirskii's paper on the relationship between phenomena on the sun and in the biosphere; it seems clear that the earth's electromagnetic field is a major ecological factor, particularly at low and ultralow frequencies, and therefore it should be considered in biometeorology and climatic medicine. The perturbations in the earth's electromagnetic field are quasiperiodic, so phenomena such as forced biorhythm synchronization may be important in coupling biological parameters to solar activity.

There were addresses from S. Pinter (Czechoslovakia), E. Bagge (Federal German Republic), and G. E. Kocharov (USSR) at the close of the Seminar.

BRITISH FUSION AND PLASMA-PHYSICS RESEARCH

G. A. Eliseev

A delegation from the State Commission on Nuclear Energy of the USSR visited the United Kingdom between Oct. 20-31, 1976, in accordance with the long-term research collaboration program, in order to examine the state of research in plasma physics and controlled thermonuclear fusion. During the tour, they visited the Culham Laboratory, the Laboratory of Plasma Physics at Oxford University, the corresponding laboratory at Imperial College in London, the laboratories of High-Voltage Engineering and Gas Discharge at Liverpool University, the Engineering Superconductivity Section at the Rutherford Laboratory, and Brentford Electric, an electrical-engineering firm.

Particular attention was given to familiarization with the state of the art and development prospects in controlled thermonuclear fusion at Culham, where virtually all major researches on this topic and plasma physics are centered (apart from researches on laser thermonuclear fusion). The staff of this laboratory is 825, of whom 260 are college graduates in science or engineering. The 1976 budget of the laboratory was 8.2. million pounds.

At Culham the delegation received detailed information on researches on the main systems (Table 1), and also on theoretical researches, engineering aspects of thermonuclear fusion, joint researches of Culham with other organizations, and so on.

Up to 1975, the CLEO system was used in tokamak mode, but then experiments were performed in stellarator mode with 0.3 angular rotational conversion and a mean radius for the inscribed surface of about 10 cm. The main results were obtained for a field of 13 kOe and a plasma current of 17 kA of duration 40 msec. It was found that the CLEO system gave no marked difference in plasma containment in the tokamak and stellarator modes. Moreover, the electron-energy containment time in stellarator mode was somewhat greater than that in

TABLE 1. Characteristics of Major Thermonuclear Systems at Culham Laboratory

Name and type	Major dimensions, cm*	Magnetic field, kOe	Plasma density, cm^{-3}	Temp., eV		Containment time, sec	β†
				electronic	ionic		
CLEO, stellarator	12; 90	<20	$2{,}5\cdot10^{13}$	350	150	$2\cdot10^{-3}$	$3\cdot10^{-3}$
DITE, tokamak	27; 117	28	$3\cdot10^{13}$	1000	350	$5\cdot10^{-3}$	$\sim10^{-2}$
HBTX I, reverse-field pinch	6; 100	10	$1\cdot10^{16}$	<100	<100	$4\cdot10^{-5}$	0,3—0,5
LEVITRON, multipole	10; 30	7	$1\cdot10^{12}$	~10	~10	2,5	$<10^{-4}$
TORSO, stellarator	6,5; 40	20	$<10^{13}$	200	50	$3\cdot10^{-4}$	$\sim10^{-3}$
TOSCA, tokamak	10; 30	14	$>5\cdot10^{13}$	300	100	$3\cdot10^{-4}$	$\sim10^{-2}$
PF, multipole	0,1·1	2000	$2\cdot10^{19}$	2000	1000	$2\cdot10^{-8}$	0,7

*Minor and major radii of the toroidal plasma chamber, respectively.

† β is the ratio of the plasma pressure to the pressure of the containing magnetic field.

Translated from Atomnaya Énergiya, Vol. 42, No. 3, pp. 248-250, March, 1977.

TABLE 2. Parameters of Thermonuclear Systems at Culham Laboratory

Characteristics	Mark I	Mark II
Power, MW		
electrical	2500	2500
thermal	5830	5830
Major radius of toroid, m	12,6	7,4
Eff. plasma radius, m	2,5	2,1
Ellipticity of plasma cross section	1,0	1,75
Magnetic field at axis, kOe	76,0	40,0
Plasma current, MA	9,7	11,7
β_t, %	1,6	9,3
Plasma density, cm^{-3}	$1,8 \cdot 10^{14}$	$3,5 \cdot 10^{14}$
Eff. containment time (energy), sec	1,8	1,5
Flux at first wall, MW/m^2	4,6	6,7
Cost, 10^6 pounds sterling		
reactor	280	?
power station	893	?

tokamak mode, which appears to be due to the smoother radial electron-temperature distribution. The relatively low ionic temperature was probably due to the high level of impurities in the plasma. It is proposed to examine the current-free containment mode on CLEO in the near future. The initial plasma will be created by a current, with maintenance by neutral-beam injection. It is also proposed to generate the plasma by evaporating D or Li tablets by means of a CO_2 laser.

The main feature of the DITE tokamak is the local (bundle) diverter; the purpose of the experiments here was to examine the operation of the diverter in plasma-heating mode with external injection. The diverter should then remove plasma moving towards the walls in the discharge chamber, and also any impurities derived from the walls. The first trials (the equipment was commissioned in 1976) gave promising results. The plasma density at the wall was reduced by a substantial factor by the diverter. Trials with pulsed oxygen inlet showed that the diverter does provide protection, since the oxygen is ionized in the diverter and displaced from the discharge chamber. Plans for future experiments include increasing the neutral-beam input power to 1.5 MW and the magnetic field (with the diverter operating) to 28 kOe.

Researches on toroidal plasma configurations with reversed fields in the plasma (the HBTX system) are traditional at Culham, since they began with the ZETA system. Such systems have an advantage over tokamaks in that stable containment can be attained at much lower toroidal magnetic field levels. Recently, the HBTX I system has provided stable operation at a discharge current of 60 kA. Also, stable self-reversal of the magnetic field in the plasma has been produced. This result has led to a decision to extend researches in this area and to build a larger RFX system, which should provide a test of similarity laws, which itself should provide sound decisions on the prospects for the design of a prototype thermonuclear reactor. The basic parameters of the RFX are as follows: major and minor radius of the toroid 180 and 60 cm, respectively, plasma current 0.7-1 MA, current containment time 10-20 msec, and plasma temperature 1-3 keV. The design has been almost completed, and certain components have already been built. The construction cost is estimated as $(5-6) \cdot 10^6$ pounds sterling, but the final decision on financing the construction has not yet been taken.

Considerable success has also been attained in the design of injectors for fast hydrogen atoms; the ion-source group has designed a gas-discharge chamber providing a uniform plasma density over a surface of 10×20 cm^2. The magnetic field is weak (about 10 Oe), which goes with a special electrode design to raise the ratio of the ion current to the discharge current to the record level of 0.78. Optimization in numerical calculations has been used to define the electrode configuration and the potential distribution that will provide ion beams of divergence less than 0.2°. The calculations have been confirmed by measurements on a model for an ion source containing a neutralizer. If the result is further confirmed on a full-scale model, the design will form an exceptional basis for injectors for thermonuclear reactor systems.

For some years, Culham has been concerned with outline design of thermonuclear reactors, in which much assistance has been obtained from fast-reactor engineers at Harwell, Risley, and Winfrith Heath. The first outline design for Tokamak Mark 1 was drawn up in 1972; economic evaluation at Risley showed that a thermonuclear power station based on such a reactor would be substantially more expensive than a nuclear

power station with the same output based on a breeder reactor. For this reason, a new project, Mark II, was drawn up in 1976, with the major objective of reducing reactor costs by increasing the ratio of the plasma pressure to the pressure of the toroidal magnetic field β_t, while at the same time the heat load at the first wall was to be increased (Table 2). An economic evaluation of Mark II is currently under way.

Various researches on plasma physics and the physics of ionized gases are in hand at the Department of Engineering Physics at Oxford University; here we may note particularly researches on the anomalous absorption of high-intensity electromagnetic radiation in plasma, which provide a means of microwave simulation of the interaction between laser beams and dense plasma. Measurements have been made on processes occurring in alkali-metal plasmas, discharge behavior in the presence of high-intensity optical pumping, and microparticle acceleration by laser beams. Oxford University is also extensively engaged in collaboration with the Rutherford Laboratory in a general program of laser fusion research.

The Department of Plasma Physics at Imperial College, London University, was set up as long ago as 1947; this is now concerned not only with instruction but also with researches on a restricted scale on plasma physics. The POLYTRON system has been used for researches on plasma containment in toroidal configurations with fields of acute-angle geometry. The magnetic field is produced by 36 one-turn coils forming a toroid and connected in opposition. Ions are accelerated in the magnetic gaps on account of the Hall effect, which reduces the radial loss of plasma. Measurements have also been made on the interactions between relativistic electrons (300 keV, 45 kA) and neutral gases or plasmas. A contract with the Culham laboratory is concerned with the scope for producing dense plasmas (up to 10^{20} cm^{-3}) by means of high-current z pinches.

Major researches on the physics of electrical breakdown in gases and on arc discharges are being performed in the Department of Electrical Engineering at Liverpool University; virtually all these researches are of applied significance and are supported by electrical-engineering firms. Researches on arc discharges in gas flows are related to the design of new high-power switches with automatic arc extinction for power-supply purposes. Several researches are designed to optimize fuses for operation at various power levels. Laser-initiated vacuum arc-discharge gaps are also being examined. Interesting results have been obtained on electrical breakdown mechanisms, and in particular it has been shown that experiment does not confirm the breakdown theory based on microparticle acceleration from the anode.

The Rutherford Laboratory provided an opportunity for seeing researches on engineering superconductivity; until recently, the main researches were concerned with accelerator topics (pulsed dipole magnets for proton synchrotrons, magnetic pipes for transporting accelerator beams, and so on). Recently, researches have been done on controlled thermonuclear fusion. At the request of the Culham Laboratory, a design has been drawn up for a superconducting magnetic system for a large tokamak, in which the stored magnetic-field energy will be $1.2 \cdot 10^{10}$ J.

Brentford Electric is a firm specializing in the design and manufacture of a wide variety of power supplies; a large fraction of the output consists of power supplies for electrophysical systems. At the request of CERN, power supplies have been manufactured for the electromagnets in beam-transport systems, for which high levels of stability were specified ($5 \cdot 10^{-6}$). Power supplies have also been designed and built for the thermonuclear laboratories at Garsching and Julich in the Federal German Republic, at Culham, and at Fontenay aux Roses (France). An interesting circuit was used in the Culham unit designed to deliver 0-60 kV at 20 A, in which the output voltage is stabilized by electromechanical control of the ratio in the primary transformer. The firm routinely produces stabilized-current sources and stabilized-voltage sources ranging up to 800 V and output up to 1500 A, with stabilization level $5 \cdot 10^{-6}$.

We would like particularly to record the warm welcome we received at the Culham Laboratory and the other scientific centers we visited.

PROCESSING AND STORAGE OF RADIOACTIVE WASTES IN CANADA

V. D. Balukova

Up to 1971, radioactive wastes constituted no problem in Canada, since over 99% of the radioactive fission products from reactors were shipped abroad. On the other hand, research reactors have been in operation for over 26 years, and during that period many research studies have been performed on reactor fuel, which had required various developments in radioactive-waste processing. The recent extension of nuclear power has made radioactive wastes an acute problem for Canada.

Researches on processing and storage of radioactive waste were illustrated during a visit of a Soviet delegation to Canada during October, 1976.

The Whiteshell Research Center is concerned with a long-term program on waste processing, which is based not only on the experience accumulated at Chalk River, but also world experience; this has been in operation since 1973. The economic situation in the country at present is unfavorable for research developments, and this will probably continue into the 1980s, and therefore waste from nuclear-fuel reprocessing will probably not accumulate on any scale in the next few years, since the spent fuel rods will be stored directly on site with a view to future extraction of the plutonium.

Relatively superficial formations have been used until recently for disposing of radioactive wastes and for storage; various engineering techniques have been developed for waste processing, which have either been checked out entirely or else are in process of checking or transfer from pilot plants to large-scale systems (reversal osomosis, combustion, and evaporation).

Spent fuel is now to be stored in a dry store after remaining for 5 years under water; a prototype concrete system for this purpose has been designed and tested at Whiteshell.

These containers are cylindrical (diameter 335.5 cm, height 488 cm, wall thickness 76.25 cm), and they are used to contain 220 assemblies from the CANDU reactor, i.e., about 4.4 tons of fuel. The fuel in its sheath is placed in a lead container, which is covered by steel plate, and then the rods are embedded in the concrete containers at the point of construction. Several such containers have been tested, particularly to simulate the temperature distribution, for which purpose electrical heaters have been fitted, and it has been found that the containers should be stable for any reasonable storage time. At the same time, means of transportation have been designed and tested for handling such assemblies.

The program also envisages the future construction of a plant for reprocessing spent fuel; the wastes are to be solidified and stored for long periods. Underground stores in deep formations are considred as the best prospect. Particular attention is now being given to the processing and storage of nuclear power station wastes. A scheme has been devised for liquid wastes that involves the following units: collection of dilute wastes → purification by reverse osmosis → purified effluent discharged to rivers; high-activity waste stored → evaporated → condensate discharged to rivers, and residue solidified with bitumen (or else stored in a vessel). There is a possibility that dispersal might also be used. Liquid wastes corresponding to national effluent standards are to be discharged to open ponds. Low-activity solid wastes should be burned, with subsequent bitumen treatment of the ash. A system has been devised for gas cleaning for use during the combustion. Special concrete stores have been set up for solidified wastes at Whiteshell, Chalk River, and the Bruce Nuclear Power Station. Previously, such storage has been performed simply underground at Chalk River.

The designed stages for the individual units vary; e.g., a full-scale system has been constructed and will shortly be commissioned for combusting solid wastes at the Bruce power station. This system includes a conveyor for handling the wastes, a primary combustion chamber (vertical, with double steel walls and internal

Translated from Atomnaya Énergiya, Vol. 42, No. 3, pp. 250-251, March, 1977.

cooling, capacity 8.5 m^3, periodic operation, chamber temperature 150-600°C), a secondary chamber (working temperature up to 1000°C), an air heat exchanger (1000-200°C), Fiberglas and asbestos filters for removing coarse and fine particles designed to work continuously at 260 and 200°C, respectively, a gas blower system, and containers for collecting and transporting the ash.

A pilot reverse-osmosis plant has also been designed and tested at Chalk River; researches are continuing on the bitumen treatment with a small plant. No general scheme for such a plant has yet been drawn up. Studies have been made on incorporating wastes containing plutonium from UO_2-PuO_2 fuel in polymers, which are based on formaldehyde, phosphoric acid, etc.

At the Chalk River, observations have been performed for 15 years on the storage of 25 vitrified blocks made by incorporating 1100 Ci of fission products in nepheline–syenite glass. This vitrification technique was originally proposed in Canada.

Much attention is also being given to the storage of wastes after processing. This aspect of the matter has been thoroughly researched from the engineering view point in Canada. Actual store construction is preceded by detailed geological and hydrogeological evaluation of the locality. Careful attention is paid to accumulating evidence on the sorption and migration of radionuclides in soil and water derived from the long-term study of underground formations at Chalk River used in storing wastes produced and shipped from elsewhere.

Such stores are envisaged only for solid or solidified wastes; major types of working system have been developed for the Pickering and Bruce nuclear power stations. A store has been constructed on the area of the Bruce power station, which includes reinforced-concrete vessels of trench type, which are transversely divided into sections for dry and solidified wastes packed in polyethylene bags (a section is closed with a concrete lid when full), and in addition there are concrete pipes buried in the ground for taking containers containing waste (144 pipes), and also ground-level concrete stores for used sorbents from the first-loop systems of reactors. The latter are shielded by banks of sand and gravel. In addition, they are fitted with drainage-pipe systems to prevent radionuclides from migrating into adjacent soil. These structures are of total volume 3400 m^3. The wastes passed to the store before the combustion system is commissioned will subsequently be removed for combustion. The stores are equipped in such a way that such removal is practicable.

Therefore, the following particular features are emphasized in Canada as regards waste processing: reverse osmosis is already operated, a novel idea of vitrification for high-level wastes in nepheline–syenite glasses has been devised and tested over many years, detailed and systematic support is provided by research on hydrogeological and physicochemical conditions in areas designed for waste storage, and it is envisaged that it should be feasible to transfer waste between stores and to build dry stores for spent fuel.

A. P. Veselkin and Yu. A. Egorov (editors)

ENGINEERING DESIGN OF NUCLEAR POWER STATION SHIELDING*

Reviewed by V. S. Yuzgin

Many books have been published on the physics of radiation shielding, but no one covers all problems in nuclear power station shielding.

This book is a practical handbook for power-station shielding designers, and it is also of value to those concerned with the design of related structure, pipework, and equipment in processing systems generally. The book generally is based on a vast amount of accumulated evidence on shielding for power stations based on thermal-neutron reactors.

Chapter 1 deals with the general concepts normally employed in shielding design, with emphasis on the correct choice of input data and the proper sequence of design studies.

Chapters 2 and 4 deal with neutron and γ-ray sources within the core of a reactor and loops and equipment generally.

Chapter 3 deals with the design sequence for a shield intended to contain penetrating radiation; here many computer programs are available, and it is suggested that radiation transmission should be determined by engineering methods with computer support, in addition to empirical studies performed manually and exact solution of the kinetic equations for radiation transport.

Chapter 4 deals with calculations on coolant activity, nonprecipitated impurities, and corrosion products in water-cooled reactors.

It is now possible to accurately forecast the radiation transfer occurring in channels, slots, and holes in shields; this is considered in Chap. 5.

Chapters 6 and 7 present the data required in calculating activation of reactor elements and shielding materials, as well as the principles of heat production under irradiation. Any extension of reactor running time requires considerable reserve radiation resistance in constructional materials, and here Chap. 8 should be of value to the designer, since it provides a method of calculating the radiation-damage margin in the body of a power-station reactor.

Unfortunately, the book does not deal with the radiation-damage safety margin for fuel-rod sheaths.

Chapter 9 deals with shielding for reactor systems, with particular emphasis on hydrogenous material. The radiation level in areas adjacent to the reactor cannot be estimated unless the scattered-radiation field is known. The last chapter presents data on such calculations.

The book contains many graphs and tables, and an extensive bibliography is given at the end of each chapter.

The book should prove of value to shielding designers for nuclear power stations, engineers concerned with radiation shielding, and students in appropriate courses at technical colleges.

*Moscow, Atomizdat (1976).

Translated from Atomnaya Énergiya, Vol. 42, No. 3, p. 252, March, 1977.

CHANGING YOUR ADDRESS?

In order to receive your journal without interruption, please complete this Change of Address notice and forward to the Publisher, 60 days in advance, if possible.

Old Address: (PLEASE PRINT)

NAME _____

STREET _____

CITY _____

STATE (or Country) _____

ZIP CODE _____

New Address: (PLEASE PRINT)

NAME _____

STREET _____

CITY _____

STATE (or Country) _____

ZIP CODE _____

Date New Address Effective: _____

Name of Journal: _____

Plenum Publishing Corporation
227 West 17 Street
New York, New York 10011

engineering science

continued from back cover

Title	# of Issues	Subscription Price
Metallurgist *Metallurg*	12	$225.00
Metal Science and Heat Treatment *Metallovedenie i termicheskaya obrabotka metallov*	12	$215.00
Polymer Mechanics *Mekhanika polimerov*	6	$195.00
Problems of Information Transmission *Problemy peredachi informatsii*	4	$175.00
Programming and Computer Software *Programmirovanie*	6	$95.00
Protection of Metals *Zashchita metallov*	6	$195.00
Radiophysics and Quantum Electronics (Formerly Soviet Radiophysics) *Izvestiya VUZ. radiofizika*	12	$225.00
Refractories *Ogneupory*	12	$195.00
Soil Mechanics and Foundation Engineering *Osnovaniya, fundamenty i mekhanika gruntov*	6	$195.00
Soviet Applied Mechanics *Prikladnaya mekhanika*	12	$225.00
Soviet Atomic Energy *Atomnaya energiya*	12 (2 vols./yr. 6 issues ea.)	$235.00
Soviet Journal of Glass Physics and Chemistry *Fizika i khimiya stekla*	6	$ 95.00
Soviet Journal of Nondestructive Testing (Formerly Defectoscopy) *Defektoskopiya*	6	$225.00
Soviet Materials Science *Fiziko-khimicheskaya mekhanika materialov*	6	$195.00
Soviet Microelectronics *Mikroélektronika*	6	$135.00
Soviet Mining Science *Fiziko-tekhnicheskie problemy razrabotki poleznykh iskopaemykh*	6	$225.00
Soviet Powder Metallurgy and Metal Ceramics *Poroshkovaya metallurgiya*	12	$245.00
Strength of Materials *Problemy prochnosti*	12	$295.00
Theoretical Foundations of Chemical Engineering *Teoreticheskie osnovy khimicheskoi tekhnologii*	6	$195.00
Water Resources *Vodnye Resursy*	6	$190.00

SEND FOR YOUR
FREE EXAMINATION COPIES

Plenum Publishing Corporation

Plenum Press • Consultants Bureau
• IFI/Plenum Data Corporation
227 WEST 17th STREET
NEW YORK, N. Y. 10011

United Kingdom: Black Arrow House
2 Chandos Road, London NW10 6NR England

Back volumes are available. For further information, please contact the Publishers.

Declassified and Approved For Release 2013/04/01 : CIA-RDP10-02196R000700090003-6

breaking the language barrier

WITH COVER-TO-COVER
ENGLISH TRANSLATIONS
OF SOVIET JOURNALS

in engineering science

Title	# of Issues	Subscription Price
Automation and Remote Control *Avtomatika i telemekhanika*	24	$260.00
Biomedical Engineering *Meditsinskaya tekhnika*	6	$195.00
Chemical and Petroleum Engineering *Khimicheskoe i neftyanoe mashinostroenie*	12	$275.00
Chemistry and Technology of Fuels and Oils *Khimiya i tekhnologiya topliv i masel*	12	$275.00
Combustion, Explosion, and Shock Waves *Fizika goreniya i vzryva*	6	$195.00
Cosmic Research (Formerly Artificial Earth Satellites) *Kosmicheskie issledovaniya*	6	$215.00
Cybernetics *Kibernetika*	6	$195.00
Doklady Chemical Technology *Doklady Akademii Nauk SSSR*	2	$65.00
Fibre Chemistry *Khimicheskie volokna*	6	$175.00
Fluid Dynamics *Izvestiya Akademii Nauk SSSR mekhanika zhidkosti i gaza*	6	$225.00
Functional Analysis and Its Applications *Funktsional'nyi analiz i ego prilozheniya*	4	$150.00
Glass and Ceramics *Steklo i keramika*	12	$245.00
High Temperature *Teplofizika vysokikh temperatur*	6	$195.00
Industrial Laboratory *Zavodskaya laboratoriya*	12	$215.00
Inorganic Materials *Izvestiya Akademii Nauk SSSR, Seriya neorganicheskie materialy*	12	$275.00
Instruments and Experimental Techniques *Pribory i tekhnika eksperimenta*	12	$265.00
Journal of Applied Mechanics and Technical Physics *Zhurnal prikladnoi mekhaniki i tekhnicheskoi fiziki*	6	$225.00
Journal of Engineering Physics *Inzhenerno-fizicheskii zhurnal*	12 (2 vols./yr. 6 issues ea.)	$225.00
Magnetohydrodynamics *Magnitnaya gidrodinamika*	4	$175.00
Measurement Techniques *Izmeritel'naya tekhnika*	12	$195.00

SEND FOR YOUR FREE EXAMINATION COPIES

Back volumes are available. For further information, please contact the Publishers.

continued on inside back cover